

*Additive Manufacturing
of metal alloys
for aerospace application:
design, production,
repair and optimization*

Ing. Paolo Argenio



Unione Europea



*Ministero dell'Istruzione,
dell'Università e della Ricerca*



Università degli
Studi di Salerno

FONDO SOCIALE EUROPEO

Programma Operativo Nazionale 2000/2006

“Ricerca Scientifica, Sviluppo Tecnologico, Alta Formazione”

Regioni dell'Obiettivo 1 – Misura III.4

“Formazione superiore ed universitaria”

Department of Industrial Engineering

***Ph.D. Course in Industrial Engineering
(XVI Cycle - New Series, XXX Cycle)***

***Additive Manufacturing
of metal alloys for aerospace application:
design, production, repair and optimization***

Supervisor

*Prof. Vincenzo Sergi
Prof. Fabrizia Caiazzo*

Ph.D. student

Ing. Paolo Argenio

Ph.D. Course Coordinator

Prof. Ernesto Reverchon

Publication list

a) Journal articles

- **“Laser beam welding of a Ti-6Al-4V support flange for buy-to-fly reduction”**
F. Caiazzo, V. Alfieri, G. Corrado, P. Argenio, G. Barbieri, F. Acerra, V. Innaro,
Metals 7, 183 (2017)
10.3390/met7050183
- **“Disk-laser welding of Ti-6Al-4V titanium alloy plates in T-joint configuration”**
F. Caiazzo, F. Cardaropoli, V. Alfieri, V. Sergi, P. Argenio, G. Barbieri
Procedia Engineering 183, pp. 219-226 (2017)
10.1016/j.proeng.2017.04.024
- **“Reduction of surface roughness by means of laser processing over additive manufacturing metal parts”**
V. Alfieri, P. Argenio, F. Caiazzo, V. Sergi
Materials 10, 30 (2017)
10.3390/ma10010030
- **“Redesign and manufacturing of a metal towing hook via laser AM with powder bed”**
D. Usera, V. Alfieri, F. Caiazzo, P. Argenio, G. Corrado, E. Ares
Procedia Manufacturing 13, 825-832 (2017)
10.1016/j.promfg.2017.09.129

- ***“Laser Powder-Bed Fusion of Inconel 718 to manufacture turbine blades”***

Fabrizia Caiazzo, Vittorio Alfieri, Gaetano Corrado, Paolo Argenio
The International Journal of Advanced Manufacturing Technology (2017)
10.1007/s00170-017-0839-3

- **“Study on the Factors Affecting the Mechanical Behavior of Electron Beam Melted Ti6Al4V”**

Carmin Pirozzi, Stefania Franchitti, Rosario Borrelli, Fabrizia Caiazzo, Vittorio Alfieri, Paolo Argenio
Journal of Materials Engineering and Performance (2017)
10.1007/s11665-017-2894-1

- **“Additive manufacturing by means of laser-aided Directed Metal Deposition of 2024 aluminum powder: investigation and optimization”**

V. Alfieri, P. Argenio, F. Caiazzo, V. Sergi
The International Journal of Advanced Manufacturing Technology 9(8), 1-12 (2017)
10.1177/1687814017714982

b) Conference Proceedings

- **“Mechanical properties of Inconel 718 in Additive Manufacturing via Selective Laser Melting – An investigation on possible anisotropy of tensile strength”**

F. Caiazzo, V. Alfieri, G. Corrado, P. Argenio
3rd International Forum IEEE “Research and Technologies for Society and Industry, RTSI 2017”, Modena, ISBN 978-1-5386-3906-1

TABLE OF CONTENTS

Abstract	I
Preface on the Additive Manufacturing	III
Chapter_I Investment casting process of turbine blade: redesign and manufacturing of mould by means of Direct Selective Laser Melting of metals	1
1.1 Principles of Direct Selective Laser Melting	2
1.2 Investment casting process	4
1.2.1 The process	5
1.3 Experimental setup	8
1.3.1 AM powder features	9
1.4 Design and manufacturing of mould	14
1.4.1 First case study	15
1.4.2 AM production	16
1.4.3 Pattern preparation	21
1.4.4 Second case study	23
1.4.5 Pattern analysis	28
1.5 Cost and time analysis for mould AM construction	30
1.6 Conclusions	32
References chapter I	33
Chapter_II Additive Manufacturing via Selective Laser Melting of turbine blades	35
2.1 Experimental setup: inconel 718 powder	36
2.2 Experimental procedure	38
2.2.1 Job preparation	39
2.3 Results and discussion	41
2.3.1 Tensile testing	41
2.3.2 Micro-hardness analysis	45
2.4 AM of the turbine blade	49
2.4.1 X-ray inspections	52
2.4.2 Am turbine blade dimensional analysis	53
2.5 Conclusions	56
References chapter II	57

Chapter_III Laser cladding as repair technology for complex component in aerospace industry	61
3.1 Introduction to powder injection Laser Cladding	62
3.2 Powder laser cladding equipment	65
3.2.1 Laser source	65
3.2.2 Powder feeder	67
3.2.3 Manipulating sistem	70
3.2.4 Laser Cladding head	71
3.2.5 Beam nozzle	72
3.3 Experimental setup	73
3.3.1 Process tuning	74
3.3.2 Powder mass flow setting	75
3.3.3 Laser spot diameter setting	77
3.4 Experimental procedure	79
3.4.1 Composition	81
3.4.2 Single-trace deposition	82
3.5 Depositions for repairing of damages	87
3.6 Repair of a superalloy CM247LC guide nozzle vane	93
3.7 Conclusions	97
References chapter III	98

Chapter_IV Reduction of surface roughness by means of laser processing over additive manufacturing metal parts	101
4.1 Sourface roughness of additive manufacturing metal parts	101
4.2 Post processing treating for surface modification	103
4.2.1 Laser surface modification	103
4.2.2 Laser surface modification by means of scanning optics	104
4.3 Experimental setup	106
4.3.1 Materials and methods	106
4.4 Results and discussion	110
4.4.1 Starting roughness for as-built samples	110
4.4.2 Roughness and geometry of the fusion zone upon LSM	111
4.4.3 Microstructure and microhardness	115
4.5 Conclusions	118
References chapter IV	119

Conclusions	121
--------------------	------------

Abstract

Since its introduction, Additive Manufacturing (AM) has been used in aerospace applications. Rapid prototyping for saving capital and time during the product development period can be accomplished; moreover, significant influences on product design, direct part fabrication, assembly, and repair are benefited. Thanks to recent developments, AM has rapidly become a strategic technology generating revenues throughout the aerospace supply chain.

In this Ph.D. thesis, some applications of AM to the purpose of part fabrication and part repairing in aerospace are addressed; advantages and crucial features are discussed.

In chapter 1, the technology of Direct Selective Laser Melting of Metals, in the family of Additive Manufacturing processes, is considered to improve the process of investment casting of turbine blade. Design, manufacturing cost and time of a mould is investigated.

In chapter 2, Direct Selective Laser Melting is considered as an advanced industrial prototyping tool to manufacture Inconel 718 turbine blades at a pre-design stage before flow production. Expediting of the evaluation of any upgrades of both the part itself and tooling for assembly is aimed. To this purpose, possible anisotropy of manufacturing is preliminarily investigated via tensile testing at room and elevated temperature as a function of the sloping angle with the building plate; the normalized strength is given and compared with similar studies in the literature. Positioning and proper supporting in manufacturing are discussed; the parts are further investigated to assess their compliance with the intended nominal geometry.

In chapter 3, laser cladding is used to repair a nozzle guide vane, one of the main structural parts of gas turbines. With respect to traditional methods, this process allows to achieve reduced changes of the metal microstructure around the repaired zone, thanks to a more accurate deposition of a small volume of the filler material. Many parameters as laser spot diameter, powder feed rate, scanning velocity and laser power have been changed as main parameters in the experimental plan. An optimal overlapping rate has been set to generate a proper track size to address the actual damage.

In chapter 4, the issue of improving, by means of post processing, the surface quality resulting from AM is analysed. Laser surface modification as an alternative to conventional technologies has been investigated; also, laser beam wobbling has been considered in comparison with linear scanning aiming to reduce the affection of the parent metal and widen the scanning trace so to reduce the overall processing time. The results are widely discussed in terms of visual inspections, reduction of roughness, geometry of the cross-

section, microstructure and microhardness. Full experimental details are provided so that the results can be reproduced.

Preface on the Additive Manufacturing

In the industrial field the employment of innovative fabrication technologies is emerging to the purpose of cost reduction and flexibility. In particular, great interest is addressed to additive manufacturing (AM) techniques, which allow to obtain complex parts based on CAD models. AM enables the fabrication of parts with complex geometry that are impractical to be manufactured using conventional subtractive manufacturing methods. In addition, AM can be used to extend the life of in-service parts through innovative repairing.

Basically, all of the AM techniques employ the same basic principle: the final component is fabricated by means of layer by layer addition of the material.

Today, in addition to plastic material, several metallic materials including steel, aluminium, nickel-based superalloys, cobalt-base alloys and titanium alloys may be processed to full dense parts with properties complying with the requirements of industrial applications. Special interest has been devoted to AM in aerospace and biomedical industries thanks to the possibility of manufacturing high performance parts with reduced overall cost. Namely, in the aerospace this could lead to a reduction of required raw materials for in-service components, which is known as the “buy-to-fly” ratio. AM could also lead to innovative lightweight structures for several applications.

In the medical industry, AM is already leading to a revolution in customized medicine where dental implants, orthopedics, and hearing aids are manufactured to fit an individual’s unique physiology.

AM processes can be classified by the nature and the aggregate state of the raw materials as well as by the energy source. In AM of metals, powder raw materials or wire are fully melted by the energy input of a laser beam or an electron beam and transformed layer by layer into a solid part of nearly any geometry (classification: Powder-based or Wire-based AM).

In the following scheme a classification of the most important AM technologies is shown.

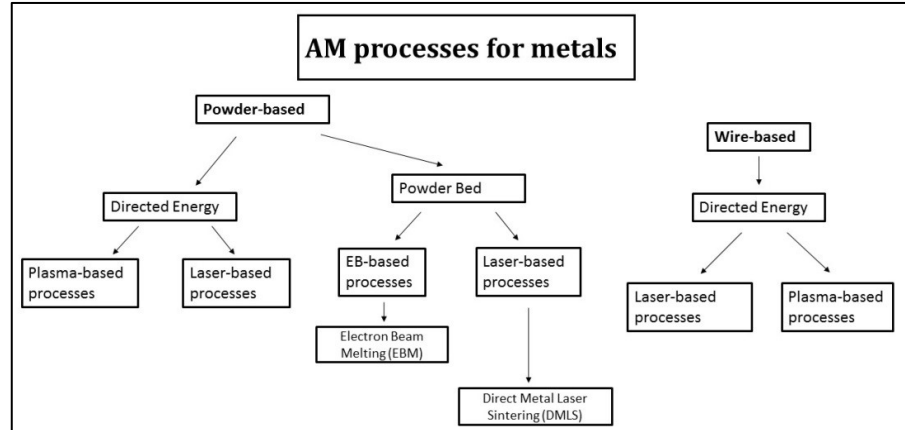


Fig. 1. AM technologies: Powder-based and Wire-based deposition AM

Powder-bed AM

In powder-bed AM systems, to prevent oxidation and possible fire due to fine particles, the process is performed in enclosed chamber which operated in vacuum or filled with an inert gas. The part and its supporting structures are manufactured in the same job, with the same material. In the center of the chamber, the metal powder is provided and layered by means of a leveling system. The chamber is then pre-heated to a pre-determined temperature depending on the process, around 100°C for laser-based processes and up to 700°C for electron beam. The laser or electron beam is then scanned over the surface of the metal powder along the pattern of the part, building up a single layer, usually between 20 and 200 μm thick. The building plate is then lowered by a single layer thickness, a leveling system provides fresh powder on top of the part, and the process is repeated until the final build is finished.

Electron Beam Melting (EBM)

In the EBM process an electron beam gun is employed as heat source. A focused beam of electrons is delivered to the powder bed, the kinetic energy is transformed into local heating to high temperatures and the powder particles melt, as a consequence.

As the process is conducted in vacuum to preserve the beam energy, gas shielding is not required. The advantage of the EBM process is that it has a faster build rate compared to laser-based powder bed systems. However, the surface roughness for EBM parts is higher and post machining is necessary depending on the applications.

Direct Metal Laser Melting (DMLM)

Direct Metal Laser Melting process was developed by EOS GmbH of Munich and has been available commercially with the EOSINT M 250 laser melting machine since 1995.

During the DMLS process a laser beam scans the surface of the metal powder layer. The laser radiation is absorbed by the powder particles and heat is generated instantaneously in the powder layer, thus producing melting and thermal stresses.

The system operates in a protective atmosphere of inert gas such as nitrogen or argon. A wide range of materials are available to be processed, including but not limited to Al-Si-10Mg, CoCr superalloys, stainless steel, Ti-6Al-4V, Nickel-based alloys 625 and 718.

The resulting surface finish is higher with respect to the EBM process. However, the building rate is slower.

Heat treatment is required to decrease the thermal residual stresses or optimize the microstructure of the produced parts. In order to improve accuracy and surface finishing depending on the application, a post-processing (usually machining) is required.

Directed energy deposition AM

Directed Metal Deposition by means of laser beam is receiving increasing interest in the frame of AM to the purpose of maintenance, repair and overhaul of condemned products when severe conditions hindering the working order have been experienced. Minimal distortion, reduced heat-affected zones and better surface quality are benefited in comparison with conventional techniques.

Laser Powder Injection (Laser cladding)

In the technology of Laser cladding a powder is injected to provide the material to be deposited. A powder nozzle in combination with a laser beam is used to build or repair components consisting of single weld tracks. Side overlapping of the individual laser traces is required to process wider surfaces on 3D complex geometries.

The laser beam creates a melting pool on the surface part and the filler material is injected by a nozzle and melts as well. The solidification results in a metallurgical bonding to the base material.

Minimal distortion of the work-piece, reduced heat-affected zones and better surface quality are benefited in laser-aided DMD in comparison with conventional coating and repairing techniques such as arc welding or plasma spraying.

The laser powder injection approach is valuable because it can be used to add material to existing high-value parts for repairing and the powder material injected can be varied to fabricate compositionally graded parts.

The powder injection approach is not constrained to a confined volume as the powder bed systems are. Therefore, these systems can be used to process large parts.

Laser Metal Wire Deposition (LMWD)

This technique is capable of producing near-net shaped components by means of a laser beam as heat source and raw material as wire. During the process, gas shielding is required.

These techniques are similar to a conventional welding process and are well suited for manufacturing parts of high deposition rate and large volumes; however, the final product is limited by the inadequate geometrical accuracy and the surface roughness, so post-processing machining of the built part is required.

Other techniques

In addition to the these AM techniques, a range of other approaches are available, based on different types of energy inputs or materials. Among these, energy inputs can be provided by means of plasma arc welding equipment.

In this process, a device is used to generate plasma, either by direct current, alternating current or radio-frequency.

The electric arc is formed between the electrodes, then an input carrier or working gas is turned into plasma. Both wire and powder filler materials can be considered to deposit metals.

A plasma torch and positioning stage are manipulated by a robot or multi-axis controller and the path is pre-programmed. Powder is introduced both through the shielding gas and the orifice gas, and the plasma arc welding system provides the energy for melting.

Chapter_I

Investment casting process of turbine blade: redesign and manufacturing of mould by means of Direct Selective Laser Melting of metals

In the industrial field, significant progress has been achieved in the development and application of Additive Manufacturing (AM), offering advantages of design freedom of structure and a wide choice of materials compared with conventional manufacturing [1].

In the aerospace the manufacturing of turbine blade is challenging since these parts are crucial for an aero-engine. Due to the significant influence of the geometrical shape and dimension of the turbine blade on the performance of the engine, strict dimensional tolerances are given for the machining process of the turbine blade. An accurate and effective machining technology is essential for the fabrication of a turbine blade. Therefore, shell-mould investment casting is widely used [2].

At present, moulds are manufactured by means of machining via CAD/CAM technologies.

Traditional investment casting suffers from high tooling costs for producing wax patterns. As such, investment casting is prohibitively expensive for low volume production like prototyping, customized or specialized component productions. The lead-time may range between several weeks to months depending on scheduling and capabilities of the factory. Therefore a toolmaker has to evaluate different mould designs before committing to manufacturing, since design errors or iterations are usually expensive and time-consuming to be amended or accommodated. Both the shape and the dimensions of tools for moulds are usually extremely accurate and, consequently, very expensive.

In this frame, in contrast to conventional, subtractive manufacturing methods, AM is increasingly investigated. Based on an incremental layer-by-layer manufacturing, any part could be theoretically made [3]. Hence the development of AM provides new possibilities to integrate materials design, structure design, and functional design, to finally achieve a new strategy of design and fabrication. Direct Selective Laser Melting is one of the main methods for AM of metals: in this section, the importance of AM techniques

integrated with the investment casting process for various applications are highlighted.

1.1 Principles of Direct Selective Laser Melting

Direct Selective Laser Melting (DSL_M) is a laser powder based technology to build objects layer by layer using metallic powder and laser. This process is structured in the following phases:

- The idea is translated into a CAD model;
- The CAD file is generally converted into STL, being it a faceted version of the model surface;
- The part is sliced, each slice having a typical thickness of 20÷40 μm;
- Supporting structures may be required, therefore a proper position of the workpiece with respect to the building plate and the scanning path for each layer must be set;
- The object is created by selectively fusing layers of powder with a scanning laser beam.

During this process, the laser radiation is absorbed by the metal powder and heat is generated instantaneously in the powder layer, thus producing melting. Stresses are produced as a consequence of heating and melting; partial release is achieved when sintering the layers.

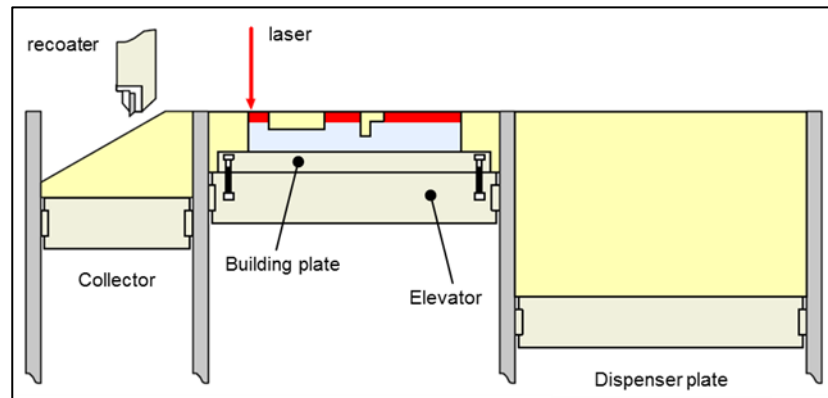


Figure 1.1: Powder bed AM process

To prevent oxidation and possible fire due to fine particles, the process is performed in closed inert chamber where inert gas atmosphere is continuously maintained so that the residual oxygen content is taken below 0.1%. Nitrogen or argon is fed into the chamber to prevent interactions of the metal powder with its environment and to protect the melt. The part and its possible supporting structures are manufactured in the same job, hence with the same material.

Investment casting process of turbine blade: redesign and manufacturing of mould by means of Direct Selective Laser Melting of metals

The powder is provided layer by layer by the recoater and a scanning head is used to deflect the laser beam.

Generally, at the end of the job, heat treatment is required to the purpose of reducing the thermal residual stresses or optimizing the microstructure of the produced parts. In order to achieve the high accuracy required for some parts or high quality surface finishing, a post-processing (usually machining) might be necessary.

The theoretical advantages of this technology are remarkable:

- tools are not required, so the issue of tool wear is prevented;
- the process is capable of manufacturing parts of complex geometry based on 3D CAD;
- delivery time is reduced at pre-design stage;
- good mechanical properties of the final part.

A number of applications of DSLM are currently considered: fabrication of inserts, injection and die casting moulds for series production and direct manufacturing of metal prototypes. This technique also offers great potential for mass customization, e.g., the fabrication of prostheses and implants for the biomedical industry.

1.2 Investment casting process

Investment casting (also known as ‘lost wax casting’ or ‘precision casting’) has been a widely used process for centuries. It is known for its ability to produce components of excellent surface finish, dimensional accuracy and complex shapes. It is especially useful for making castings of complex and near-net shape geometry, where machining may not be possible or too wasteful. It is also considered to be the most ancient process of making art castings. Technological advances have also made it to be the most modern and versatile one among all the metal casting processes.

In the field of aerospace technology, turbine blade is one of the critical components of aero-engine. Due to the significant influence of the geometrical shape and dimension of the turbine blade on the performance of engine, close dimensional tolerances are specified for the machining process of the turbine blade. The accurate and effective machining technology is essential for the machining of turbine blade. To do this, the shell-mould investment casting is widely used [2]. An appropriate die profile, which takes into account of the various shrinkages involved in casting process, is important for enhancing the quality of net-shaped products. Due to the shrinkages of the wax and solidifying alloy material, the geometrical size of the part produced by the investment casting process is smaller than that by the die cavity. In order to ensure the dimension accuracy, the position accuracy and the surface roughness, the wax pattern die profile design for turbine blade needs to consider the compensation of shrinkages brought by the solidification process.

Due to the complex, time-consuming and expensive process of investment casting, traditional methods for designing die profile assume constant shrinkage rate.

Properties and considerations of manufacturing by investment casting:

- Investment casting is a manufacturing process that allows the casting of extremely complex parts, with good surface finish;
- Very thin sections can be produced by this process. Metal castings with sections as narrow as .015 in (.4 mm) have been manufactured using investment casting;
- Investment casting also allows for high dimensional accuracy. Tolerances as low as .003 in (.076 mm) have been claimed;
- Practically any metal can be investment cast. Parts manufactured by this process are generally small, but parts weighing up to 75 lbs (34 kg) have been found suitable for this technique;
- Parts of the investment process may be automated;
- Investment casting is a complicated process and is relatively expensive.

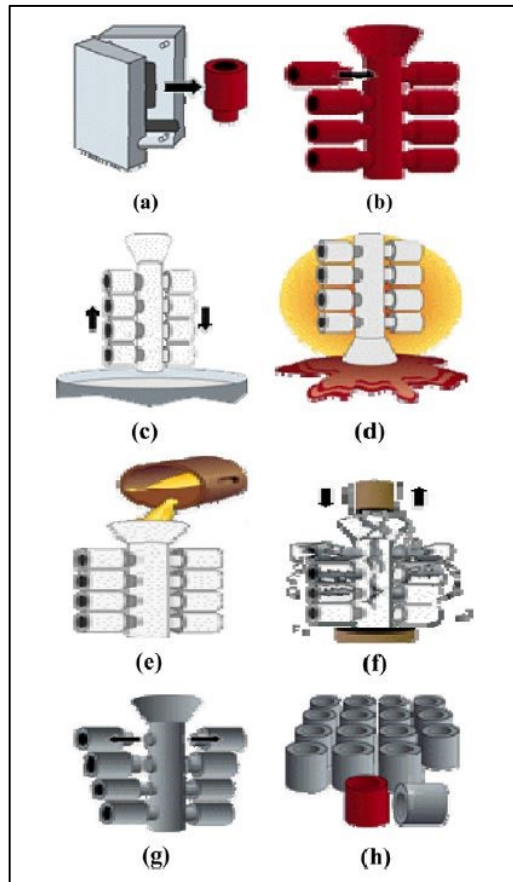
Consequently the investment casting process has increasingly been used to produce components for the aerospace industry and it has been particularly successful for the production of single crystal turbine blades.

1.2.1 The process

The first step in investment casting is to manufacture the wax pattern for the process. The pattern for this process may also be made from plastic; however it is often made of wax since it will melt out easily and wax can be reused.

Since the pattern is destroyed in the process, one will be needed for each casting to be made. When a lot of parts are produced, a mould for manufacturing patterns is needed.

The mould to create wax patterns may be cast or machined. The size of this master die must be carefully calculated. It must take into consideration shrinkage of wax, shrinkage of the ceramic material invested over the wax pattern and shrinkage of the metal casting. It may take some trial and error to get just the right size, therefore these moulds can be expensive.



Basic steps involved in ceramic shell investment casting:

(a) pattern production,

(b) pattern assembly,

(c) investment,

(d) dewaxing,

(e) casting,

(f) knock-out,

(g) cutoff,

(h) finishing and inspection

(Kalpakjian and Schmid, 2008).

Figure 1.2: Basic steps involved in ceramic shell investment casting

Often many wax patterns may be connected and poured together producing many castings in a single process. This is done by attaching the wax patterns to a wax bar, the bar serves as a central sprue. This arrangement is called a tree, denoting the similarity of casting patterns on the central runner beam to branches on a tree.

The metal casting pattern is then dipped in a refractory slurry whose composition includes extremely fine grained silica, water and binders. A ceramic layer is obtained over the surface of the pattern. The pattern is then repeatedly dipped into the slurry to increase the thickness of the ceramic coat. In some cases the pattern may be placed in a flask and the ceramic slurry poured over it.

Once the refractory coat over the pattern is thick enough, it is allowed to dry in air in order to harden.

The next step in this manufacturing process is the key to investment casting. The hardened ceramic mould is turned upside down and heated to a temperature of around 200F - 375F (90°C - 175 °C). This causes the wax to

Investment casting process of turbine blade: redesign and manufacturing of mould by means of Direct Selective Laser Melting of metals

flow out of the mould, leaving the cavity for the metal casting. The ceramic mould is then heated to around 1000F-2000F (550°C -1100°C). This will further strengthen the mould, eliminate any leftover wax or contaminants and drive out water from the mould material. The metal casting is then poured while the mould is still hot. Pouring the casting while the mould is hot allows the liquid metal to flow easily through the mould cavity, filling detailed and thin sections. Pouring the metal casting in a hot mould also gives better dimensional accuracy, since the mould and casting will shrink together as they cool. After pouring of the molten metal into the mould, the casting is allowed to set as the solidification process takes place. The final step in this manufacturing process involves breaking the ceramic mould from the investment casting and cutting the parts from the tree.

1.3 Experimental setup

The machine used for the experimental plan is an EOSINT M270 dual mode, including a laser unit, a control computer, a building chamber, a powder dispenser and a wiper blade. An ytterbium-fibre laser of 200 W, with a wavelength of 1.08 μm is used (implying high absorption of the laser radiation in the metal and good melting efficiency). The laser system uses a “dual focus” technology as a compromise to achieve resolution of details, reliable part density and high mechanical properties. Indeed, the spot size can be changed between 0.1÷0.5 mm. Namely:

- A shorter spot size is used to generate high definition “skin”, thus offering higher density, better surface quality and hardness;
- A larger spot size is used for “core” areas in order to reduce the building time and residual inner stresses, so to obtain uniform mechanical properties.

Laser is guided through the optical fibre and focuses onto the powder bed. To prevent oxidation during melting and explosions because of thin powders, the process is performed in a chamber filled with nitrogen or argon gas which reduces the initial oxygen to 0.8%. In order to foster the junction between parts and building platform, which are usually made of the same or similar metal to be processed, and to reduce distortions the second one is heated and melting process starts when plate reaches 80 °C.

CAD data are downloaded, and then slicing is done on the workstation through EOS RP-Tools software. Multiple parts can be build in a single run on the steel base plate.



Figure 1.3: EOSINT M270

Investment casting process of turbine blade: redesign and manufacturing of mould by means of Direct Selective Laser Melting of metals

Table 1.1: Technical data EOS M270 (source: EOS)

Effective buiding volume (including building platform)	250 mm x 250 mm x 215 mm
Building speed (material-dependent)	2 – 20 mm ³ /s
Layer thickness (material-dependent)	20 – 100 μm
Laser type	Yb – fibre laser, 200 W
Precision optics	F–theta – lens, high – speed scanner
Scan speed	up to 7.0 m/s
Variable focus diameter	100 – 500 μm
Current supply	32 A
Maximum power consumption	5.5 kW
Nitrogen generator	standard
Compressed air supply	7000 hPa; 20 m ³ /h
Dimensions (B x D x H)	
System	2000 mm x 1050 mm x 1940 mm
Recommended installation space	approx.. 3.5 m x 3.6 m x 2.5 m
Weight	approx.. 1130 kg

Higher precision is benefited with respect to additive manufacturing via electron beam; engineering tolerances are in the order of tenths of millimeters, that is with maximum deviation in the order of 0.2% when processing parts whose dimensions are comparable to the building chamber; deviation is lower for smaller parts.

1.3.1 AM powder features

Pre-alloyed, argon gas atomized virgin commercial EOS GP1 stainless steel powder, 20 μm mean grain size, corresponding to standard UNSS17400 chromium-copper precipitation hardening steel in terms of nominal chemical composition (Table 1.2) has been considered.

This kind of steel is characterized by having good corrosion resistance and mechanical properties, especially excellent ductility in laser processed state, and is widely used in a variety of engineering applications.

This material is ideal for many part-building applications (DirectPart) such as functional metal prototypes, small series products, individualised products or spare parts. Standard processing parameters use full melting of the entire geometry with 20 μm layer thickness, but it is also possible to use Skin & Core building style to increase the build speed. Using standard parameters the mechanical properties are fairly uniform in all directions.

Parts made from EOS StainlessSteel GP1 can be machined, spark-eroded, welded, micro shot-peened, polished and coated if required. Unexposed powder can be reused.

Typical applications are:

- engineering applications including functional prototypes, small series products, individualized products or spare parts;
- parts requiring high corrosion resistance, sterilisability, etc;
- parts requiring particularly high toughness and ductility.

Table 1.2: Nominal composition (wt. %) of the powder; single values to be intended as maximum

Cr	Ni	Cu	Mn	Si	Mo	Nb	C	Fe
15.0÷17.5	3÷5	3÷5	1	1	0.5	0.15÷0.45	0.07	balanced

The powders have been produced by argon gas atomization. Compared with the process of atomization in water, regular spherical shape is achieved. Electron microscopy has been performed to check the shape (Figure 1.4) and size distribution (Figure 1.5) of the virgin powder.

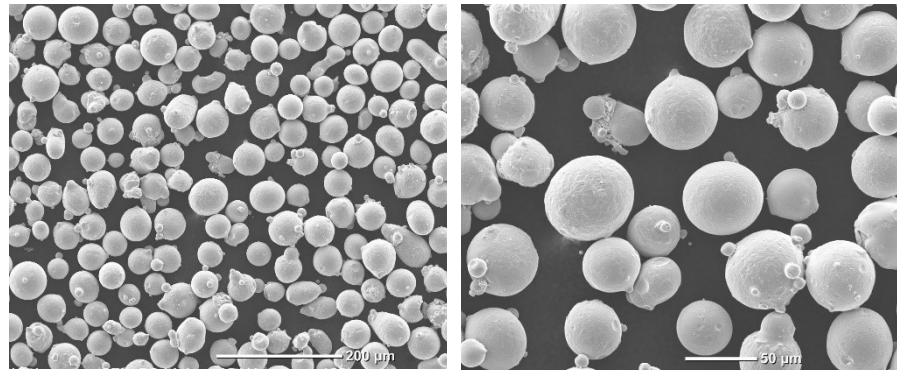


Figure 1.4: EOS GP1 electron microscopy powder particles morphology

Namely, the shape is found to be spherical and regular; as regarding the size, dimensions are consistent with the expected range.

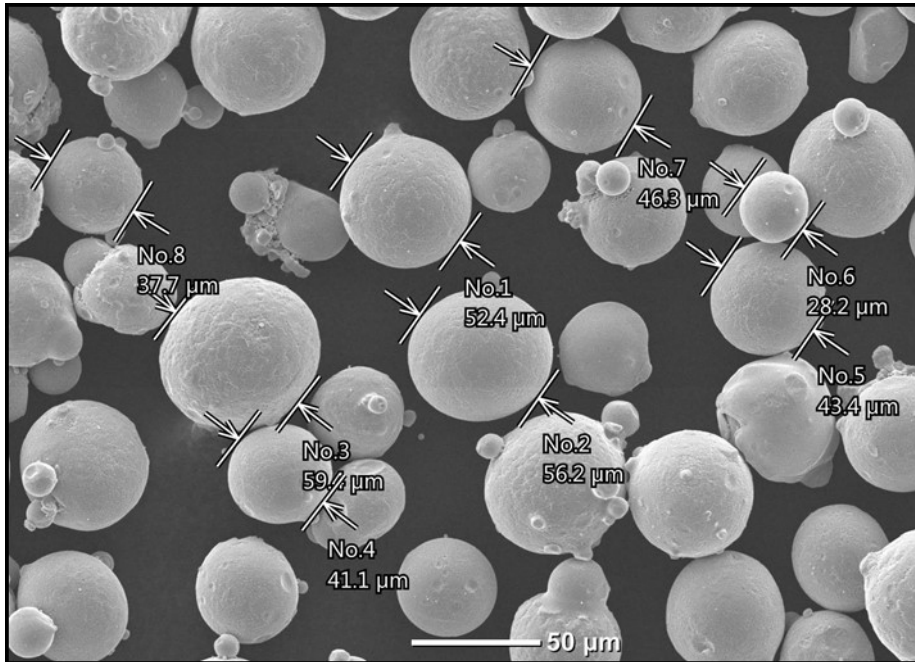


Figure 1.5: EOS GP1 powder particles size.

Furthermore, the virgin powder and some test samples have been investigated via aeral and punctual EDS inspections. The acquired spectra and the chemical compositions have been compared (Figure 1.6, Table 1.3). An average overall fitting coefficient of the quantitative analysis (i.e., the residual between the acquired and the synthetic spectra) of 0.89% and 0.78% resulted for the powder and the samples, respectively. At first, the EOS GP1 data sheet is matched in terms of nominal chemical composition; certain elements below 1% wt. have not been detected. Random transverse and longitudinal cross-sections of the samples have been considered; based on these, one may infer the referred nominal chemical composition has been taken during processing.

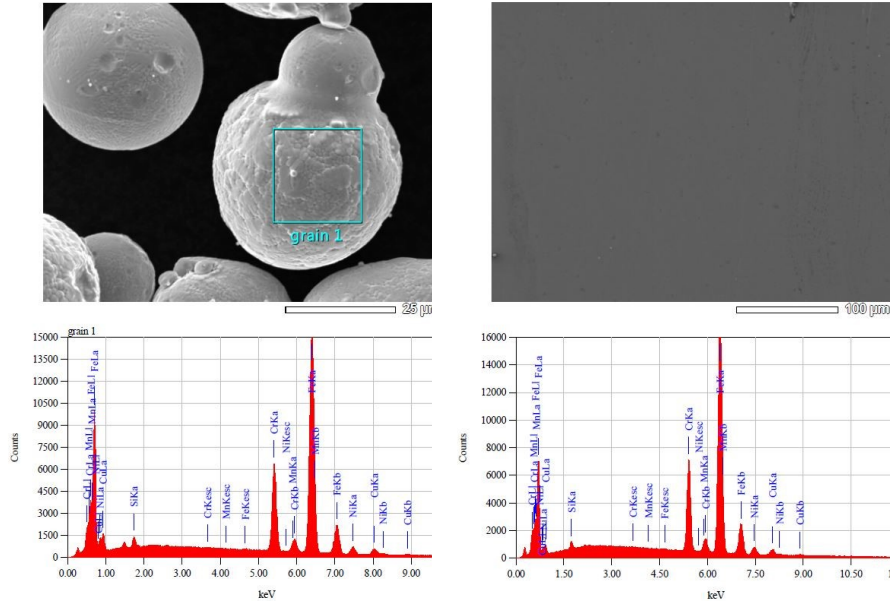


Figure 1.6: Examples of acquired EDS spectra for powder and samples, respectively

Table 1.3: EDS inspections, average chemical composition (wt.%) of powder and samples

	Fe	Cr	Ni	Cu	Mn	Si	Mo	Nb	C
Powder	72.70	16.75	4.46	4.87	0.33	0.90	-	-	-
Std. dev.	0.14	0.06	0.06	0.07	0.03	0.02	-	-	-
Samples	73.61	16.32	4.42	4.43	0.61	0.62	-	-	-
Std. dev.	0.13	0.06	0.05	0.07	0.03	0.02	-	-	-
Eos GP1	Bal.	15-17.5	3-5	3-5	max 1	max 1	max 0.5	0.15-0.45	0.07

Uniform fusion has been experienced in the samples (Figure 1.7), as proven by EDS mapping of the main alloying elements.

Investment casting process of turbine blade: redesign and manufacturing of mould by means of Direct Selective Laser Melting of metals

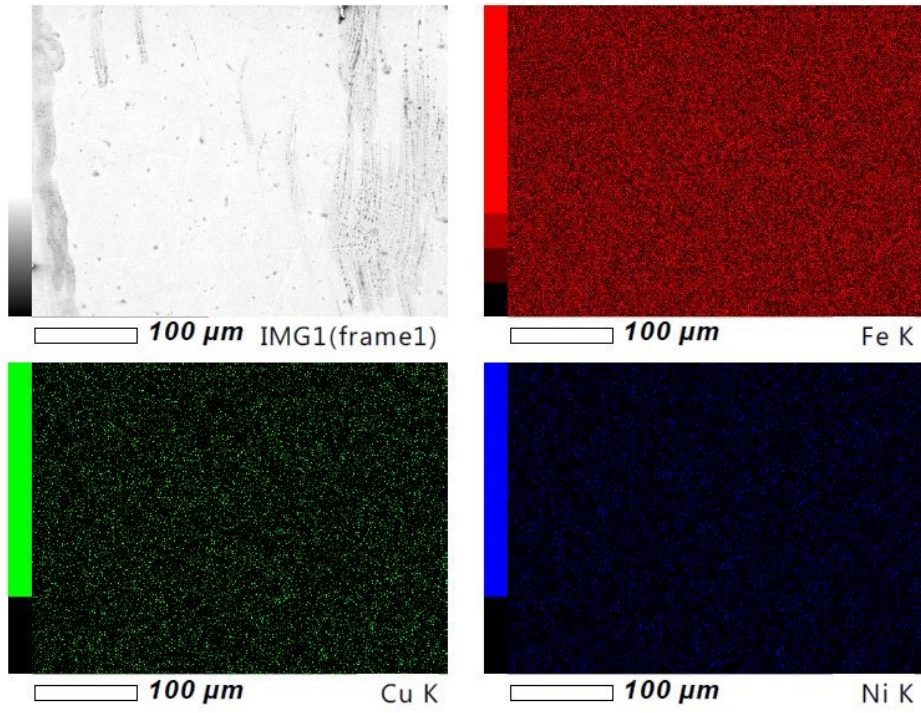


Figure 1.7: Examples of acquired EDS mapping for samples

1.4 Design and manufacturing of mould

The investment casting process has been increasingly used to produce components for the aerospace industry and it has been particularly successful for the production of single crystal turbine blades. When producing parts in any quantity, a mould from which to manufacture patterns is required. Today the mould to create wax patterns is usually made by means of machining.

Conventional manufacturing methods, such as turning and milling, may limit possible geometries of the final assembly. These limitations often result in structures that are inefficient, as many areas of a component have specific allowance that cannot be removed physically or via economically viable operations; indeed, conventional methods such as electrical discharge machining are employed.

The use of Additive Manufacturing process in the production of mould, improves current casting quality (optimize the cooling system), reduces manufacturing costs and explores new markets in order to remain competitive [4, 5]. In addition new features can be accomplished reducing the total number of parts of the assembly.

The aim of the present study is the development of a framework for redesigning existing components in order to exploit the benefits of AM [6,7]. This has been tested and validated through the redesign of an actual component, currently designed to be manufactured using conventional techniques. The objectives were to present a reduction of lead time and to preserve the overall mechanical and thermal features of the parts, so to bear with the shock loads.

1.4.1 First case study

Two different steel moulds have been evaluated. The first model is composed of two parts and three tool insert. The latter are required to be machined to achieve complex geometry.

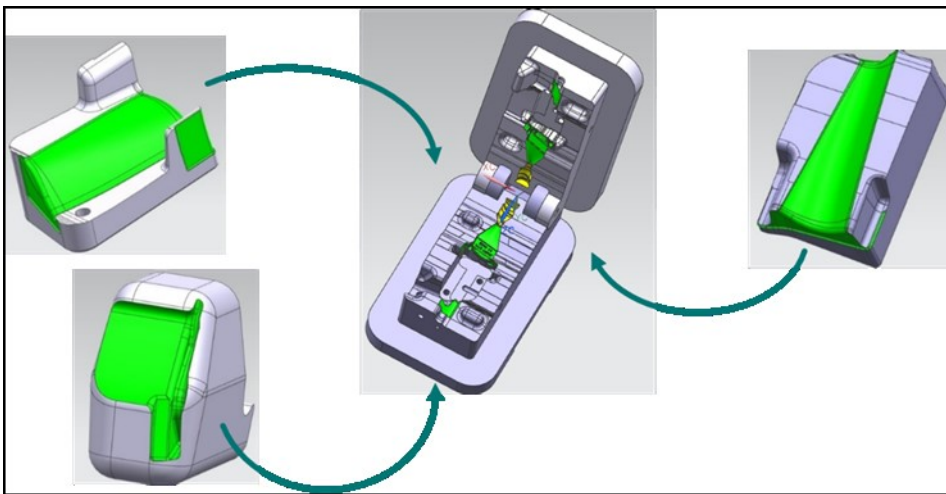


Figure 1.8: first model of mould

First of all a redesign of the mould has been implemented. The kind of redesign has been made taking into account the major feature of additive manufacturing that is the possibility to manufacture regardless the complexity of component geometry to be fabricated.

The redesign consist of the following stages:

- The part is build directly on the construction platform;
- Tool inserts are integrated in the mould;
- Only mould core is manufactured to simplify the job.

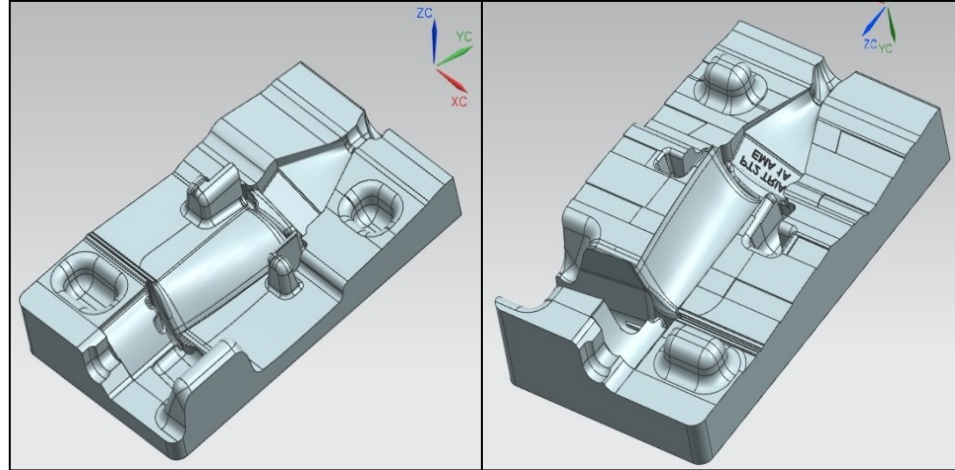


Figure 1.9:redesign of mould

1.4.2 AM production

An EOSINT M270 commercial laser melting system (EOS, Krailling, Germany) has been used to manufacture a job.

Processing power, speed, layer thickness, and hatching strategies are based on preliminary trials aimed to optimize the process and full dense structure (Table 1.4); a nitrogen inert atmosphere has been arranged.

Table 1.4: Main features and processing parameters in selective laser melting of stainless steel powder

Gain medium	Fibre, Yb:YAG
Operating laser power [W]	195
Linear processing speed [mm·s⁻¹]	1
Hatch spacing [mm]	0.10
Layer thickness [μm]	20
Focused spot diameter [μm]	90

Before performing the building job, proper corrective factors must be evaluated by means of a test-job to measure the effective processing diameter and take into account possible dimensional shrinkage.

Investment casting process of turbine blade: redesign and manufacturing of mould by means of Direct Selective Laser Melting of metals

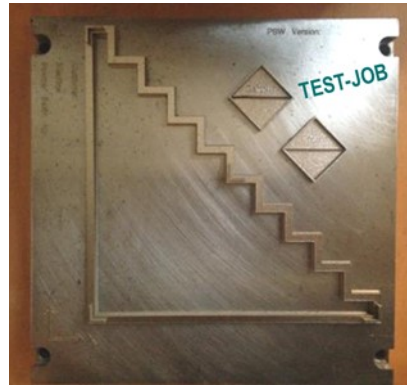
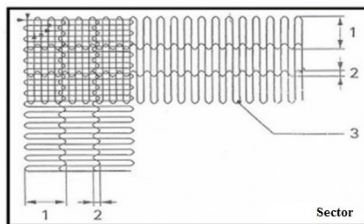


Figure 1.10: test job for calibration machine

Moreover, a proper scanning strategy has been arranged. Namely, each layer is scanned in stripes and sectors: the section is subdivided into areas, each of them is scanned by the laser with side-to-side stripes.



- 1) stripes width
- 2) stripes overlapping
- 3) laser center trajectory

Figure 1.11: scanning strategy

Based on the test-job and the scanning strategy, the dimensional accuracy of the components is expected to result in the order of tenths of a millimeter. The AM process has been performed, improper surface roughness resulted, therefore post-processing steps has been required.

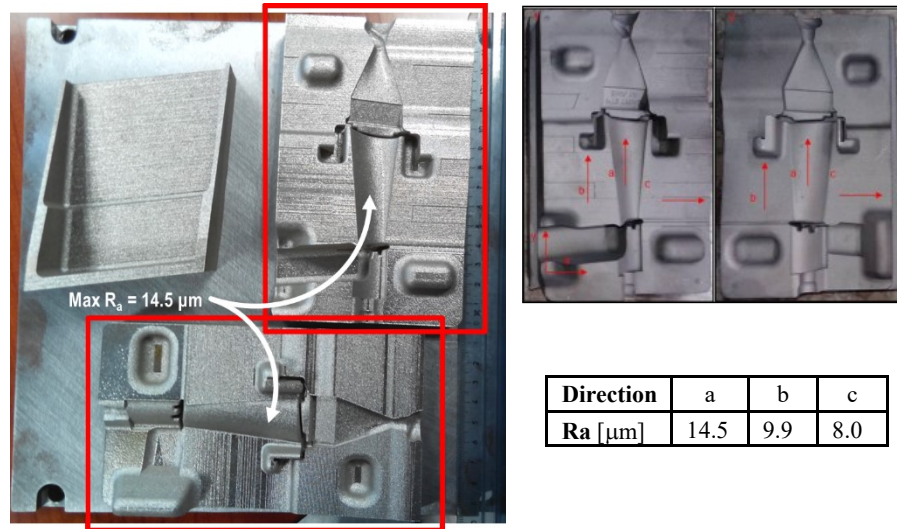


Figure 1.12: mould after production and measure of roughness

The first step is a post-process stress-relieving at 650 °C for 1 hour. After stress-relieving, a dimensional analysis with the optical scanner ATOS 3D scanner GOM has been performed. The resulting deviation is in the order of tenths of millimeter, as a consequence of buckling of the building plate.

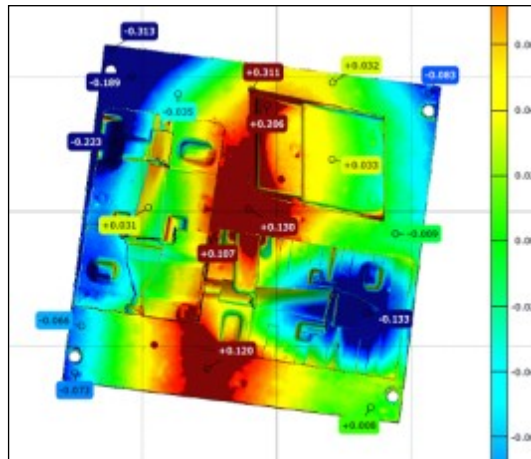


Figure 1.13: dimensional analysis with the optical scanner

The second step is shot-peening process of the surface to improve the surface quality. Therefore, in order to prepare the mould for wax injections, the surface roughness has been reduced. Shot-peening has been performed using the following parameters.

Investment casting process of turbine blade: redesign and manufacturing of mould by means of Direct Selective Laser Melting of metals

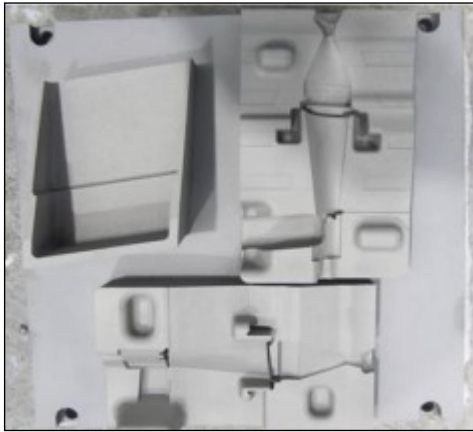


Figure 1.14: job after sand blasting

Table 1.5: Shot peening parameters

Pressure	80 psi
Sand	Washington mills
Composition	Aluminum oxide
Granulometry	120/220 Mesh
Time	4 min
Distance	5 cm

The treatment of shot peening reduced the roughness to an average value of $5.6 \mu\text{m}$ with a standard deviation of $1.75 \mu\text{m}$.

The third step has been wire cutting via Electrical Discharge Machining (EDM) to cut the parts from the building plate.

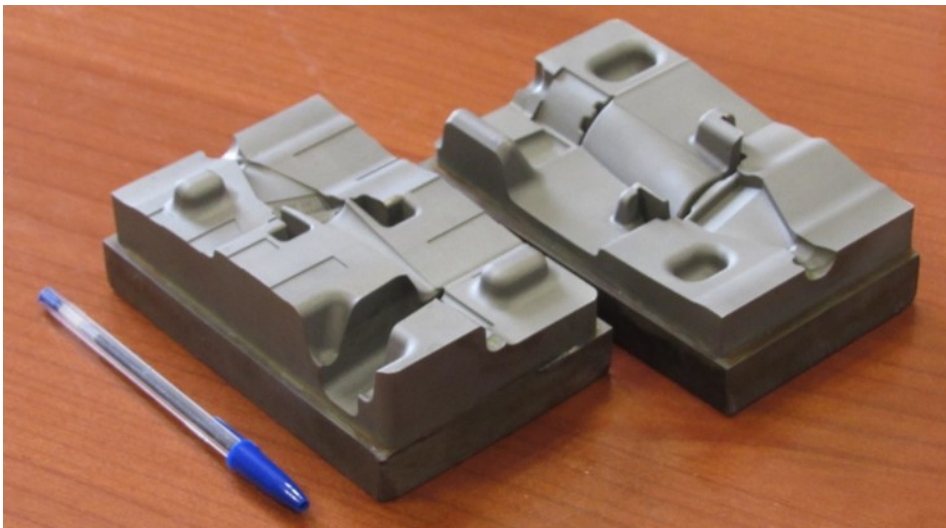


Figure 1.15: final configuration mould

Subsequently a series of non-destructive test have been carried out, such as 3D measurements by means of a laser scanner and x-ray inspection.

First of all scanning by means of laser metrology has been performed to assess the geometry; the mismatch with respect to the intended original CAD file has been measured. Deviations in the order of hundredths of millimeter

have been found for the surface reproducing the airfoil of the turbine blade. The results are shown in Figure 1.16.

Based on X-ray inspections using a General Electric CRx flex CR scanner, all of the moulds have been found to be defect-free, as no indications have been shown in Figure 1.17.

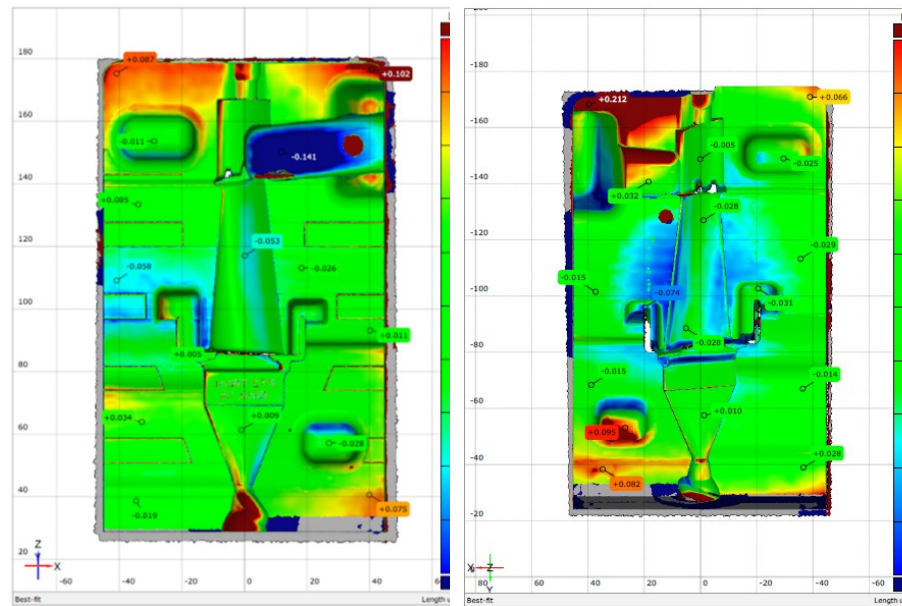


Figure 1.16: dimensional analysis with the optical scanner

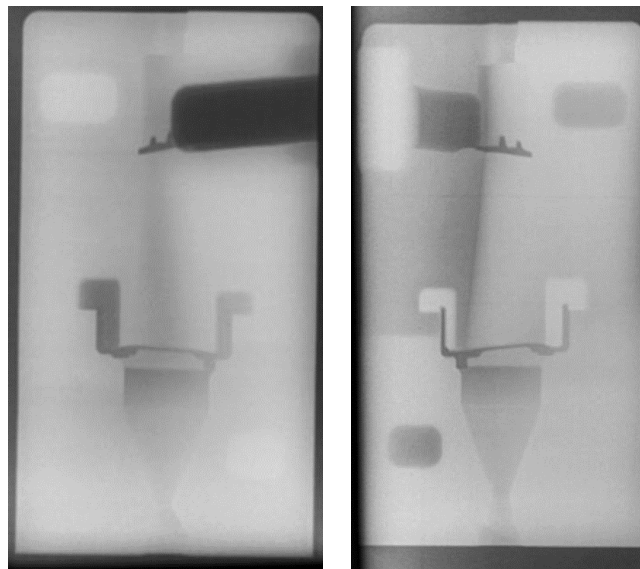


Figure 1.17: X-ray inspections

1.4.3 Pattern preparation

The pattern in investment casting has the exact geometry of the required final cast part but with dimensional allowances to compensate its own volumetric shrinkage as well as the solidification shrinkage of the cast metal in the ceramic mould. Wax, plastic or polystyrene are the common pattern materials among which wax is most widely used.

For the mould in question a pattern wax has been used. The wax have the following characteristics:

- It should have the lowest possible thermal expansion so that it can form a shape with highest dimensional accuracy;
- Its melting point should not be higher than the ambient temperature so that distortion of thick sections and surface cavitations can be prevented;
- It should be resistant to breakage, i.e. it is of sufficient strength and hard enough at room temperature so that it can be handled without damage;
- It should have a smooth and wettable surface so that a finished cast part with a smooth surface can be obtained;
- It should have a low viscosity when melted to fill the thinnest sections of the die;
- It should be released from the die easily after formation;
- It should have very low ash content so that it does not leave any ash inside the ceramic shell;
- It should be environmentally safe, i.e. does not lead to the formation of environmentally hazardous or carcinogenic materials upon combustion.

Costs, availability, easy of recycling, toxicity, etc., are the other important factors while selecting a pattern wax. The working efficiency of investment casting can be increased by improving one or more characteristics of the wax, by mixing additives, blending with different waxes and varying the process parameters.

Finally a pattern of desired shape, has been produced by injecting molten wax into the AM-made mould. Then wax has been assembled to form a cluster to be casted to form the blades.

The result is shown in Figure 1.18. It is worth noting that the first injected pattern (first from left) is incomplete since the mould was improperly polished.



Figure 1.18: wax blades built to test the mould

After casting, the ceramic shell is removed through mechanical methods to obtain the alloy blades. Roughness measures have been carried out on cast alloy blades in the longitudinal and transverse directions. The roughness is found to be higher with respect to the allowed standard.

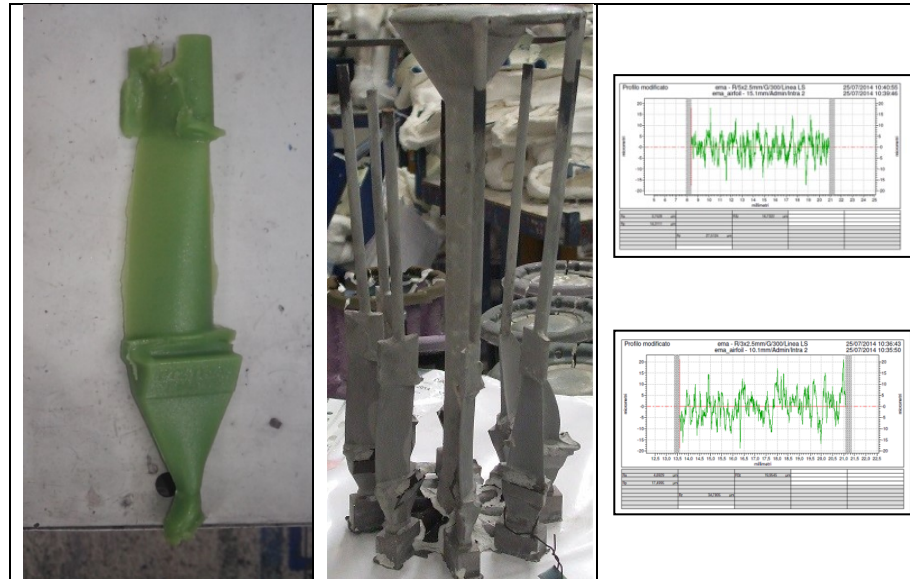


Figure 1.19: turbine blade casting with AM mould (longitudinal and transverse profile, respectively)

1.4.4 Second case study

As second case study, a more complex mould consisting of 5 components has been considered. In this model the mould is decomposable to allow removal of the wax blade. The overall external dimensions are 250 mm × 60 mm × 65 mm.

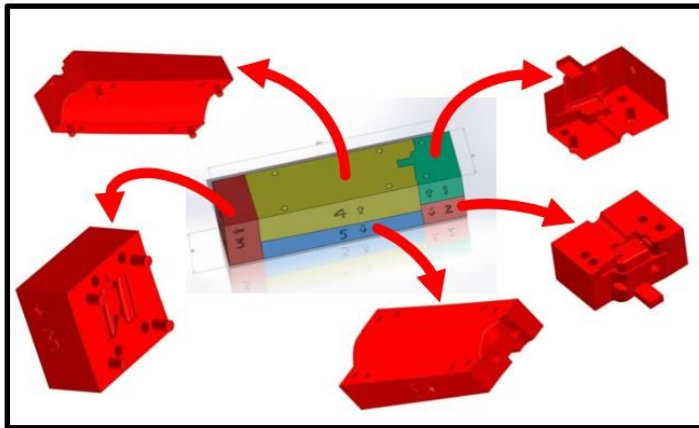


Figure 1.20: second model of mould

Redesign for manufacturing is required to allow the fabrication via AM. Therefore, the following changes have been made to the original model:

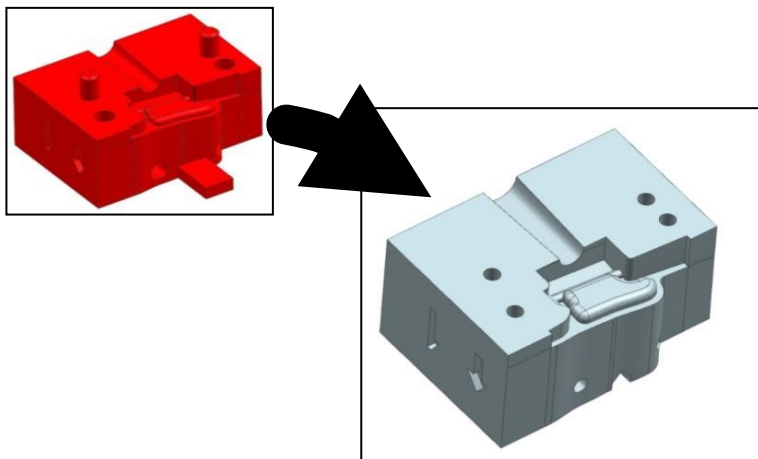


Figure 1.21: redesign of a component of mould

- Reduction of the diameter of the plug holes from 6.5 mm to 4 mm; since an optimal surface roughness is not possible in AM, machining is required, hence the nominal dimensions are restored afterwards;
- Replacement of the centering pins by holes for subsequent plug insertion;
- Reduction from 2 mm to 0.1 mm of the depth of the component mark, so as not to apply internal supporting structures;
- Addition of 1 mm thickness allowance at the bottom of the part so to allow detaching of the component from the buildingn plate via wire EDM;
- Replacement of the centering block by a suitable geometric groove of proper shape and angle to prevent supporting during building.

The application of the re-engineering criteria on the five components determines the variations shown in the Figure 1.22 obtained overlapping the original configurations and redesigned configurations.

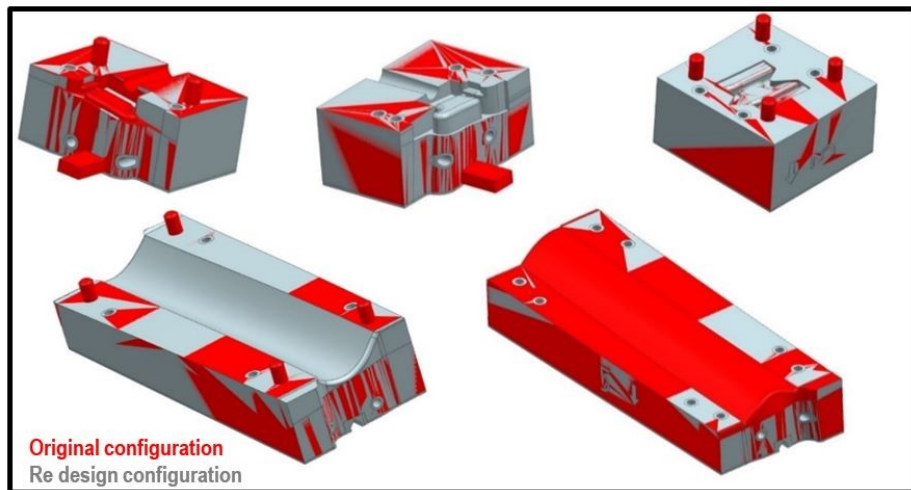


Figure 1.22: overlapping the original configurations and redesigned

Mould elements are made in three separate job, using the same methodology and material as the previous mould. The components were arranged as shown in the Figure 1.23 to reduce deformations of buiding plate caused by material retraction.

Investment casting process of turbine blade: redesign and manufacturing of mould by means of Direct Selective Laser Melting of metals

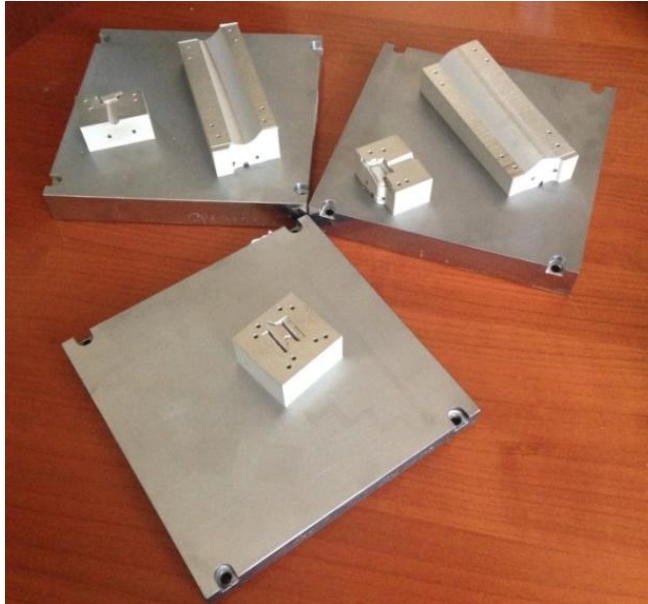


Figure 1.23: moulds fabricated with AM on the construction plate

After fabrication, post processing must be performed, consisting in the following steps:

1. Heat treatment for stress relieving (650 ° C for one hour, in argon inert chamber)
2. Wire cutting by EDM to remove components from the building plate
3. Sandblasting
4. Mechanical machining to allow mechanical coupling of the moulds.

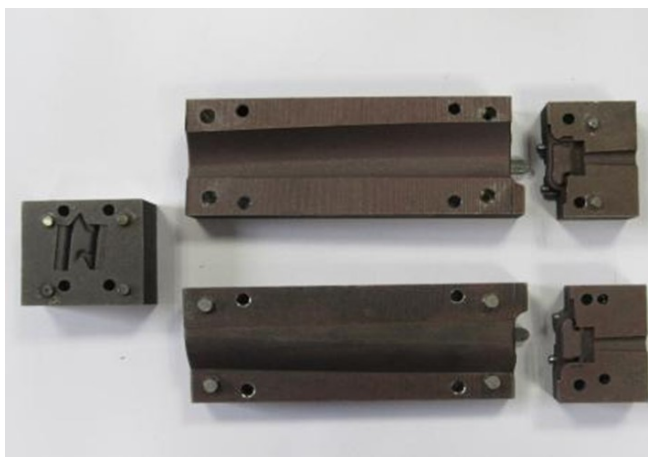


Figure 1.24: parts of the mould fabricated with AM

As mentioned above the main problem is the surface roughness of the component built. The first step was to perform roughness measurements on the aerofoil. The following table shows the values measured in orthogonal directions, i.e., horizontal (H) and vertical (V).

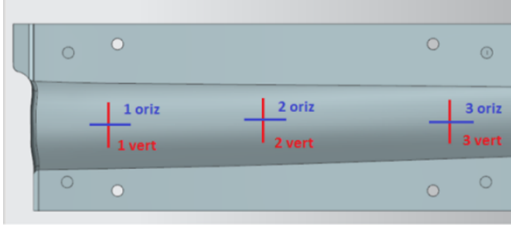
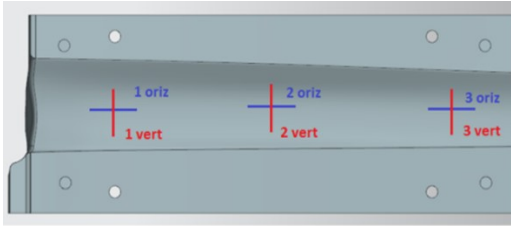
	Ra [μm]	Rz [μm]
	1 H 12.2	75.7
	1 V 10.4	54.6
	2 H 14.1	84.4
	2 V 8.2	46.7
	3 H 13.9	81.3
	3 V 13.3	72.3
	Ra [μm]	Rz [μm]
	1 H 11.6	74.3
	1 V 10.6	54.2
	2 H 11.8	76.0
	2 V 13.2	66.5
	3 H 13.5	86.8
	3 V 9.3	49.7

Figure 1.25: roughness measurements on the aerofoil

After AM fabrication, without additional machining, the average roughness is around $12 \mu\text{m}$, which is still high for the application of the investment casting. Therefore, sandblasting has been conducted as for the first case study, thus improving the overall surface finish, with resulting reduced roughness in a measure of 50%, approximately.

Subsequently, in order to clean the mould from residuals of sandblasting, the moulds have been treated by ultrasonic washing. The cycle has been performed for a period of 10 minutes into water with proper cleaning agent. The surface of the mould after the treatments appeared under the following conditions with improved roughness.

Investment casting process of turbine blade: redesign and manufacturing of mould by means of Direct Selective Laser Melting of metals

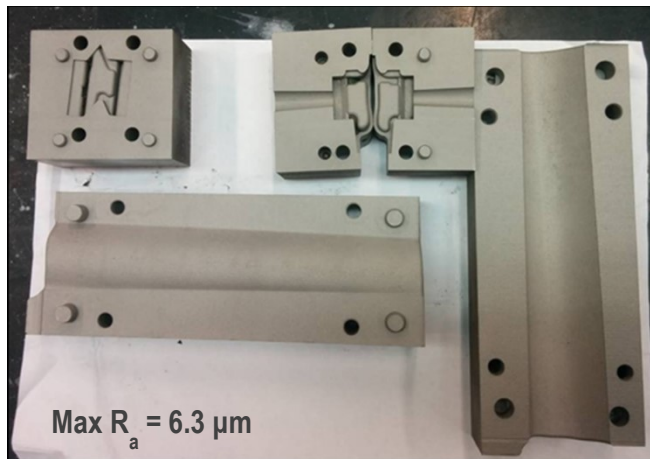


Figure 1.26: mould after sandblasting and ultrasonic washing

Based on the test-job and the processing strategy, tolerances are expected again to match the tenths of a millimeter. A DEA Global Image Clima Coordinate Measuring Machine (CMM) has been employed to check these.

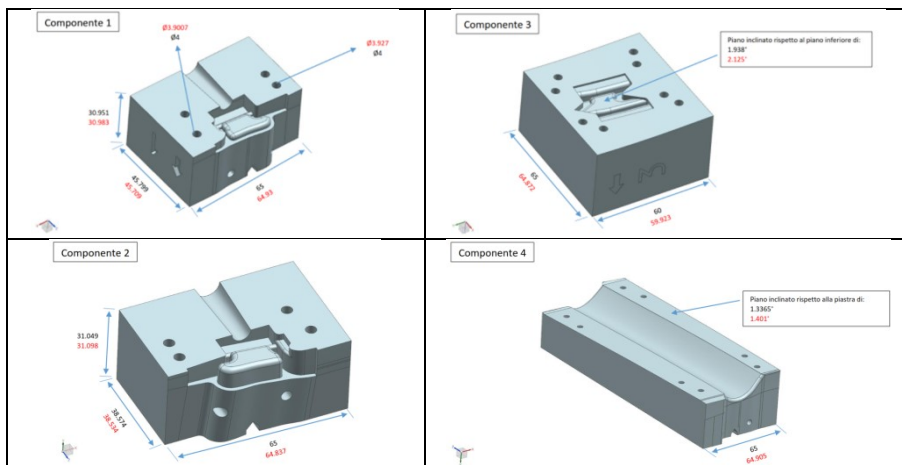


Figure 1.27: measurements detected by a CMM machine

Based on X-ray inspections, all of the mould have been found to be sound and defect-free, as no indications have been shown in Figure 1.28.

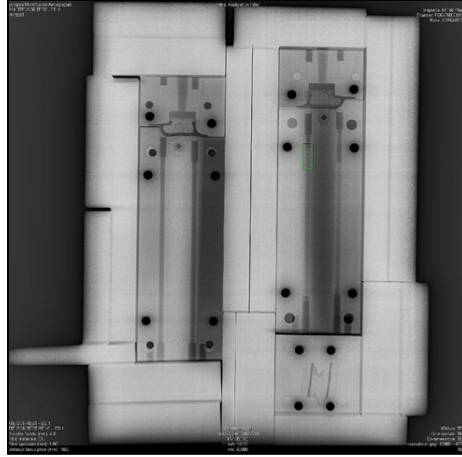


Figure 1.28: X-ray inspections

1.4.5 Pattern analysis

Castings with wax have been made to test the mould. After sand blasting the mould, an improvement in the injections has been noticed, both in terms of surface quality and in terms of extraction of the wax blades from the mould (i.e., the blades were intact).



Figure 1.29: wax blades casting with AM mould

Roughness analysis has been conducted on wax blades. Roughness values higher than the standard (1.6 μm) have been found.

Two measurements of roughness have been made on each sample as shown in the following table.

Investment casting process of turbine blade: redesign and manufacturing of mould by means of Direct Selective Laser Melting of metals

Table 1.6: roughness performed on wax blades

Sample	Ra(μm)
1	4.72
	4.96
2	6.04
	5.59
3	6.62
	4.40

1.5 Cost and time analysis for mould AM construction

In the field of AM of metals, the purchase of the machine is the main cost. Indeed, the energy cost only contributes to minor level. Also simultaneous building of parts in the working chamber, rather than building a single part at a time, resulted in massive cost reduction. So it has become evident that in order to minimize the overall cost of the part, significant care must be taken to reduce the building time. It has been even proved that simultaneous building of an optimum number of parts is crucial to reduce time consumption.

In this case study, mould components have been produced in three jobs because the manufacturing of many parts in the same job would result in severe deformation during building. In the following table, the times and costs of each job are given.

*Job 1**Job 2**Job 3*

<u>Time scheme [hours]</u>	<i>Job 1</i>	<i>Job 2</i>	<i>Job 3</i>
Redesign	3	3	1.5
Additive manufacture	75	78	30
Preparation job and cleaning machine	3	3	2.5
Heat treatment	16	16	16
	97	100	50
<u>Cost scheme [€]</u>	<i>Job 1</i>	<i>Job 2</i>	<i>Job 3</i>
Material	300	300	120
Machine	2150	2250	850
Labour	405	405	250
Heat treatment	220	220	220
	3075	3175	1440

Table 1.7: time and cost for AM production of mould

Investment casting process of turbine blade: redesign and manufacturing of mould by means of Direct Selective Laser Melting of metals

It is worth noting that the longest time is the time for manufacturing; the higher cost is the cost of the machine. In detail, the cost of the manufacturing are given in Table 1.8.

Table 1.8: Detail of cost items

Material	Powder 70 €/kg	Construction plate 5 €/job		
Machine	Energy	Inert gas 0.8 €/hour	Filter 1.2 €/ hour	Depreciation
Labour	Redesign	Job design	Preparation and cleaning machine	
Heat treatment	Energy	Inert gas 0.8 €/ hour		

The partial cost of the whole mould is **7690,00 €**. The cost of the mechanical machining to obtain the required tolerances must be considered as well.

Table 1.9: Times and costs for post-process mechanical machining

<u>Time scheme [hours]</u>	<i>Job 1, 2, 3</i>
Component removal with wire EDM	63
Sandblasting	2
Hole finishing	7
Plate grinding	3
	75
<u>Cost scheme [€]</u>	<i>Job 1, 2, 3</i>
Component removal with wire EDM	3200
Sandblasting	150
Hole finishing	360
Plate grinding	100
	3810

Wire EDM to remove the parts from the buiding parts results in a significant effect of the overall price of the finishing.

As a consequence of this the total cost of the mould made by additive manufacturing is 11.500 €.

1.6 Conclusions

Fabrication of moulds by means of AM tecnique is possible, but the related costs are still high [5, 8]. However, it should be noted that the costs are evaluated in the assumption of prototyping activity, in fact similar moulds made with traditional techniques would present a comparable or even lower cost. With the development of these technologies and with the reduction in the cost of machinery and raw materials, great benefits in terms of time and cost of production would result.

In addition, conformal cooling channels could be considered [9, 10], as shown in the Figure 1.30, to increase mould productivity with the control of mould temperature and part dimensions.

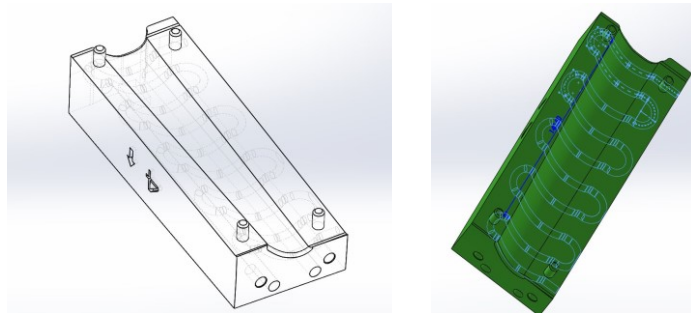


Figure 1.30: design of cooling channels conformal for thermal control of mould

References chapter I

- 1) Dirk Herzog, Vanessa Seyda, Eric Wycisk, Claus Emmelmann, « Additive manufacturing of metals, 2016 Acta Materialia Inc. Published by Elsevier Ltd.».
- 2) S. Jones, C. Yuan, «Advances in shell moulding for investment casting, Journal of Materials Processing Technology 135 (2003) 258–265».
- 3) Sunpreet Singha, Seeram Ramakrishnab, Rupinder Singhc, « Material issues in additive manufacturing: A review, Journal of Manufacturing Processes,2016».
- 4) Konstantinos Salonitis, Saeed Al Zarban, « Redesign Optimization for Manufacturing Using Additive Layer Techniques, Procedia CIRP 36 (2015) 193 – 198»
- 5) Heidi Piili, Ari Happonenb, Tapio Väistöc, Vijaikrishnan Venkataramanana, Jouni Partanend, Antti Salminenena, « Cost Estimation of Laser Additive Manufacturing of Stainless Steel, Physics Procedia 78 (2015) 388 – 396».
- 6) Mary Kathryn Thompson, Giovanni Moroni, Tom Vaneker, Georges Fadel,R. Ian Campbell, Ian Gibson, Alain Bernard, Joachim Schulz, Patricia Graf, Bhriгу Ahuja, Filomeno Martina, Vijaikrishnan Venkataramanana, Jouni Partanend, Antti Salminenena, « Design for Additive Manufacturing: Trends, opportunities, considerations, and constraints, CIRP Annals - Manufacturing Technology 65 (2016) 737–760».
- 7) Sebastian Hällgrenena, Lars Pejrydb, Jens Ekengrenb, « (Re)Design for Additive Manufacturing, Procedia CIRP 50 (2016) 246 – 251»
- 8) Wei Gaoa, Yunbo Zhanga, Devarajan Ramanujana, Karthik Ramaniana, Yong Chenc,Christopher B. Williams, Charlie C.L. Wange, Yung C. Shin, Song Zhanga, Pablo D. Zavattieri, « The status, challenges, and future of additive manufacturing in engineering, Computer-Aided Design 69 (2015) 65–89»
- 9) Vegard Brøtana, Olav Åsebø Bergb, Knut Sørbya, « Additive manufacturing for enhanced performance of moulds, Procedia CIRP 54 (2016) 186 – 190»
- 10) Suchana A. Jahan and Hazim El-Mounayri , « Optimal Conformal Cooling Channels in 3D Printed Dies for Plastic Injection Moulding, Procedia Manufacturing Volume 5, 2016, Pages 888–900»

Chapter II

Additive Manufacturing via Selective Laser Melting of turbine blades

In the frame of Additive Manufacturing of metals, the aerospace industry has become increasingly interested in the use of Additive Manufacturing (AM) methods for the production of Ni-based high-temperature components.

Selective Laser Melting is investigated in this chapter as an advanced industrial prototyping tool to manufacture Inconel 718 turbine blade at a pre-design stage before flow production.

As mentioned in the previous sections, new possibilities in lightweight design and direct fabrication of functional end-use parts are offered by Additive Manufacturing where the base material is provided layer-by-layer, unlike conventional turning and milling relying on removal from the bulk. Namely, Selective Laser Sintering (SLS) and Melting (SLM) are solid freeform fabrication techniques based on laser irradiation of metal powder. Assemblies are turned into single parts, hence streamlining of manufacturing and potential elimination of tooling are benefited. Moreover, customization is allowed and the mechanical strength of the bulk is achieved upon proper set-up, although the resulting surface quality may limit the application if compared with conventional metal manufacturing. Post processing treating is required indeed to the purpose of surface modification.

Among a wide range of possible applications of AM, interest is currently devoted to processing superalloys for aerospace and automotive where outstanding combination of superior mechanical properties and wear resistance are required in demanding environments.

Typically, the Inconel 718 superalloy has been developed and applied in wrought, cast, and powder metallurgy forms, and the parts manufactured using these methods have demonstrated superior mechanical properties and performances [1] [2]. However, it is difficult to control the performance of this material when casting or forging. Furthermore, rapid development of modern industry and advanced engine designs, which require complex structures, high dimension precision, and further elevated mechanical properties, puts more pressure on Ni-based super alloys and their production. Therefore, an application of novel processing methods is necessary for the net shape production of Inconel 718 parts with complex configurations and high performance requirements.

2.1 Experimental setup: inconel 718 powder

Inconel 718 (IN718), a solid-solution or precipitation strengthened Ni-based austenite superalloy [3], has been used for produce prototype turbine blade. This superalloy receiving increasing interest, as being widely used to produce exhaust pipes, parts for rocket motors, gas turbines and nuclear reactors.

Two main reasons are driving both scientific and industrial investigation about IN718 AM - made parts. At first, challenges are faced when addressing fabrication of IN718 parts at room temperature with conventional machining due to high shear strength and low material removal rate [4]; in addition, complex parts with specific internal geometries and tight dimensional accuracy are usually required in aerospace and nuclear industries, hence conventional machining would be unfeasible [5]. Since IN718 is well known for good weldability, thanks to slow precipitation strengthening kinetics resulting in reduced cracking occurrence, SLM is enabled [6].

Pre-alloyed, 20 μm mean grain size, virgin EOS IN718 powder resulting from argon gas-atomization has been considered.

The powder has been preliminarily inspected in terms of size and geometry, since specific requirements of shape must be matched to the purpose of proper manufacturing. Spherical and near-spherical grains have been found (Figure 2.1), thus efficient flowing and layer packaging are expected to result in uniform melting [7].

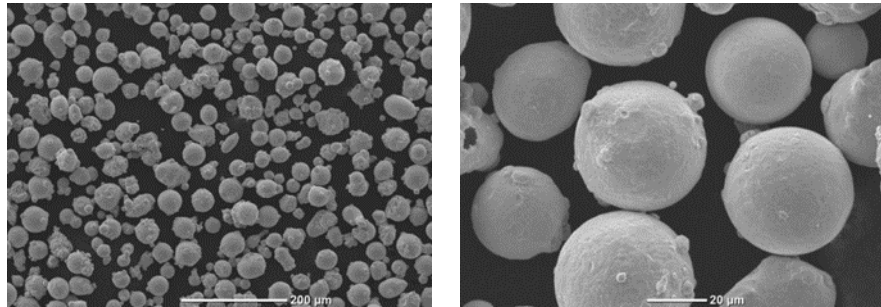


Figure 2.1: Pre-alloyed, argon gas-atomized, virgin IN718 powder; electron microscopy

Furthermore, the virgin powder and the samples have been investigated via aeral and punctual EDS inspections using a JEOL Neoscope.

EDS inspections have been conducted both on virgin powder and random cross-sections of the samples, to assess possible variation in the nominal composition upon AM; 15 kV accelerating voltage, 1 nA probe current and 3 min probing live time have been set.

The acquired spectra and the chemical compositions have been compared (Figure 2.2, Table 2.1). An average overall fitting coefficient of the quantitative analysis (i.e., the residual between the acquired and the synthetic

spectra) of 1.9% and 2.9% resulted for the powder and the samples, respectively.

At first, the ASTM B637 standard is matched in terms of nominal chemical composition; certain elements below 1% wt. have not been detected. Random transverse and longitudinal cross-sections of the samples have been considered; based on these, one may infer the referred nominal chemical composition has been taken during processing.

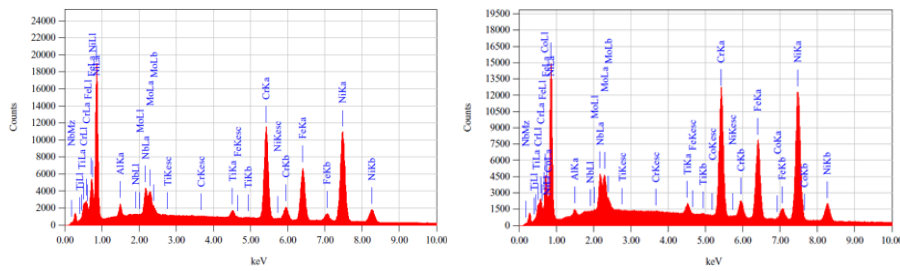


Figure 2.2: – Examples of acquired EDS spectra for powder and samples

Table 2.1: EDS inspections, average chemical composition (wt.%) of powder and samples

	Ni	Cr	Fe	Nb	Mo	Al	Ti
Powder	52.28	19.74	17.30	5.35	2.88	0.40	1.03
Std. dev.	0.12	0.05	0.06	0.04	0.04	0.02	0.01
Samples	52.29	19.19	18.29	5.30	3.35	0.48	1.08
Std. dev.	0.12	0.05	0.05	0.04	0.04	0.01	0.01
ASTM B637	50-55	17-21	Bal.	4.8-5.5	2.8-3.3	0.2-0.8	0.7-1.2

2.2 Experimental procedure

As for any other metal alloy, the resulting mechanical properties upon AM are expected to depend on the final density, as a function of heat and mass transfer in turn [8], based on the main processing parameters such as the size of the laser beam, the laser power, the scanning speed, the layer thickness and the hatch spacing [9] [10]. Therefore, extensive research has been conducted to draw a correlation between densification and microstructure of IN178 AM-made parts; it has been shown that optimum processing strategies result in 0.3% residual porosity, with elongated grains along the building direction [5]. Wear and high-temperature oxidation tests have been also implemented [11] [12], since poor resistance would lead to severe degradation of service life in the operating environment.

Anisotropy in the mechanical behavior is expected upon layering, depending on the direction of building, due to columnar grain growth as a consequence of directional thermal conduction. As regarding SLM, anisotropy has been discussed in the literature for stainless steel [13] [14], titanium [15] and Ni-based alloys [16]; anisotropy has also been reported when AM is conducted by means of electron beam [17]. This issue is expected to be crucial for Ni-based super alloys which are highly anisotropic and are conveniently processed to the purpose of producing functionally graded components [18], indeed.

An approach to measure the degree of AM-induced anisotropy as a function of the direction of building has been proposed in the literature [14]: the normalized yield or ultimate tensile strengths are evaluated with respect to their counterpart as resulting from an in-plane (i.e., flat-built) specimen. Depending on the base metal [13] [14] [16], normalized strength in SLM is found to range from 0.8 to 1.1. The position of building in the working area has even been suggested as possible additional reason of anisotropy [14], although this effect is thought to be negligible when focusing and deflecting are driven by means of an F-theta lenses providing uniform irradiance and approaching speed over the working surface [19].

It is worth noting that depending on the manufacturer and the powder size, arithmetic as-built roughness in SLM usually ranges from 8 to 20 μm [20]: since rough and rippled surfaces are reported to have larger stress concentrations, the rate of crack growth when testing as-built samples is affected [17]. In addition, residual stresses resulting from thermal cycles during laser AM, may exceed the yield strength, thus involving delamination during processing, as well as affecting corrosion resistance, fracture toughness, crack growth behavior and fatigue performance of the part. With respect to this issue, IN718 parts have been found to be very susceptible to warping and buckling because of their higher residual stress to yield strength ratio [21]. Given this, neutron diffraction has been presented as a valid method to validate thermo-mechanical models so to predict the residual stresses on

Ni-based AM-made parts [22]. Heat treatment is usually suggested to the concurrent purposes of stress relieving and precipitation of parent strengthening phase [6].

To provide further understanding of the mechanical properties of IN718 AM-made parts, possible anisotropy is investigated in this study as a function of the direction of growth. Flat-, 45°- and upright-built samples have been produced. The tensile response at room and elevated temperature is discussed. Eventually, a batch of turbine blade, which are currently made via casting, has been manufactured and inspected by means of X-rays and 3D laser scanning metrology.

Three possible direction of growing are considered; corresponding supporting structures are designed, accordingly. Although AM is not deemed to be a current viable option to casting, the process is intended to offer a valuable technical test model in the frame of advanced industrial prototyping to evaluate any possible upgrade at a pre-design stage before flow production; furthermore, a preliminary evaluation of clamping and tooling for assembly is aimed. Therefore, proper mechanical features must be achieved and the same base metal must be used.

2.2.1 Job preparation

An EOSINT M270 commercial laser melting system with Yb:YAG fibre-laser source has been used to manufacture a convenient number of cylinders (12 mm diameter, 90 mm height); an F-theta lens is used to focus and deflect the laser beam over the working area. Flat-, 45°- and upright-built samples have been produced (Figure 2.3) in 99.4% pure argon inert atmosphere; supporting structures have been required on downward facing surfaces, depending on the sloping angle with the building direction, hence for flat- and 45°-built samples.

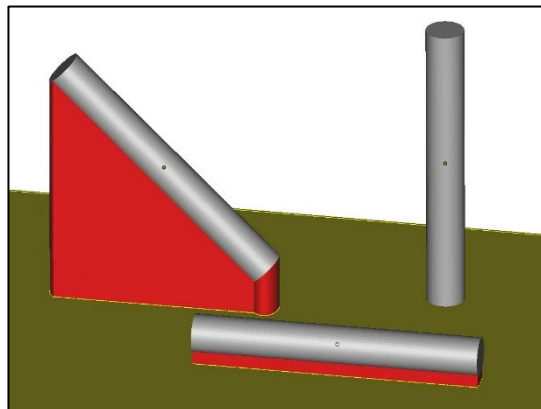


Figure 2.3: Positioning of flat-, 45°- and upright-built cylinder samples on the building plate

Operating laser power, speed and hatching strategies are based on preliminary trials aimed to optimize SLM and full dense structure (Table 2.2).

A number of quality jobs have been performed to assess and fine-tune the beam offset and the scaling factor to address possible dimensional shrinkage. Namely, a checkerboard scanning pattern with 67° rotation of the scanning direction between consecutive $20\ \mu\text{m}$ thick layers has been set. To the concurrent purpose of stress relieving and ductility improvement [3], heat treatment as per AMS 5664 standard (i.e., solution annealing at $1065\ ^\circ\text{C}$ for 1 hour, ageing at $760\ ^\circ\text{C}$ for 10 hours, cooling to $650\ ^\circ\text{C}$ and holding for 8 hours in argon inert atmosphere) has been eventually conducted before removal of the parts from the building plate, as suggested by the powder manufacturer [23].

Table 2.2: Main features and processing parameters in SLM of IN718 powder

Gain medium	Fibre, Ytterbium-doped YAG (Yb:YAG)
Operating laser power	195 W
Linear processing speed	$1.2\ \text{m}\cdot\text{s}^{-1}$
Hatch spacing	$90\ \mu\text{m}$
Layer thickness	$20\ \mu\text{m}$
Focused spot diameter	$90\ \mu\text{m}$

2.3 Results and discussion

Uniform fusion is experienced. Overlapping lenticular-shaped melting pools result as a consequence of building and layer development [24] when investigating the samples (Figure 2.4); it is worth noting that although a scanning beam of theoretical 90 μm diameter is used, a wider scanning trace of approximately 120 μm width is found due to thermal conduction. Moreover, the typical 67° scanning angle between exposures over consecutive layers is measured if a cross-section is made orthogonal to the direction of growing (Figure 2.5).

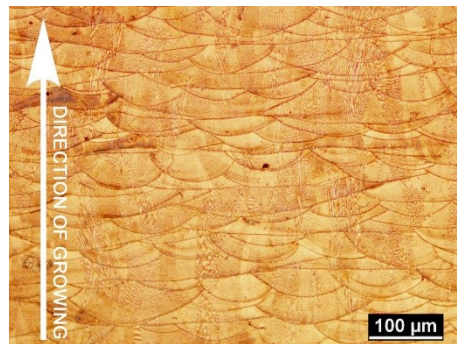


Figure 2.4: Layer development, longitudinal cross-section in the upright-built sample

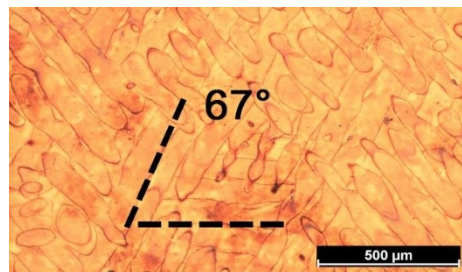


Figure 2.5: Exposures over consecutive layers; transverse cross-section in the upright-built sample

2.3.1 Tensile testing

Subsize specimens with round cross-section, as allowed by ASTM standards [25] [26], have been produced via turning of the cylinders, in agreement with similar research in the literature [16]. The same standards have been referred for testing at room and elevated temperature; namely, tensile testing at 650 °C has been conducted, being this the maximum operating temperature for IN718 AM-made parts under load, as per material data sheet [23]. Investigation on near-net-shape AM-made tensile specimens, with no

effort to machine or grind the resulting surface, has been reported in the literature in case of flat specimens [14].

In this experimental campaign instead, an investigation on as-built parts is not feasible, given a mean arithmetic roughness ranging from 5 to 20 μm over as-built surfaces, depending on the sloping angle with the building direction. Therefore, in order to provide uniform, improved surface quality to the purpose of reliable tensile testing, post processing would be required anyway. Eventually, average roughness has been reduced below 0.5 μm upon turning.

The outcome of tensile testing has been discussed as a function of temperature T and sloping angle with the building direction (Table 2.3, Figure 2.6) in comparison with the referred expected mechanical properties as per material data sheet [23], where available. Three specimens for each building direction have been tested; average values of yield strength for a 0.2% offset ($YS_{0.2}$) and ultimate tensile strength (UTS) are given; the degree of AM-induced anisotropy is measured in terms of normalized strength R with respect to a flat-built specimen, as suggested in the literature [14].

Table 2.3: IN718 yield-strength ($YS_{0.2}$) and ultimate tensile strength (UTS), room and elevated temperature

Sample	T [°]	$YS_{0.2}$ [MPa]	R_{YS} [/]	UTS [MPa]	R_{UTS} [/]
EOS reference	24	1239	<i>n.a.</i>	1384	<i>n.a.</i>
Flat-built		1295	1.00	1484	1.00
45°-built	24	1368	1.06	1521	1.02
Upright-built		1240	0.96	1398	0.94
Flat-built		1033	1.00	1139	1.00
45°-built	650	1124	1.09	1187	1.04
Upright-built		978	0.95	1114	0.98

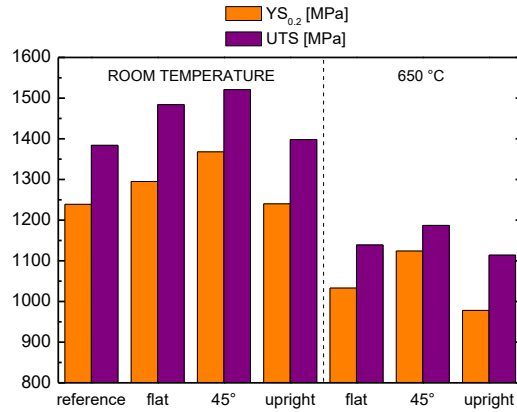


Figure 2.6: IN718 yield-strength ($YS_{0.2}$) and ultimate tensile strength (UTS), room and elevated temperature

Ductile fracture has been experienced, irrespective of the sample and the temperature. As regarding testing at room temperature, both the referred average $YS_{0.2}$ and UTS are available with 100 MPa uncertainty [24] to take account of possible anisotropy, hence the results are found within the expected range. Also, based on the normalized strengths, the degree of AM-induced anisotropy is negligible, its value being in agreement with similar, available findings in the literature (Figure 2.7).

Therefore, the optimization of the processing parameters and the scanning patterns is effective; one may infer uniform mechanical properties are achieved on a complex real component experiencing different loading conditions (i.e., loading directions) when in service.

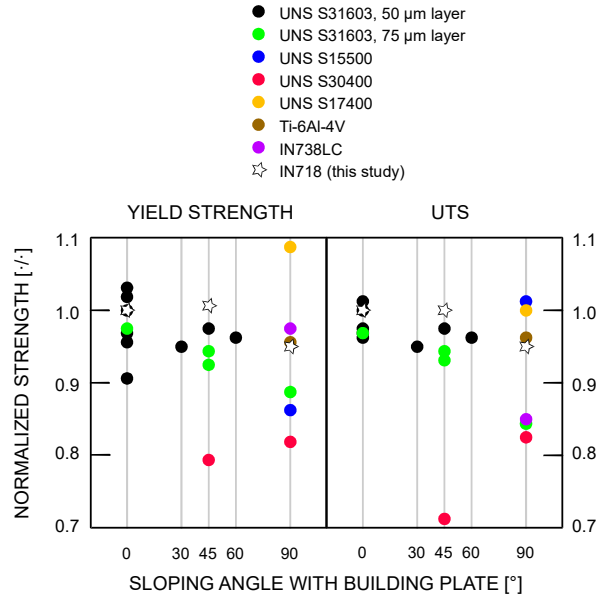


Figure 2.7: Normalized strength resulting from SLM; adaptation and upgrade based on the literature [27]

Nevertheless, it is worth noting that higher YS0.2 and UTS are found for the 45°-built specimen. A favorable stress state can be referred as possible reason: as a general rule, fracture is induced over planes where maximum shear stress occur; these are 45° from the direction of loading, hence are parallel to layering when testing 45°-built specimens. Since bonding among layers may be incomplete, failure is thought to be deferred when layers are pulled together in parallel. As a consequence of the same effect, improved ductility is found for the upright-built sample instead; the same has been reported in the literature when discussing AM of titanium via electron beam [17].

As regarding testing at elevated temperature, reference properties are not available by the manufacturer, although possible comparisons could be drawn based on wrought parent metal. Nevertheless, to the purpose of this paper, it is worth noting that any decrease Δ of YS0.2 and UTS is deemed to be independent on the building direction (Table 2.4). Moreover, as for testing at room temperature, although the degree of anisotropy is found to be low, higher YS0.2 and UTS are found for the 45°-built specimen; the same reason apply.

Table 2.4: Average decrease of mechanical properties at 650 °C with respect to room temperature

Sample	$\Delta YS_{0.2}$ [%]	ΔUTS [%]
Flat-built	20	23
45°-built	18	22
Upright-built	21	20

2.3.2 Micro-hardness analysis

Vickers micro-hardness of the parts has been discussed based on the outcome of both optical microscopy and Vickers microhardness testing. Namely, an indenting load of 300 g has been used for a dwell period of 10 s; a step of 420 μm has been allowed between consecutive indentations, in compliance with ISO standard for hardness testing on metallic materials.

Two types of cylinder specimens have been investigated, i.e., 0° and 90°-built specimens with respect to the building plate.

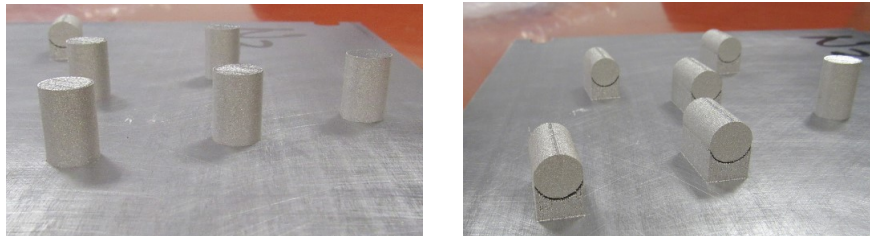


Figure 2.8: 90°, 0°- built specimens, positioning in building

On each specimens, micro-hardness scanning paths in different directions have been performed. In the following figure, the directions are shown.

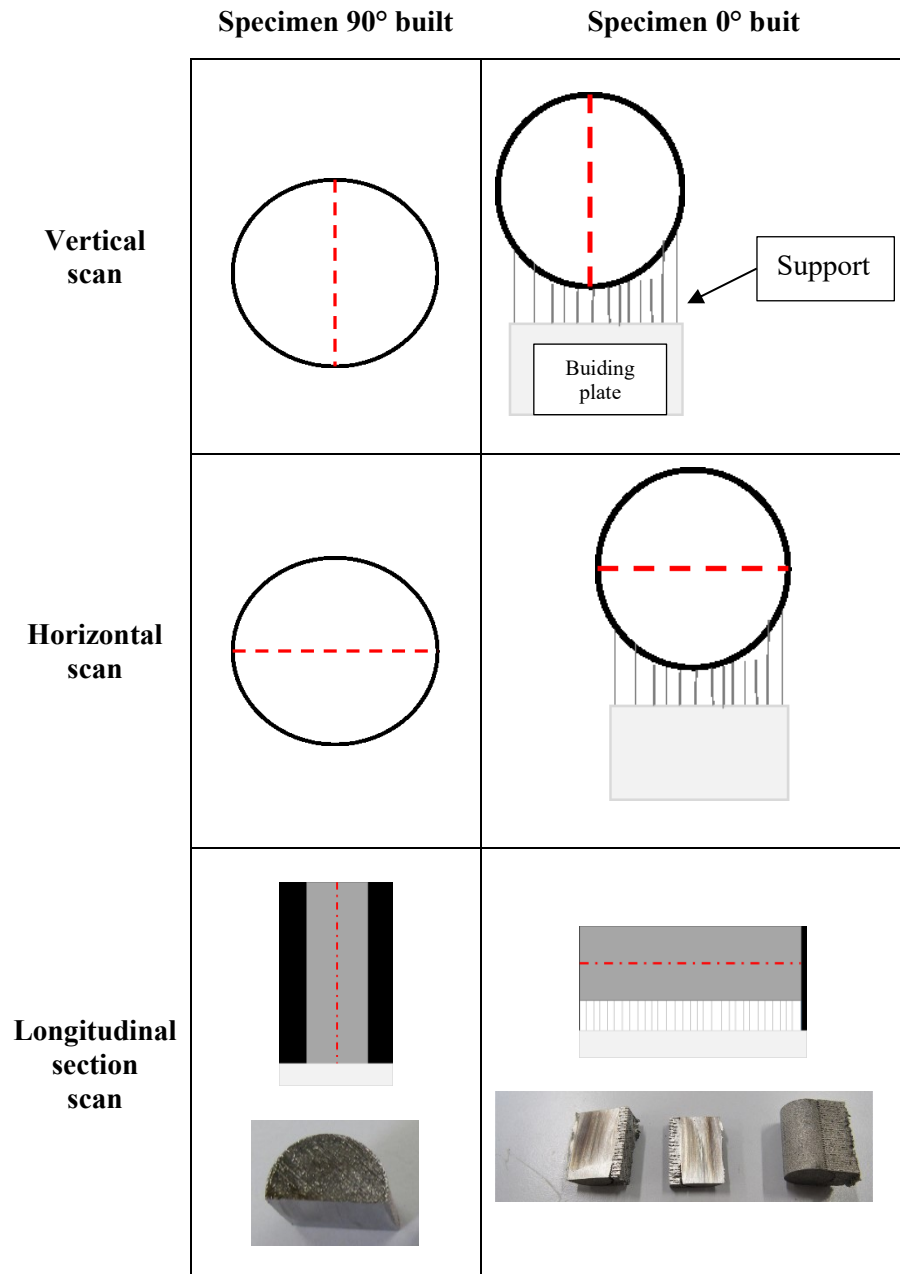
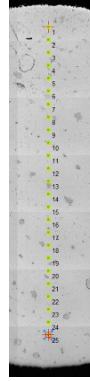
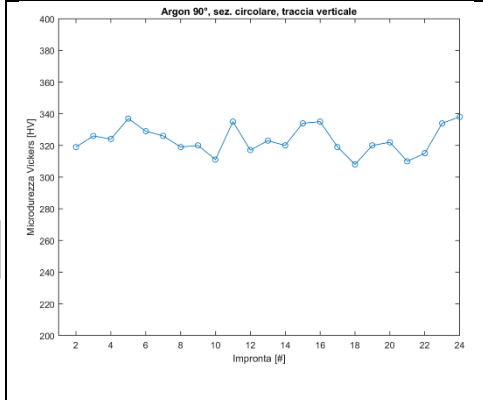


Figure 2.9: micro-hardness scanning direction

Additive Manufacturing via Selective Laser Melting of turbine blade

Specimen
90°
vertical
scan

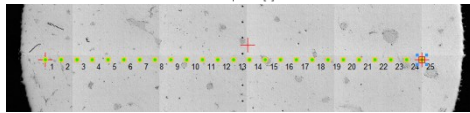
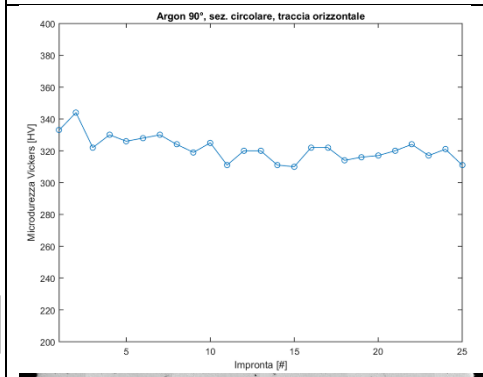
μ	323
σ	9



Field [#]	Hard. [HV]
1	319
2	326
3	324
4	337
5	329
6	326
7	319
8	320
9	311
10	335
11	317
12	323
13	320
14	334
15	335
16	319
17	308
18	320
19	322
20	310
21	315
22	334
23	338
24	316

Speciment
90°
horizontal
scan

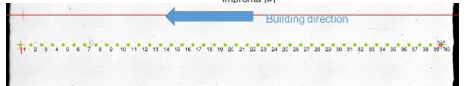
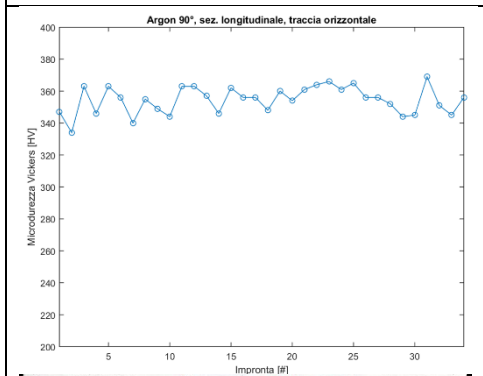
μ	322
σ	8



Field [#]	Hard. [HV]
1	333
2	344
3	322
4	330
5	326
6	328
7	330
8	324
9	319
10	325
11	311
12	320
13	320
14	311
15	310
16	322
17	322
18	314
19	316
20	317
21	320
22	324
23	317
24	321
25	311

Speciment
90°
longitudinal
section
scan

μ	355
σ	8

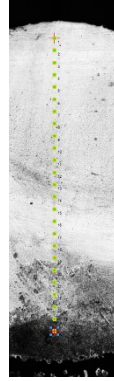
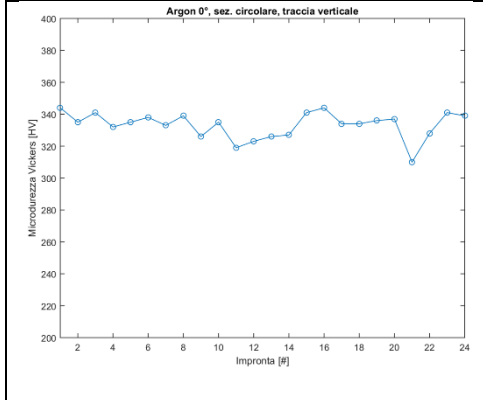


Field [#]	Hard. [HV]	Field [#]	Hard. [HV]
1	347	18	348
2	334	19	360
3	363	20	354
4	346	21	361
5	363	22	364
6	356	23	366
7	340	24	361
8	355	25	365
9	349	26	356
10	344	27	356
11	363	28	352
12	363	29	344
13	357	30	345
14	346	31	369
15	362	32	351
16	356	33	345
17	356	34	356

Chapter II

Speciment
0°
vertical
scan

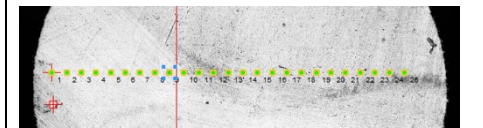
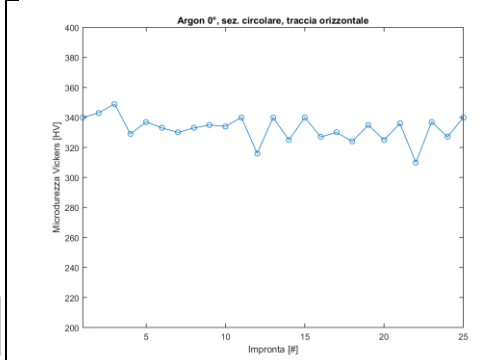
μ	333
σ	8



Field [#]	Hard. [HV]
1	344
2	335
3	341
4	332
5	335
6	338
7	333
8	339
9	326
10	335
11	319
12	323
13	326
14	327
15	341
16	344
17	334
18	334
19	336
20	337
21	310
22	328
23	341
24	339

Speciment
0°
horizontal
scan

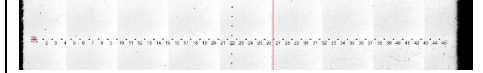
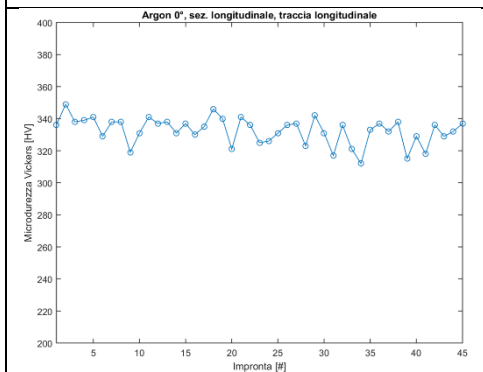
μ	333
σ	9



Field [#]	Hard. [HV]
1	340
2	343
3	349
4	329
5	337
6	333
7	330
8	333
9	335
10	334
11	340
12	316
13	340
14	325
15	340
16	327
17	330
18	324
19	335
20	325
21	336
22	310
23	337
24	327
25	340

Speciment
90°
longitudinal
section
scan

μ	333
σ	8



Field [#]	Hard. [HV]	Field [#]	Hard. [HV]
1	336	24	326
2	349	25	331
3	338	26	336
4	339	27	337
5	341	28	323
6	329	29	342
7	338	30	331
8	338	31	317
9	319	32	336
10	331	33	321
11	341	34	312
12	337	35	333
13	338	36	337
14	331	37	332
15	337	38	338
16	330	39	315
17	335	40	329
18	346	41	318
19	340	42	336
20	321	43	329
21	341	44	332
22	336	45	337
23	325		

2.4 AM of the turbine blade

The same processing parameters and scanning strategies have been used to manufacture the turbine blade. Based on the outcome of tensile testing, anisotropy is negligible, hence the overall mechanical properties are not affected by positioning when proper preliminary optimization of processing parameters and scanning strategies is conducted to achieve uniform fusion and reduced porosity. Therefore, any part with a shape suggesting a natural preferential direction of growing can be equally manufactured to the purpose of accommodating proper supports and concurrently reducing the overall building time; the same mechanical strength is expected, irrespective of positioning.

Among all possible directions of growing, three of these have been investigated, the longitudinal axis of the airfoil being taken to 0° , 45° and 90° to the building plate (Figure 2.10). Depending on positioning, proper supporting by means of auxiliary structures would be required. Namely, an ideal balance must be found between two needs: reducing the amount of supports to preserve functional surfaces and allow the removal of the part; preventing warping and collapse for crucial surfaces exceeding a given threshold depending on both the material and the machine [28]. Cone-shaped supports (Figure 2.11) have been preferred at the edge of the dovetail to increase the extent of the interface with the building plate; line supporting has been provided along the dovetail instead. Teeth at the interface between block supports and parts (Figure 2.12) have been conveniently adjusted in number and size (i.e., height, length and spacing) depending on the supported part. The airfoil is self-supported in the upright-built sample, hence additional supporting is prevented on a crucial surface.

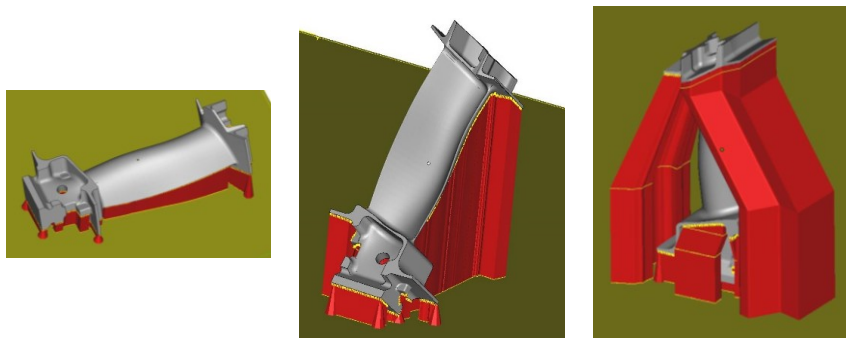


Figure 2.10: Flat-, 45° - and upright-built turbine blade, positioning in building (not to scale)

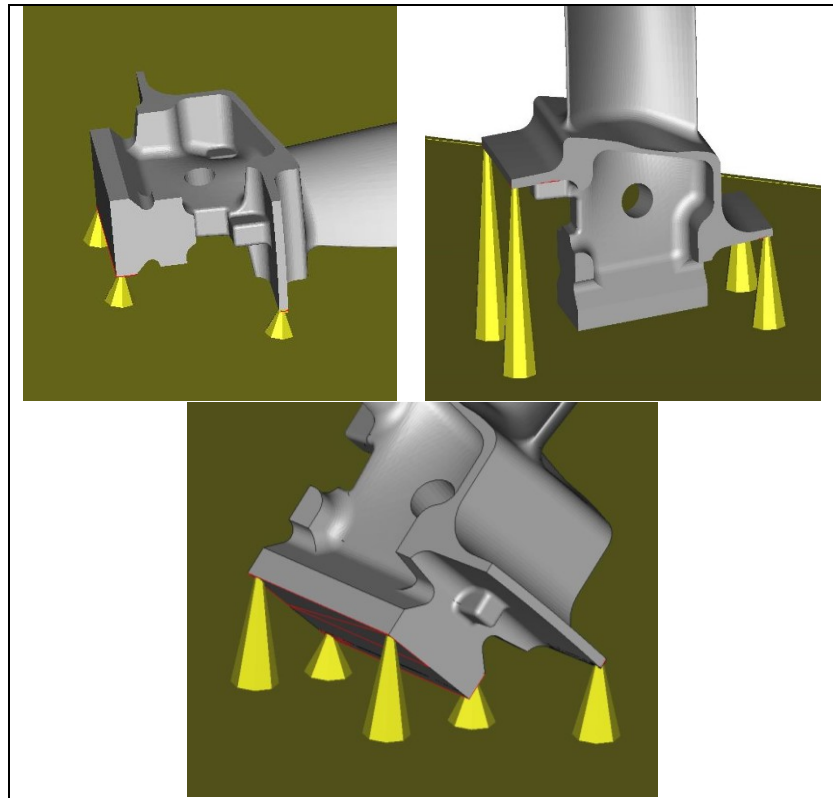


Figure 2.11: Flat-, 45°- and upright-built turbine blade, detail of cone-shaped supports on the dovetail; dismissed line and block supporting along the dovetail (not to scale)

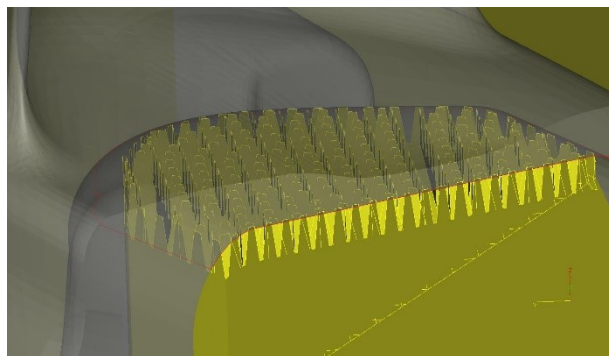


Figure 2.12: – Detail of teething at the interface between block supports and part, upright building

Reduced building time has been benefited for flat- and 45°-built samples in comparison with the upright-built sample, thanks to shorter building height (Table 2.5). On the other hand, reduced and easier post-processing has been required for the latter, since the surface quality of the airfoil has not been affected by supporting.

Table 2.5: Building time of the turbine blade as a function of positioning; manufacturing of one part per job

Positioning	Manufacturing time	Building height
Flat-built	8 h, 26 min	33 mm
45°-built	17 h, 13 min	75 mm
Upright-built	22 h, 10 min	90 mm

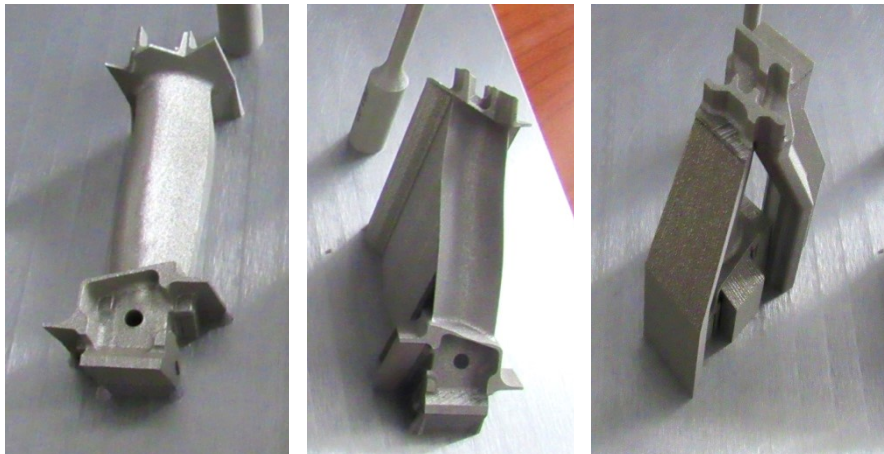


Figure 2.13: Flat-, 45°- and upright-built turbine blade, as-built, with supporting structures on the building plate



Figure 2.14: Flat-, 45°- and upright-built turbine blade, removed from the building plate, heat treated

2.4.1 X-ray inspections

X-ray inspections have been performed to assess the occurrence of possible lack of fusion, inclusions and cracks. Manufacturing of the turbine blades has been possible for any given positioning (Figure 2.13, Figure 2.14); sound and defect-free parts resulted, as no indications have been shown via X-ray inspections using a General Electric CRx Flex CR scanner (Figure 2.15).

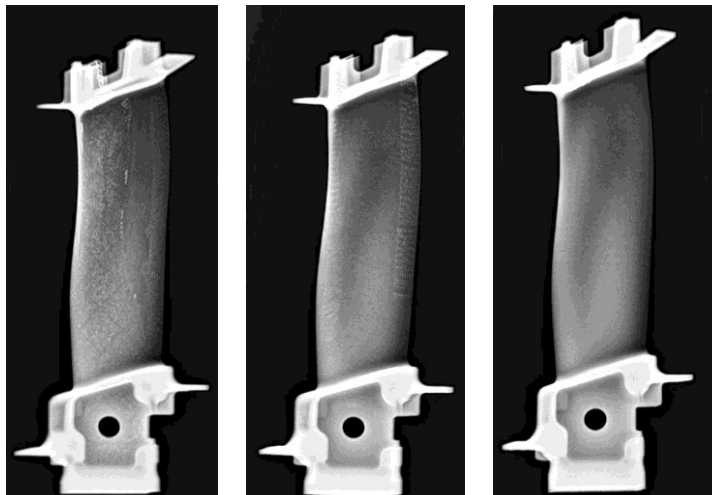


Figure 2.15: Flat-, 45°- and upright-built turbine blade, removed from the building plate, X-ray transmitted images

2.4.2 AM turbine blade dimensional analysis

Laser scanning has been eventually conducted to evaluate any possible deviation from the intended geometry.

Further conclusions can be drawn based on the outcome of laser metrology (Figure 2.16). Irrespective of positioning, the dovetails are found to comply with the intended geometry, hence cone-shaped supports are deemed to be effective. As expected, removal of the supports from the flat-built sample has been challenging and time-consuming; this direction of growing is not suggested, accordingly. As regarding the upright-built sample, it is worth noting that although the airfoil being self-supporting, warping resulted with a maximum mismatch in the order of 0.3 mm at the trailing edge.

Convincing results have been achieved with the 45°-built sample instead: a mismatch in the order of 0.2 mm has been measured at the convex side of the airfoil, but since the nominal curvature is matched, the issue is deemed to result from improper dressing in post-processing. The effectiveness of the part in a preliminary evaluation of tooling and clamping is not affected; nevertheless, proper machining allowance could be set to prevent any minimal mismatch. Therefore, when balancing the overall processing time and the general features, manufacturing of the 45°-built sample should be preferred, being this an ideal compromise among multiple needs.

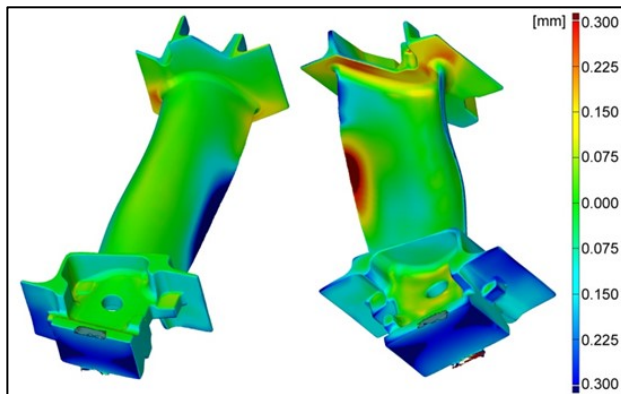


Figure 2.16: Flat built turbine blade, laser metrology in comparison with the intended nominal geometry

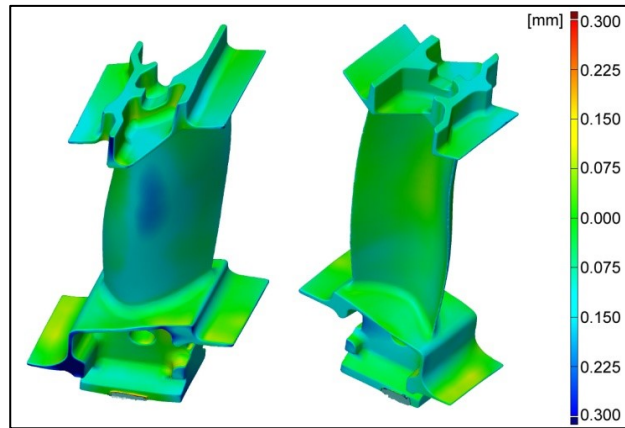


Figure 2.17: 45° built turbine blade, laser metrology in comparison with the intended nominal geometry

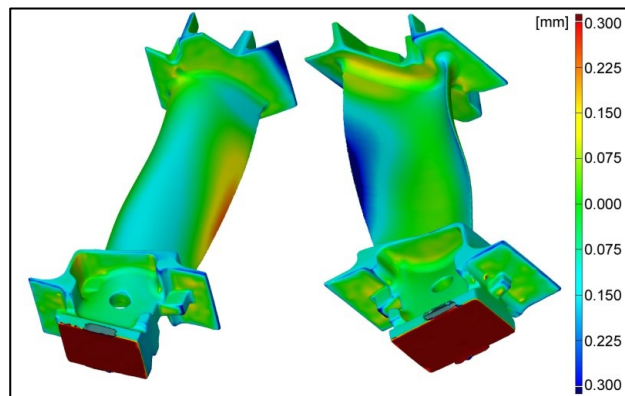


Figure 2.18: upright built turbine blade, laser metrology in comparison with the intended nominal geometry

Additive Manufacturing via Selective Laser Melting of turbine blade

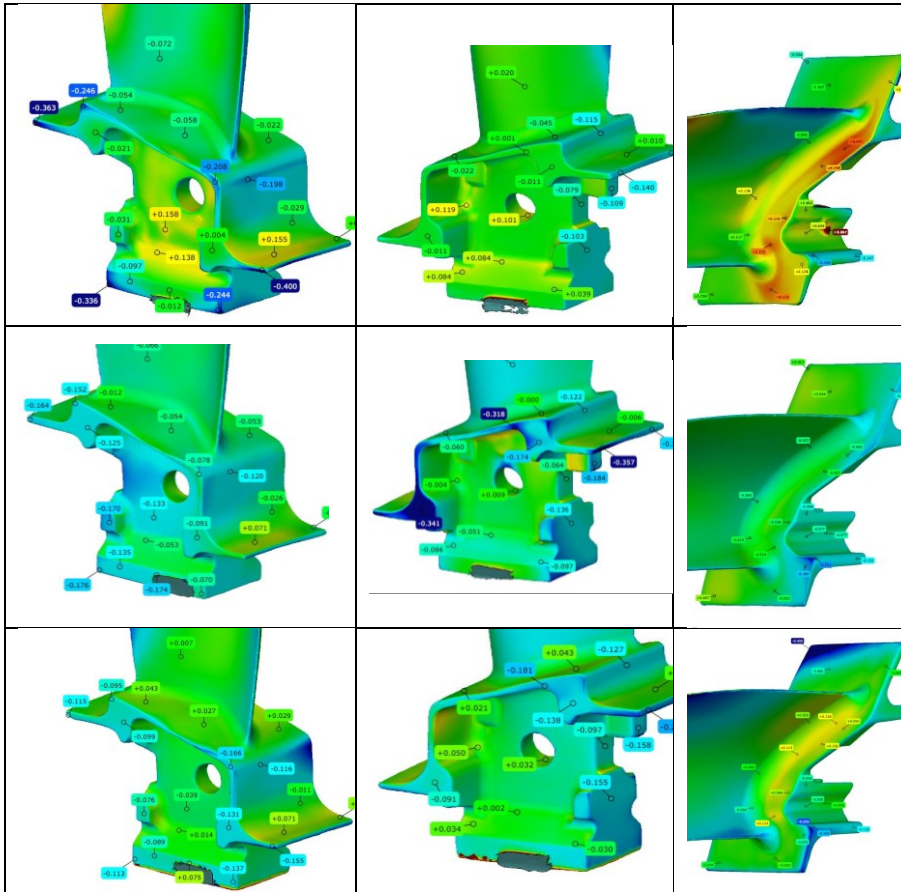


Figure 2.19: detail 0°, 45° and 90° turbine blade, laser metrology in comparison with the intended nominal geometry

2.5 Conclusions

A number of main findings have been drawn in the frame of Additive Manufacturing of superalloy Inconel 718 by means of Selective Laser Melting. At first, uniform fusion is experienced and convincing matching with the intended geometry can be achieved upon proper settings of the processing parameters, based on preliminary optimization and fine-tuning.

As regarding the mechanical properties, anisotropy is considered to be negligible when measured in terms of normalized strength, both at room and elevated temperature; moreover, any decrease of both the yield and the ultimate tensile strength at the maximum allowed operating temperature of the parts has been found to be independent on the building direction.

Three possible direction of growing have been proposed to manufacture real parts: all of them resulted in effective building, with sound and defect-free quality. Nevertheless, although the mechanical properties are expected to be the same, multiple issues must be taken into account, including the overall processing time and the need for post-processing to remove the supporting structures and reduce the surface roughness.

References chapter II

- [1] L. Zheng, «Mechanism of intermediate temperature embrittlement of Ni and Ni-based superalloys, Crit. Rev. Solid State Mater. Sci. 37 (3) (2012) 181–214.».
- [2] S. Sufiiarov, «Selective Laser Melting of Heat-resistant Ni-based Alloy Non-ferrous Metals, 1(38), 2015 32–35.».
- [3] R. Reed, «The superalloys, Fundamentals and Applications, New York: Cambridge University Press, 2006.».
- [4] H. A. Youssef, «Machining of Stainless Steels and Super Alloys: Traditional and Nontraditional Techniques, New York: John Wiley & Sons, 2016.».
- [5] P. Choi et al., ««Densification and microstructural investigation of Inconel 718 parts fabricated by selective laser melting,» Powder Technology, vol. 310, pp. 60-66, 2017.».
- [6] M. Tucho et al., ««Microstructure and hardness studies of Inconel 718 manufactured by selective laser melting before and after solution heat treatment,» Materials Science & Engineering A, vol. 689, p. 220–232, 2017.».
- [7] G. Murr, ««Metal Fabrication by Additive Manufacturing Using Laser and Electron Beam Melting Technologies,» Journal of Materials Science and Technology, 2012.».
- [8] M. Xia et al., ««Influence of hatch spacing on heat and mass transfe, thermodynamics and laser processability during additive manufacturing of Inconel 718 alloy,» International Journal of Machine Tools & Manufacture, vol. 109, 20.».
- [9] Steen, «Laser material processing.».
- [10] Cardaropoli, ««Dimensional analysis for the definition of the influence of process parameters...,» Journal of Engineering Manufacture, 2012.».
- [11] Q. Jia et al., ««Selective laser melting additive manufactured Inconel 718 superalloy parts: High-temperature oxidation property and its mechanisms,» Optics&LaserTechnology, vol. 62, pp. 161-171, 2014.».
- [12] Q. Jia et al., ««Selective laser melting additive manufacturing of Inconel 718 superalloy parts: Densification, microstructure and properties,» Journal of Alloys and Compounds, vol. 585, pp. 713-721, 2014.».
- [13] E. Tolosa et al., ««Study of mechanical properties of AISI 316 stainless steel processed by 'Selective Laser Melting', following

- different manufacturing strategies,» *International Journal of Advanced Manufacturing Technology*, vol. 51, n. 5-8, pp. 639-647».
- [14] E. Luecke et al., ««Mechanical Properties of Austenitic Stainless Steel Made by Additive Manufacturing,» *Journal of Research of the National Institute of Standards and Technology*, vol. 119, 2014.».
- [15] S. Rafi, ««A comparison of the tensile, fatigue, and fracture behaviour of Ti6Al4V and 15-5 PH stainless steel parts made by selective laser melting,» *International Journal of Advanced Manufacturing Technology*, vol. 69, n. 5-8, pp. 1299-1309, 2013.».
- [16] W. Rickenbacher, ««High temperature material properties of IN738LC processed by selective laser melting (SLM) technology,» *Rapid Prototyping Journal*, vol. 19, n. 4, pp. 2082-2090, 2013.».
- [17] R. Ladani, ««Mechanical behavior of the Ti-6Al-4V manufactured by electron beam additive fabrication,» in *Proceeding of the ASME 2013 International Manufacturing Science and Engineering Conference MSEC2013, Madison, WI, 2013.*».
- [18] V. Popovich et al., ««Functionally graded Inconel 718 processed by additive manufacturing: Crystallographic texture, anisotropy of microstructure and mechanical properties,» *Materials and Design*, vol. 114, p. 441–449, 2017.».
- [19] Muth, ««Optimized x/y scanning head for laser beam positioning,» in *Proceedings of SPIE 2774, Design and Engineering of Optical Systems, Glasgow, 1996.*».
- [20] Alrbaey, ««On Optimization of surface roughness of selective laser melted stainless steel parts: a statistical study,» 2014.».
- [21] T. Mukherjee et al., ««An improved prediction of residual stresses and distortion in additive manufacturing,» *Computational Materials Science*, vol. 126, p. 360–372, 2017.».
- [22] Z. Wang et al., ««Residual stress mapping in Inconel 625 fabricated through additive manufacturing: Method for neutron diffraction measurements to validate thermomechanical model predictions,» *Materials and Design*, vol. 11».
- [23] EOS, «EOS NickelAlloy IN718 for EOSINT M 270 Systems, EOS.».
- [24] Argenio, Caiazzo, Sergi, Alfieri, ««Reduction of Surface Roughness by Means of Laser Processing over Additive Manufacturing Metal Parts,» *Materials*, vol. 10, n. 30, pp. 1-12, 2017.».
- [25] ASTM International, «ASTM E8 / E8M-16a, Standard Test Methods for Tension Testing of Metallic Materials, West Conshohocken: ASTM International, 2016.».

- [26] ASTM International, «Standard Test Methods for Elevated Temperature Tension Tests of Metallic Materials, West Conshohocken: ASTM International, 2009.».
- [27] N. T. e. al., ««Selective laser sintering of single- and two-component metal powders,» Rapid Prototyping Journal, vol. 9, n. 2, p. 68–78, 2003.».
- [28] Calignano, ««Design optimization of supports,» 2014.».

Chapter_III

Laser cladding as repair technology for complex component in aerospace industry

A number of innovative technologies are offered in the literature to the purpose of additive manufacturing to keep parts and devices in working order when local manufacturing imperfections or demanding conditions of temperature, wear and mechanical stresses have been experienced. Since part replacement would result in increased costs for any component of complex geometry, mainly in aerospace and automotive, proper actions are required to the purpose of cost saving. Also, overhaul of new parts could be required to fix minor local imperfection resulting from improper casting.

Among possible technologies, laser-aided Directed Metal Deposition (DMD) or Laser Cladding is thought to be capable of producing near-net-shape and sound clads to successfully perform coating for maintenance, repair and overhaul of condemned parts of high complexity and expensive manufacturing cost [1, 2, 3, 4].

This process is receiving increasing interest in aerospace industry: minimal distortion of the work-piece, reduced heat-affected zones and better surface quality are benefited in laser-aided DMD in comparison with conventional coating and repairing techniques such as arc welding or plasma spraying are benefited [5].

In this chapter a specific process for laser metal deposition is presented: Laser cladding by powder injection: powder particles are fed into the melt pool generated by laser to produce a reported trace [6]. The method is more flexible with respect to powder bed fabrication: it allows the on-line variation of clad dimensions and clad composition; more elements and alloys are available given that larger particle sizes can be employed. Minimal distortion of the work-piece, reduced heat-affected zones and better surface quality are hence benefited in comparison with conventional coating and repairing techniques such as arc welding or plasma spraying.

3.1 Introduction to powder injection Laser Cladding

The process of laser cladding, in the common industrial application, is conducted in single-stage: a melting pool is produced by irradiation of laser beam and an additive metal is fed, concurrently. Generally the laser head is moved by a positioning device [7]. A deposited metal trace results by cladding materials added to the surface of the substrate.

For this investigation, the powder injection laser cladding has been used, where the additive cladding material has been fed in the form of powder.

Powders can vary in size and shape and in terms of how they are produced. For most laser cladding applications, the powders are larger in size compared to those used in laser melting processes. For laser cladding, it is common to see powders range between 10 and 100 μm and are typically spherical in shape. Spherical-shaped particles can reduce any entrapment of inert gas within the melt pool and can thus lead to a final part with less porosity. Powders for alloyed materials will consist of all alloyed constituents as they are produced from the alloyed metal in its molten state. Gas atomization, water atomization and plasma rotating electrode processes (PREP) are typical means for producing powders effective for laser cladding application. The particle feed rate is the average mass of particles leaving the nozzle with respect to time and can range between 1-30 g/min.

Powder particles are fed and melt into the heat zone to produce a layer of clad, complete coating is achieved by overlapping the tracks in order to improve the surface properties of the substrate material or to repair a component.

This method is more flexible: it allows the on-line variation of clad dimensions and clad composition and many more elements and alloys are available as powder; furthermore products with a complex geometry can be treated, because material is fed continuously to the interaction zone.

In this process, inert gas is required to the purpose of shielding the zone of processing and carrying the powder. Powder is delivered to the laser deposition line via a carrier gas. Generally it is an inert gas, Argon or Helium. The pressure and the flow rate have an important effect on the physics of the process. A high carrier gas flow rate has the effect of increasing the overall depth of the pool, compared to a low flow rate during both pulsed and continuous wave deposition. It can be seen that in continuous wave deposition the area of the melt pool produced with a high carrier gas flow rate is larger than the area produced with a low gas flow rate [8].

Three different concepts of powder injection are possible [9], depending on the type of nozzle used:

- Off-axis powder injection: a single powder stream is fed lateral into the laser beam;

- Continuous coaxial powder injection: a powder stream cone is produced which encloses the laser beam;
- Discontinuous coaxial powder injection: three or more powder streams are fed coaxial to the laser beam.

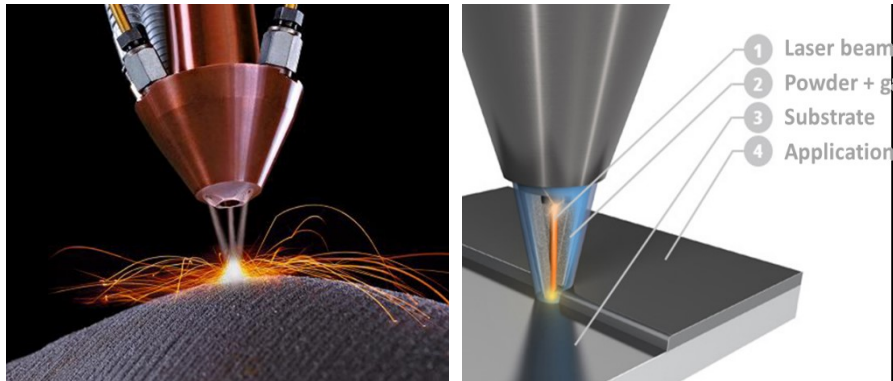


Figure 3.1: Laser cladding by powder injection

Laser cladding process is essentially a fusion and solidification process, which involves complex interactions between the laser beam, metal powders, the base material (substrate), and processing gases. It is influenced by a lot of processing parameters which are also correlated to each other. Therefore, the process results to be really complex so that the relationship between the variables and the effect of the process parameters on the process results must be analysed and modeled. In the Figure 3.2 the physical and process variables that affect the clad results are shown.

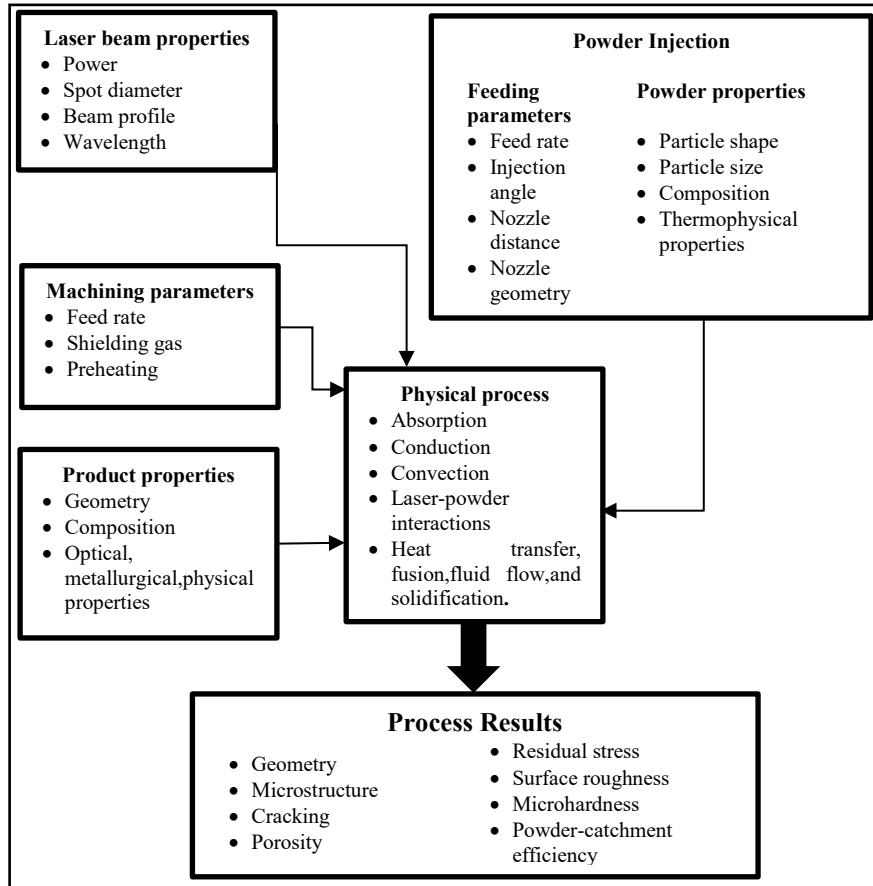


Figure 3.2: A scheme of the process

The process parameters regarding the laser beam properties and the machining parameters will be discussed in the next paragraph, where the laser cladding equipment is described. The feeding parameters depend on the nozzle configuration, therefore these variables are presented also.

3.2 Powder laser cladding equipment

The process of powder laser cladding equipment requires the following equipment:

- Laser source: energy source
- Powder feeder: powder is mixed with the carrier gas and delivered to the deposition line via an antistatic powder conveyor
- Shielding gas: is required to prevent oxidation during fusion/solidification
- Laser deposition line: motion device, optics, nozzle

The following scheme show how these components are connected.

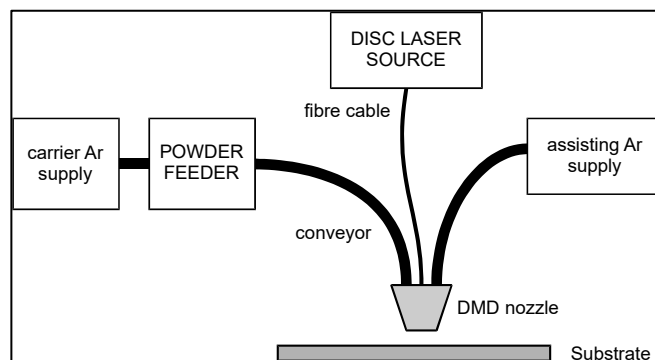


Figure 3.3: Laser deposition line, base components

At present, two possibilities of filler material are offered: wire and powder, the former being preferred in general for its lower cost and lower oxide content, the latter for being flexible in materials and allowing higher precision for local repairing with better surface quality and bonding strength.

3.2.1 Laser source

The experimental work has been performed using a Yb:YAG disk-laser source in continuous wave emission. The wavelength of 1030 nm is well suited for transport by optical fibers cable of 300 μm diameter.

The main technical features are given in Table 3.1.

Table 3.1: Main technical features of the laser system

Parameter	Value
Maximum output power [kW]	4.0
Operating nominal wavelength [nm]	1030
Beam Parameter Product [mm × mrad]	8.0
Core diameter of the delivering fibre [μm]	300
Spot size of the laser beam on the surface [mm]	3
Spot size of the powder stream [mm]	2.5

The principle of the disk laser operation is based on the use of an active element in the form of a disk with a cooled surface. High cooling efficiency of the laser medium is provided by a large area of the disk surface, which is important from the point of view of the heat transfer process. Therefore, the scheme is capable of delivering laser power up to 4 kW. It is important to note that due to effective heat transfer within the disk area there is no thermal lensing effect, which is a disadvantage in case of ‘rod’ and ‘slab’ (optical range) geometries of the active element. In the latter, cooling is performed through a side surface of the active element; a two-dimensional heat flow, forming a parabolic profile of thermal distortion, propagates through this side surface.

The disk lasers advantages are:

- Active medium in quasi-three levels;
- Pumping diode;
- Limited effect of thermal lens;
- Reduction of losses in the resonant cavity;
- Reduction of parasitic effects;
- Higher efficiency compared to traditional laser (25% wall-plug, 65% opt-opt);
- Possibility to increase the power by expanding the diameter of the pumping;
- Low values of BPP in combination with acceptable values of M^2 ;
- Rayleigh ranges are higher compared to Nd:YAG laser.



Figure 3.4: Laser source

3.2.2 Powder feeder

One of the most important and crucial aspects of the process is consistency of the powder flow. Therefore, a flow monitoring system has been employed to check the feeding rate during testing.

The powder feeder significantly affects the powder flow. In the prototype station at the University of Salerno, the powder delivery system consists of a hopper powder feeder from Medicoat. This kind of feeder is based on the volumetric control of the powder flow, which is continuously fed to an oscillating channel from a hopper as shown in the following figure.



Figure 3.5: Medicoat vibrating powder system and oscillating channel

The quantity of delivered powder is determined based on the vibrational frequency of the conveyor. A relation must be found to express the mass flow as a function of input voltage inducing vibration to the conveyor by a command and control unit Reovib 168. The voltage signal changes in the range 0-10 V.

It is well known that a carrier gas is needed to the purpose of delivering the powder. In this case, helium has been considered. Therefore, an additional system to set the carrier and the shielding gas flow is required.

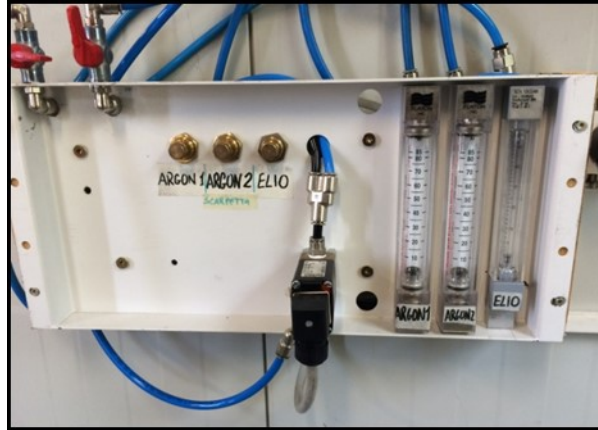


Figure 3.6: System regulator of Helium and Argon gas

As shown in the following figure, the carrier gas input is the brass fitting close to the plug and is connected via a 3/8" pipe. A similar pipe is used for the powder output, connected via a stainless steel fitting. Since the metallic powder could cause the formation of electrical discharges, an antistatic cable has been used.

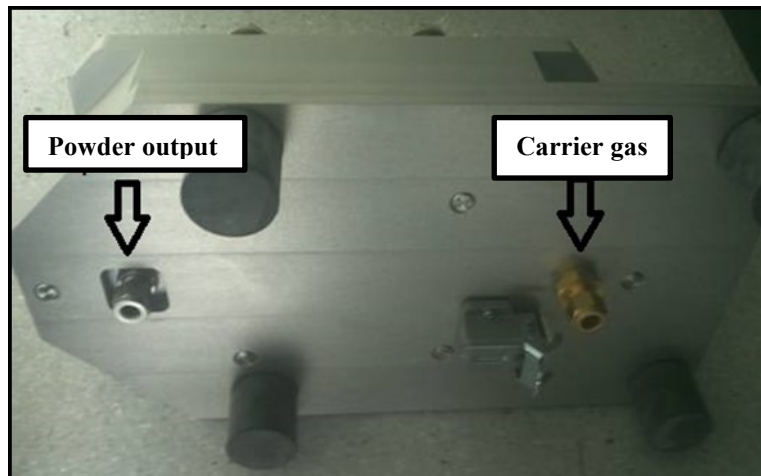


Figure 3.7: Gas and powder fitting

The unit as provided by Medicoat presents some technological limits: it is recommended for a variable shielding gas flow rate in the range of 0-10 l/min and the maximum pressure should not exceed 6 bar. The powder feeder, as already mentioned, is connected to a frequency converter REOVIB MFS 168. It is a command and control system which generates an output frequency

independent of the main supply parameters, in particular the set output frequency corresponds to the frequency of mechanical oscillation of the conveyor, thus allowing regulation of the powders flow. This frequency may be set manually or automatically. The setting of the vibration is adjusted via an external control voltage in the range 0÷10 V.

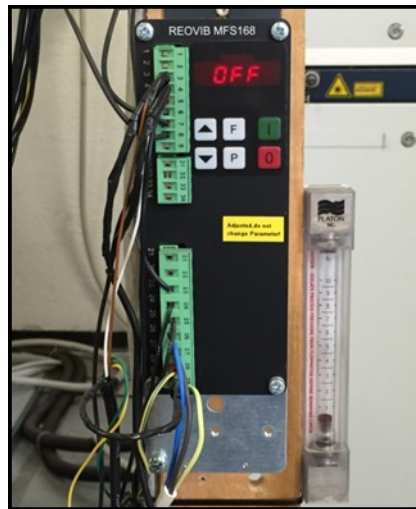


Figure 3.8: Drive unit component

In order to check the steadiness of the powder flow, a flow watch sensor connected to a led display unit is used in the process. This component checks if the powder rate is constant during the process to ensure the proper execution. The flow watch supervises the powder flow needed for the coating application. It is very important because hidden defects into the coating could be the result of a disturbed powder flow. To the purpose of a reliable measurement, the flow watch has been connected as near as possible to the powder line output. Then, it has been connected with the LED display that indicates precisely the trend based on the number of LEDs turned on: 10 LEDs are available and are proportional to the powder flow from 0 to 100%.

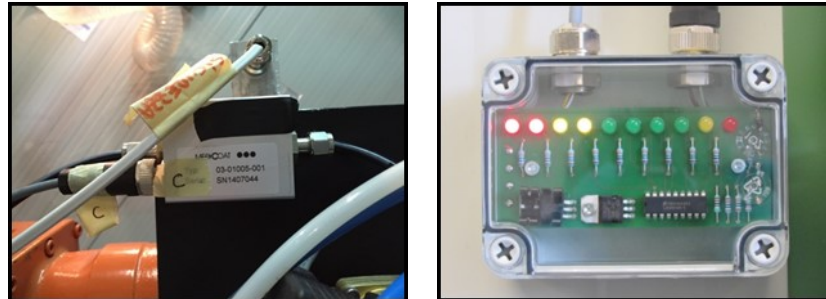


Figure 3.9: Flow-watch and display unit

3.2.3 Manipulating system

A six-axis industrial robot (ABB IRB 2400) with a dedicated controller is used to manipulate the laser beam over the cladding substrate. Its characteristics are given in the following table:

Table 3.2: Manipulate system technical characteristics

Model	IRB2400/16 Type B
Carrying capacities	16 kg / 1.55 m
Speed	100 ÷ 1000 mm/s
Absorption	0.37 ÷ 0.67 kW



Figure 3.10: ABB industrial robot

3.2.4 Laser Cladding head

Laser cladding head is composed of an optical system, with a collimator and focusing lens, and a nozzle to deliver the powder to the melt pool.

As known, laser cladding, in contrast to laser cutting or welding, requires a larger laser spot. This is achieved by moving of the focal plane. In particular, the cladding head is equipped with a motorized (mobile) collimator lens, which changes the beam profile. A voltage set drives the movimentation of the lens as described in the following section.

The collimator length is the distance between the end of the fibre cable and collimator lens position, instead the focal length is the distance between the focal lens and the point of minimum spot laser diameter. In this research the focal length of the lens and the focal length of collimation are respectively 200 mm and 100 mm.

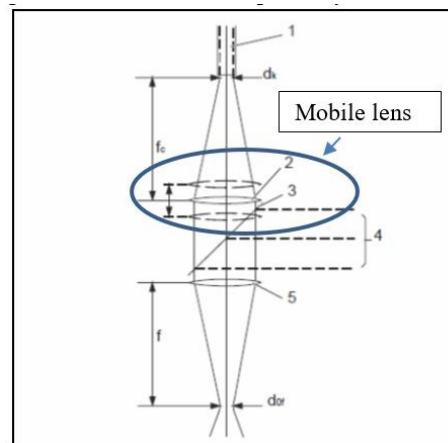


Figure 3.11: Collimating and focusing lens

The minimum spot laser diameter is called focal diameter d_{of} and depends on the diameter of the fiber cable, the used collimator and focusing lens, in according to the following relation:

$$d_{of} = \frac{f}{f_c} d_k$$

where

d_{of} : focal diameter [mm]

f : focal length [mm]

f_c : collimating length [mm]

d_k : fibre cable diameter [mm]

The minimum laser spot diameter in this configuration is hence:

$$d_{of} = \frac{200}{100} \cdot 0.300 = 600 \mu\text{m}$$

3.2.5 Beam nozzle

The laser cladding head is composed of a three-beam nozzle to blow the powder on the base substrate in the deposition line: namely, three stream cones of metal powder are provided coaxially around the laser beam; each stream is injected by a separate inert gas conveying flow, then the powder meets the laser beam in the cladding area on the top surface of the substrate. The nozzle used is the model SO12, with stand-off distance of 12 mm, corresponding to a powder flow diameter onto the surface base material of 2.5 mm. The highest laser power which could be employed with this nozzle is 3 kW.



Figure 3.12: three-beam nozzle

3.3 Experimental setup

The component considered for laser cladding repairing is a nozzle guide vane (Figure 3.13) made by means of investment casting. A number of research papers in the literature have been referred [10, 11, 12].

First of all, preliminary tests have been carried out by powder laser cladding technique using the prototype station available. The powder for repair is homologous to component material.



Figure 3.13: nozzle guide vane

In the experimental test, two different nickel alloy have been considered: C1023 and CM247LC. These superalloy are widely used in manufacturing of equiaxed nozzle guide vanes and seal segments for aero gas turbines, especially in low-pressure turbines. However, in spite of its extensive applications in many different types of engines, this alloy is considered difficult to be welded, repaired, and machined, although some studies have successfully addressed these issue for C1023 [13].

The high strength of this alloy is mainly due to a fine distribution of γ' (gamma prime) precipitates that are formed directly after casting. The quick formation of these precipitates does not allow processing of components in a soft condition, such as that of other superalloys in a solution annealed state.

However, it is desirable to achieve some kind of temporary soft condition that could improve the manufacture of C1023 and CM247LC components.

3.3.1 Process tuning

Before starting the experiments, tuning of the process has been required. The laser cladding process tuning has been carried out in according to the next steps:

- Carrier and shielding gas setting;
- Powder mass flow setting as a function of the drive unit voltage and setting of the head position in order to focus the powder to the workpiece;
- Laser spot diameter as a function of the collimator lens position setting by a voltage signal.

Two inert gases are required:

- Shielding gas, in order to protect the clad on the surface of the workpiece from the air of the external environment;
- Carrier gas, to transport the metal powders from the conveyor to the nozzle.

In this case, argon is used as both shielding gas and carrier gas. Moreover, in order to facilitate the process analysis influenced by a lot of parameters, carrier gas and shielding gas have been defined at a constant value of pressure and mass flow.

3.3.2 Powder mass flow setting

The quantity of delivered powder is determined based on the vibrational frequency of the conveyor. Therefore, a relation must be found to express the mass flow as a function of input voltage inducing vibration to the conveyor by a command and control unit Reovib 168. The voltage signal changes in the range 0-10 V.

After setting the carrier gas flow rate, a number of trials are carried out changing the voltage signal. Each trial is 5 min long, and the container, used to collect the powder, is weighed before and after the trial so to evaluate the powder flow rate. Argon as carrier gas has been set at 3,5 bar and 3 l/min.

Two different nickel-base superalloy powders with mean particle size ranging from 50 to 100 μm have been used. The feeding powder has been preliminary dried at 100 °C for one hour.

In the next table, the value of the parameters are shown.

Table 3.3: Powder C1023 mass flow as a function of the voltage

Voltage [V]	Powder mass flow [g/min]
3	3,7
4	4,3
5	5,8
6	7,2
7	9,6
8	11,2
9	12,9
10	15,5

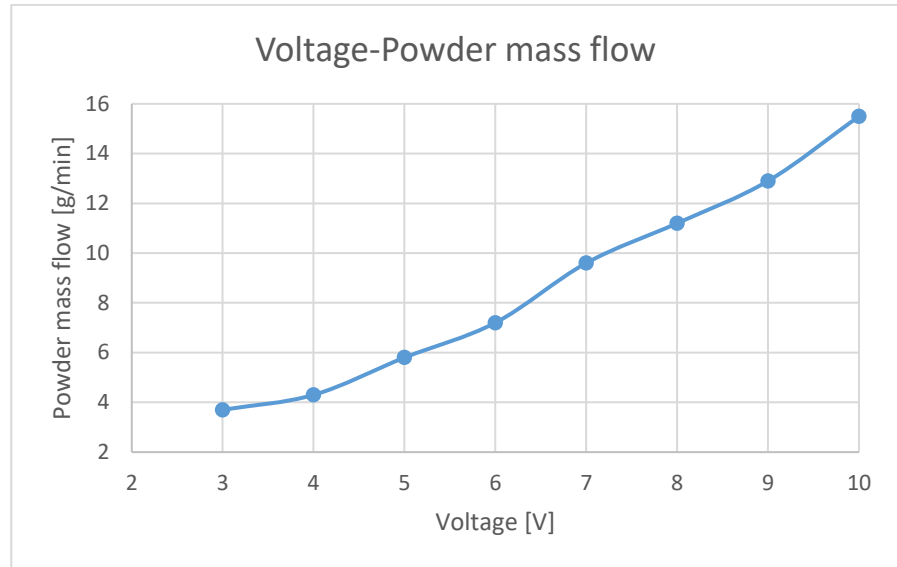


Figure 3.14: Powder C1023 mass flow as a function of voltage

Upon setting of the powder mass flow, the head stand-off has been set so that the laser beam and the powder flow are focused onto the surface. With a three-way nozzle the stand-off has been allowed between the tip of the feeding nozzle and the reference plane, so that the minimum size of the streams is delivered to the surface of the component. To this purpose, the distance between the end of the nozzle and the workpiece must be 12 mm (Figure 3.15).

A tilting angle of 4° has been given to the laser head, in agreement with common practice, to prevent back-reflections from entering the optics train.

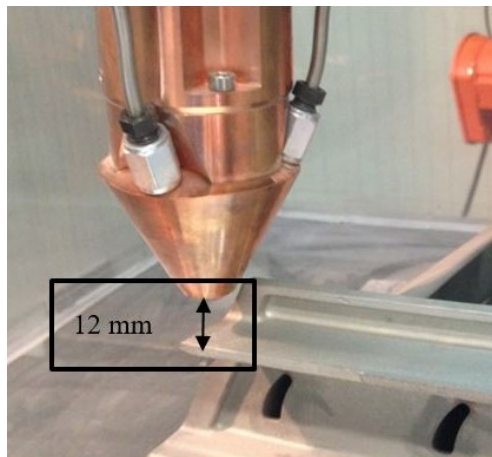


Figure 3.15: Position of the head

3.3.3 Laser spot diameter setting

Since the focal beam diameter is 0.6 mm and a laser spot of 3-5 mm is needed, the laser beam must be defocused. Hence defocusing of the beam is achieved through a mobile collimator lens which changes the beam profile. Defocusing the laser beam through the handling of the laser head is not possible, because the powder beam profile would be affected and would result in focusing far from the workpiece.

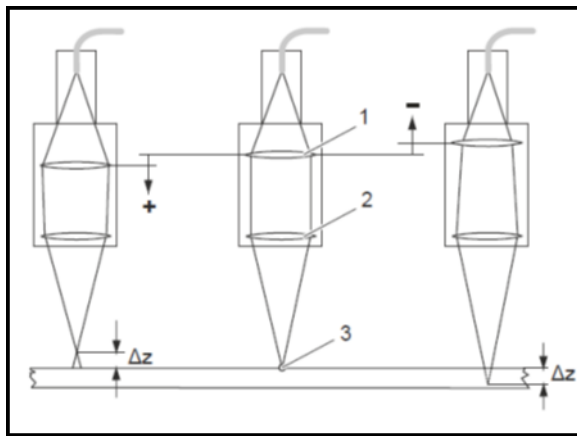


Figure 3.16: Setting of the collimator lens

Before analyzing the relationship between the voltage and the focal position Δz , a function of the spot laser diameter onto the surface has been found via the caustic equation. Namely, the Rayleigh range and the angle of divergence are defined as follow:

$$z_R = \frac{d_0^2}{4 * \frac{BPP}{1000}} = 7,5 \text{ mm}$$

$$\vartheta = \left(\frac{4 * BPP}{d_0 * 1000} \right) = 0,08 \text{ rad} = 4,6^\circ$$

From the caustics equation we know that:

$$d(z) = d_0 \sqrt{1 + \left(\frac{z}{z_R} \right)^2}$$

In the following graphic the relationship between the laser spot diameter and the Δz is given.

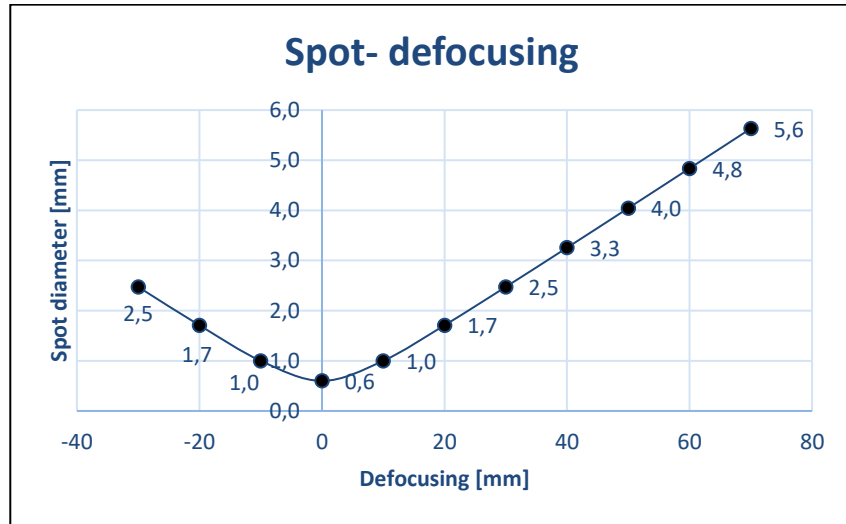


Figure 3.17: Spot diameter as a function of defocusing

A correlation between the position of the focal spot and the voltage of the collimator lens can be defined. In particular the focal position in the control range is proportional to the setpoint voltage. The setpoint voltage to be entered is calculated according to the following formula:

$$V = \frac{\Delta z - B}{A}$$

Where:

Table 3.4: Setpoint voltage and focal position

Parameter	Description	Unit
V	Setpoint voltage	V
Δz	Focal position	mm
	$\Delta z = 0$ Focal point is on the workpiece surface	mm
	$\Delta z > 0$ Focal point is above the workpiece surface	
	$\Delta z < 0$ Focal point is in the workpiece	
A	Coefficient A	mm/V
B	Coefficient B	mm

Depending on the focal length of the lens and the focal length of collimation the following values are given for the coefficients A and B.

Table 3.5: Coefficients for the Setpoint voltage calculation

Focal lengths	A	B
$f=200$ mm	4,82 mm/V	21,03 mm
$f_c=100$ mm		

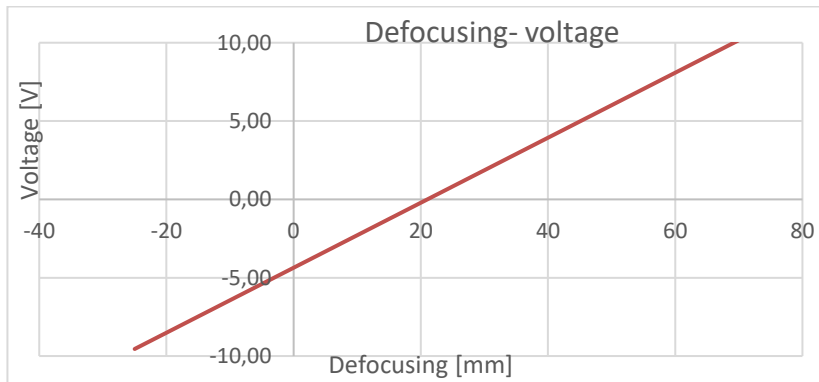


Figure 3.18: Laser beam defocusing as a function of voltage

3.4 Experimental procedure

At first stage, preliminary trials in form of single deposition over 3.3 mm thick Ni-based plates have been conducted to investigate the response of the base metal to laser-aided DMD with injection of homologous powder. The main input variables have been selected based on the referred literature: the effects of laser power P and laser scanning speed s have been discussed for given powder feeding rate of $13 \text{ g}\cdot\text{min}^{-1}$ and given positive defocusing providing a processing laser beam diameter of 3 mm on the substrate. A full-factorial, 2-factor, 2-level experimental plan has been considered, with the addition of the central point (Figure 3.19); according to the literature [14] and previous studies [15] on DMD of metal powder, setting a 2-level plan is expected to be valid, as only weak interactions are in place. Therefore, five processing conditions of trial resulted; three replications have been considered for each testing point to evaluate the average responses. A random testing procedure has been arranged.

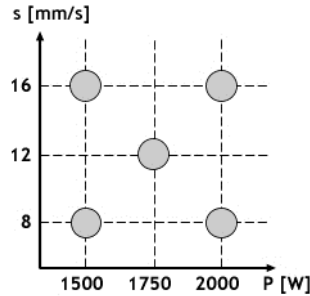


Figure 3.19: Processing conditions in preliminary trials

The general approach to find the operating window is given in the following. In terms of specific delivered power and feeding, the processing levels are deemed to agree with similar works in the literature [16] and have been properly adjusted so to result in valuable outcomes (i.e., preventing detachment, balling, lack of clad, excessive dilution or surface oxidation of the traces). With respect to speed, this must be taken below a threshold value so to promote homogenization of the interface between trace and substrate. Defocusing of the laser beam has been required to improve catchment, which is crucial when DMD is performed by powder injection [1]; namely, the size of the melting pool has been increased so to match the powder stream cones; lower irradiance has been benefited as well, to the purpose of reduced penetration depth and dilution in turn. The flow rate for both carrier and shielding argon has been taken as a constant, 3 and 10 l·min⁻¹, respectively.

The geometry as a function of the processing parameters has been discussed: in agreement with common practice in DMD, trace width in the cross-section, depth and height with respect to the reference plane have been measured (Figure 3.20) over three specimens for each sample in order to assess the main effects.

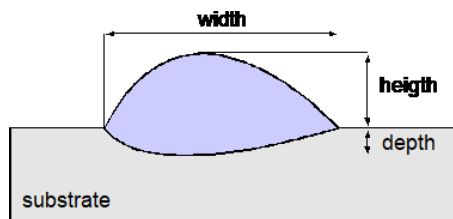


Figure 3.20: Scheme of the geometrical responses in the cross-section

Moreover, dilution must be investigated. Although a chemical definition is usually given involving the weight percentage composition of the main alloying elements in the substrate with respect to the reported metal [1], it has been shown that an alternative geometric definition can be given [17]; namely, the ratio of the fused (i.e., mixing) area of the substrate to the total area in the

transverse cross-section can be measured. To a first approximation [18], this can be even given as:

$$\text{dilution} = \frac{\text{depth}}{\text{height} + \text{depth}}$$

The geometrical approximation involving depth and height has been used in this study.

3.4.1 Composition

The powder has been preliminarily inspected in terms of size and geometry, since specific requirements of shape must be matched to the purpose of proper manufacturing. Spherical and near-spherical particles have been found (Figure 3.21), thus efficient flowing and layer packaging are expected to result in uniform melting.

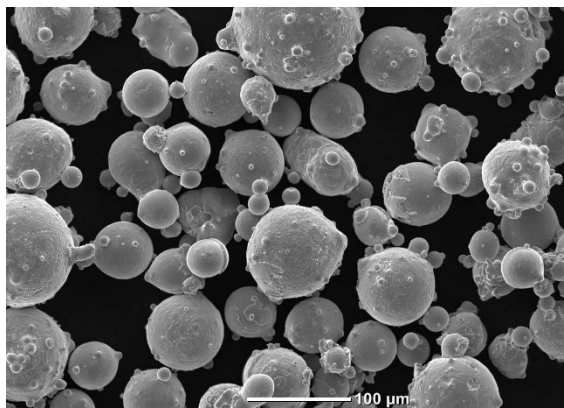


Figure 3.21: Electron microscopy of pre-alloyed, argon gas-atomized, virgin Ni-based powder

The chemical composition of both the substrate and the powder has been investigated via areal and punctual EDS inspections. An average overall fitting coefficient of the quantitative analysis (i.e., the residual between the acquired and the synthetic spectra) of 2.4% and 2.5% resulted for the substrate and the powder, respectively; certain elements below 1% wt. have not been detected.

Table 3.6: Average chemical composition (wt.%) of substrate and virgin powder resulting from EDS inspections

	Ni	Cr	Co	Mo	Al	Ti
Substrate	59.4	14.8	10.6	7.7	4.5	3.0
Powder	58.4	15.5	10.3	8.3	4.0	3.5

3.4.2 Single-trace deposition

At this stage, the nozzle centering of the laser beam and the powder transfer streams have been preliminarily checked. The regular stream of powder was also checked; the flow rate has been fixed at 13 g / min, as determined by previous exploratory tests with same composition and granulometry powders of $50 \div 100 \mu\text{m}$; due to possible risk of reflection, all depositions have been conducted by tilting the 4° head in the forward direction. The stand-off between the tip of the nozzle and the surface is fixed at 12 mm. Finally, argon has been used both for powder transport and for oxidation protection. The constant process parameters are shown in Table 3.8.

Table 3.7: Process conditions

Condition	Power [W]	Speed [mm/s]
1	2000	8
2	1500	8
3	2000	16
4	1500	16
5	1750	12

Table 3.8: Constant process parameters

Stand-off	12 mm
Defocusing laser beam	32 mm
Focused spot diameter	3 mm
Powder flow rate	13 g/min
Argon flow rate for powder transport	3 l/min
Argon flow rate for oxidation protection	10 l/min

Based on visual inspections (Table 3.9), all of the conditions of the experimental plan resulted in successful processing, therefore inert shielding is deemed to be effective. The deposited metal has been found to be sound, at macroscopical scale at least. Nevertheless, a number of indications (i.e., surface cracks) have been found via FPI (Fluid Penetrant Inspections). These are mostly common when the conditions with higher thermal input are investigated. Based on this, the condition with 1.5 kW power, 16 mm·s⁻¹ speed, resulting in the lowest thermal input (approx. 95 J·mm⁻¹) within the investigating domain should be selected.



Figure 3.22: Visual appearance of single trace deposits

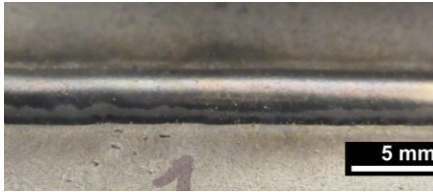
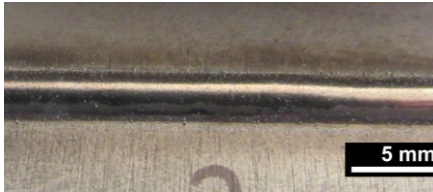
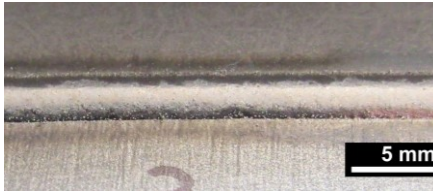

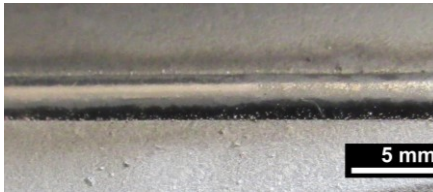
Condition	Power [W]	Speed [mm/s]	Clad aspect
1	2000	8	 Micrograph showing the clad surface for condition 1. The surface is relatively smooth with a dark, thin layer. A scale bar in the bottom right corner indicates 5 mm.
2	1500	8	 Micrograph showing the clad surface for condition 2. The surface shows some vertical striations and a dark layer. A scale bar in the bottom right corner indicates 5 mm.
3	2000	16	 Micrograph showing the clad surface for condition 3. The surface shows some vertical striations and a dark layer. A scale bar in the bottom right corner indicates 5 mm.
4	1500	16	 Micrograph showing the clad surface for condition 4. The surface shows some vertical striations and a dark layer. A scale bar in the bottom right corner indicates 5 mm.
5	1750	12	 Micrograph showing the clad surface for condition 5. The surface is relatively smooth with a dark, thin layer. A scale bar in the bottom right corner indicates 5 mm.

Table 3.9: Details of the traces for each processing condition

As regarding the soundness at microscopical scale, a number of micropores, 60 μm at most in size, have been found in the cross-section (Figure 3.23). One may assume this would not result in rejection at quality checks. Indeed, since no specific regulations are currently available for DMD, usual international standards for quality in laser welding [19] are borrowed: the standard is matched in terms of allowed pore size and accumulated length. Interestingly, the total amount of pores did not show any correlation with the processing parameters, therefore a random sources must be ascribed to; with this respect, it has been suggested that pores may be induced by trapped processing gases [20].

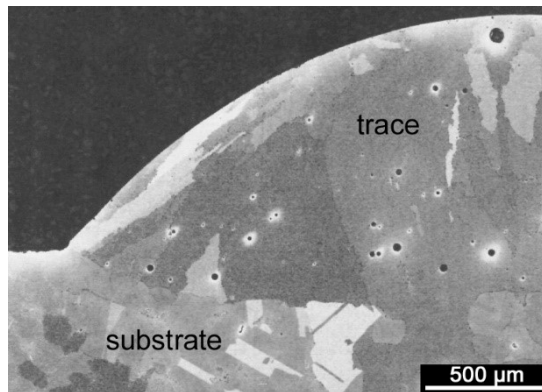


Figure 3.23: Micropores in the fusion zone (1.5 kW laser power, 16 mm·s⁻¹ speed)

Irrespective of their possible imperfections in terms of cracks and porosity, all of the processing conditions of the experimental plan are valuable to draw a general overview of the process in terms of dependence on the governing factors. Trace width, depth, height and dilution have been measured (Table 3.10) and discussed via main effect plots (Figure 3.24) as a function of the processing parameters.

Table 3.10: Average geometrical responses for each processing condition

Power [W]	Speed [mm·s ⁻¹]	Width [mm]	Depth [mm]	Height [mm]	Dilution [%]
1500	16	3.43	0.20	0.80	20%
2000	16	3.59	0.22	0.71	24%
1750	12	3.64	0.28	0.90	24%
1500	8	3.95	0.31	1.54	17%
2000	8	4.15	0.34	1.23	22%

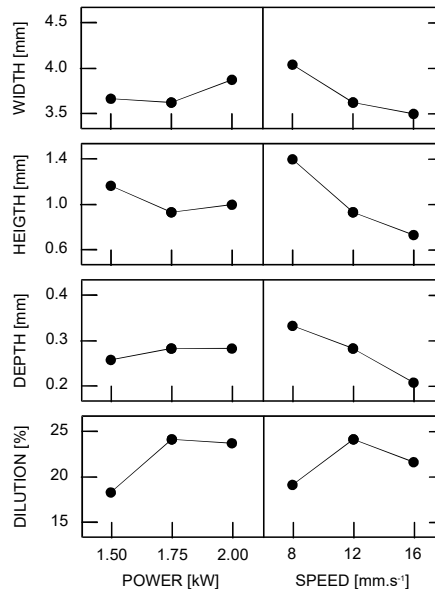


Figure 3.24: Main effect plots for mean responses as a function of the governing factors

As expected, width is found to increase for increasing power, decrease for increasing speed otherwise, as a reduced thermal input is provided. The same reasons apply for depth. As regarding the height, an increase of power yields a decrease in height as a larger pool is induced, hence powder is laid over a wider trace; on the other hand, an increase in speed yields a decrease in height since the feeding nozzle is moved with the laser head, hence less powder is laid per unit length. Dilution is found to be lower than 25%, hence the operating window is deemed to be suitable for both repairing and fabrication of parts; its results from concurrent effects of the governing factors on depth and height. All of the trends are in agreement with similar findings on DMD of metals [15, 21]. For each response, no interactions among the governing factors are inferred based on the interaction plots, therefore the choice of a 2-level plan is deemed to be consistent and effective.

All conditions are acceptable to visual inspection and have no oxidation or geometric irregularity, so all of them have been transferred to the next stage of experimentation, or to the execution of side-by-side and partially overlapped depositions for the purpose of repairing damage to the airfoil.

3.5 Depositions for repairing of damages

In the actual industrial process, grooves are made before DMD to preliminarily remove any local imperfections upon improper casting of the part.

The outer surface of the component has been machined to reproduce the surface conditions that could result when damage or imperfections are preliminarily prepared for repairing. In particular, five holes (Figure 3.25) of 3.5 mm diameter have been considered. The holes are marked by the numbers corresponding to the process conditions; the component has been carefully positioned and oriented under the deposition nozzle (Figure 3.26) so that the addition of powder is made in an orthogonal plane about the laser beam propagation direction so as to maintain irradiance constant.

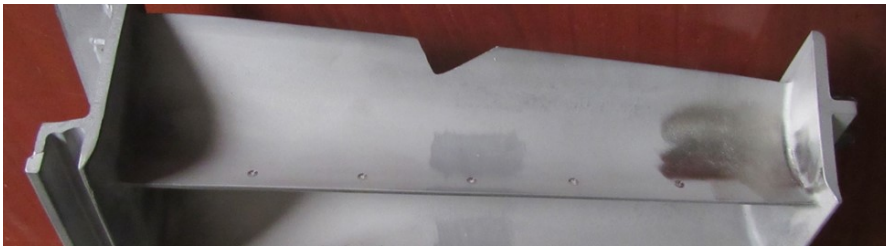


Figure 3.25: damage



Figure 3.26: Align the component with respect to the deposition direction

For each hole to be properly filled and coated, two deposition traces have been performed with a constant offset of 0.8 mm with respect to the reference points H and K on the theoretical circumference of the hole edge (Figure 3.27).

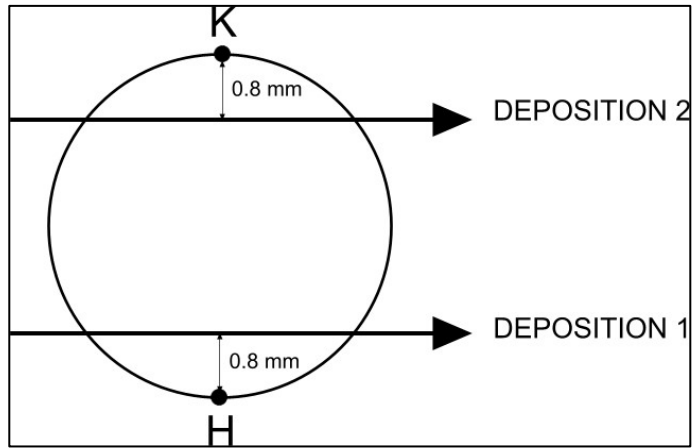


Figure 3.27: Deposition scheme

After the deposition of the first track the surface has been cleaned with steel brushes and acetone before the deposition of the second one. All the process conditions resulted in proper local reconstruction; a local discoloration due to oxidation has been observed (Figure 3.28). The details of the visual aspects are shown in Table 3.11.

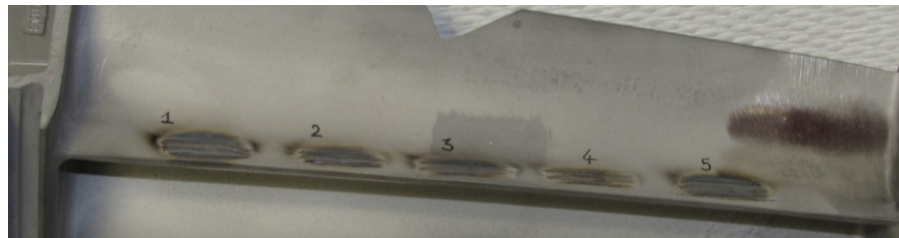


Figure 3.28: Visual aspect of the deposition traces on the component

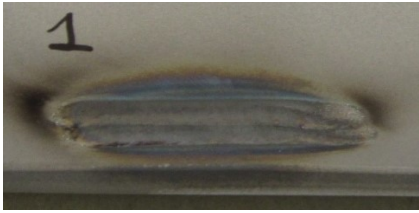
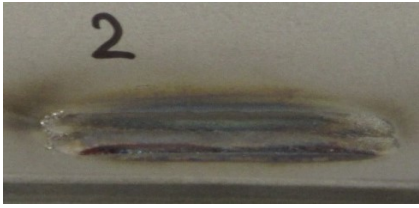
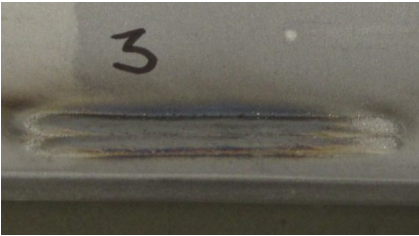
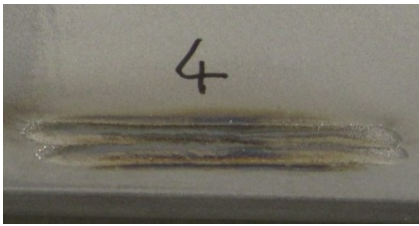
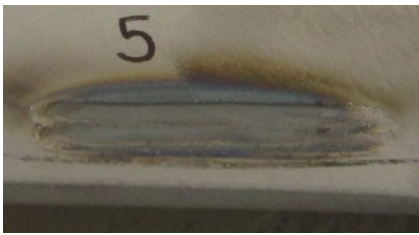
Condition	Power	Speed [mm/s]	Visual aspect
1	2000	8	
2	1500	8	
3	2000	16	
4	1500	16	
5	1750	12	

Table 3.11: Visual aspect of the deposition traces on the component

In order to assess the feasibility of this repair technology in conditions closer to real cases, further testing has been carried out with filling rather than

deposition, aiming to provide an appropriate repair strategy and a suitable deposition scheme, since side-by-side and overlapping deposition are usually required, depending on the local imperfection to be repaired. To this purpose, the company supplier performed a number of slots by means of front milling (Figure 3.29) with a mean depth of 2.2 mm, a mean width of 6.3 mm and a length ranging from 15 to 19 mm, those simulating the actual condition resulting from material removal of cast imperfections prior to cladding. The grooves to be filled have been progressively numbered from 1 to 5.

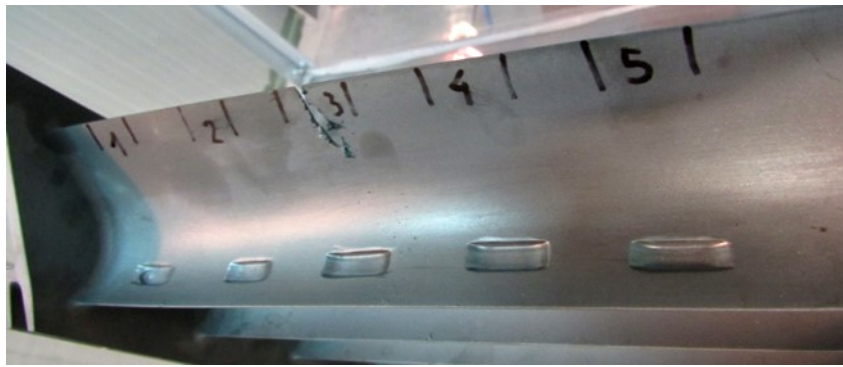


Figure 3.29: slots on the nozzle guide vane

Based on the analysis of the preliminary trials, the geometric dimensions of the traces in the optimal condition are known, although complete and proper actual repairing must be made by means of multiple layers and side by side depositions. From previous experience in the field of DMD of superalloys, it is also known that the geometric size of single-deposited traces on flat surfaces may differ from multi-layer, side-by-side deposition; the extent of this difference is not predictable and must be investigated. Moreover, a number of deposition strategies should be compared to assess a proper method of repairing. Three strategies have been proposed, the slots 2, 3 and 4 have been considered. The offset of each deposition for a given layer is measured with respect to the slot edge (Figure 3.30); since a larger width than 2 mm is expected, overlapping is allowed, hence a continuous process is made.

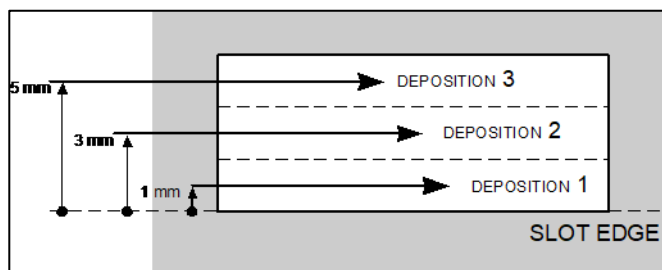


Figure 3.30: Horizontal section, offset of the deposition axis with respect to the slot edge

The order of deposition of the traces (Figure 3.31) for a given deposition strategy is the same for each layer (Figure 3.32). Once the deposition of each layer is completed, the stand-off is progressively adjusted of 0.8 mm, so to locate the beam focus at the new surface. Four layers of deposition have been required, one of them being incomplete in strategy 2.

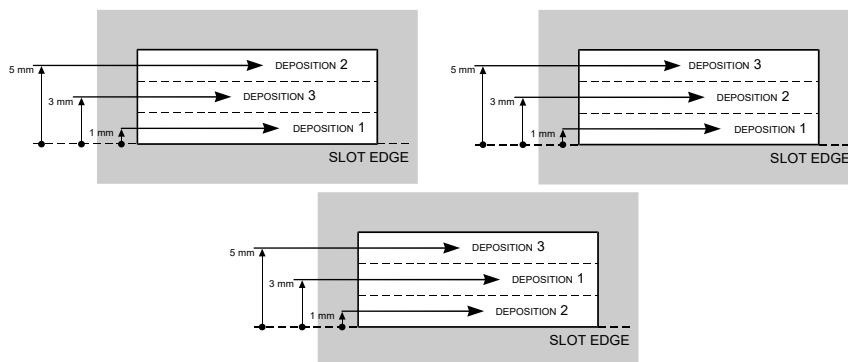


Figure 3.31: Horizontal section, order of track deposition in strategies 2, 3 and 4

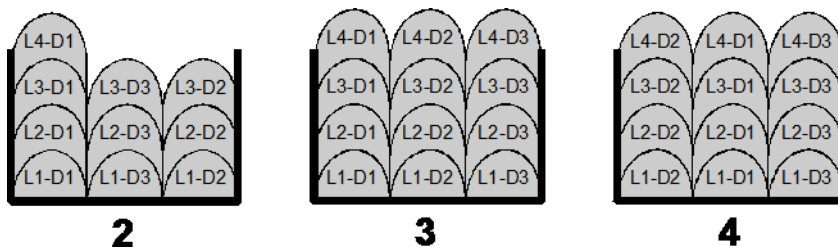


Figure 3.32: Cross section, deposition order for the strategies under consideration (L identifies level, D deposition)

All traces have been made with the optimum process parameters previously identified; after each deposition, the component has been cleaned of excess powder that could affect the next deposition. In the visual aspect, the traces are homogeneous and uniform (Figure 3.33).



Figure 3.33: Visual aspect of the component at the end of deposition strategies

Upon single and multi-trace processing, solution heat treating at 1190 °C, in vacuum, for one hour has been performed; then, non-destructive tests in form of FPI have been conducted.

With respect to repairing, eventual post-processing of the machining allowance (i.e., part of the last deposition exceeding the groove) has been required.

Uniform fusion resulted (Figure 3.34); the total percentage of pores is found to be consistent with respect to the single-trace counterpart. As a consequence, the referred standard is still matched [19]. One may infer the process can be successfully shifted from single- to multi-trace depositions within a defined bound.



Figure 3.34: Longitudinal cross-section of the groove upon repairing and milling of the allowance

3.6 Repair of a superalloy CM247LC guide nozzle vane

Laser cladding technique has been also evaluated for repairing a guide nozzle vane of nickel-based alloy, CM247LC, which is considered to be difficult to weld for propensity to form hot cracks. In this case preliminary tests have been conducted to repair a surface damage with the prototype station available at L5 Laboratory of the University of Salerno.

The multijet three-way nozzle has been used. Powder for repair is homologous to component material.

In order to define the optimum values of power and processing speed, some linear depositions have been carried out in the form of a single track with lengths of about 30 mm on flat parts of the component. The process parameters already tested on the component in Alloy C1023, for which no particular criticalities have been highlighted, have been considered. Therefore, a two-factor experimental plan with a central point has been performed (Figure 3.35) with a total of 5 test conditions, listed in Table 3.12.

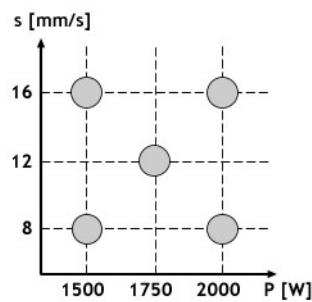


Figure 3.35: Levels of process factors and test conditions

Table 3.12: Process conditions

Condition	Power [W]	Speed [mm/s]
1	2000	8
2	1500	8
3	2000	16
4	1500	16
5	1750	12

All the preliminary activities, such as powder flow adjustment, nozzle centering and standoff definition have been performed in according to previous trials. The flow rate was fixed at 5 g / min. Due to possible risk of reflection, all depositions have been conducted by tilting the 4 ° head in the forward direction. Argon has been used both for powder transport and for oxidation protection. The constant process parameters are shown in Table 3.13.

Table 3.13: Process parameters maintained constant

Stand-off	12 mm
Defocusing laser beam	32 mm
Focused spot diameter	3 mm
Powder flow rate	5 g/min
Argon flow rate for powder transport	3 l/min
Argon flow rate for oxidation protection	10 l/min

In according to visual inspection (Figure 3.36), the process conditions are suitable for deposition, and the parameters are suitable to adequate adhesion of the powder to the component. The visual aspects of individual deposition traces, by stereoscopic microscope, are shown in Table 3.14. However, cracks are present in conditions 1 and 2; in particular, in both cases there is a crack at the end of the deposition (Figure 3.37) [22]. A smaller crack, is present in condition 3 (Figure 3.38).



Figure 3.36: Visual aspect of single traces deposits


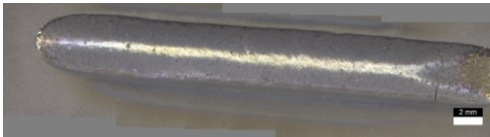
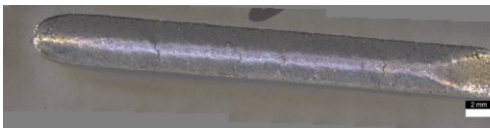
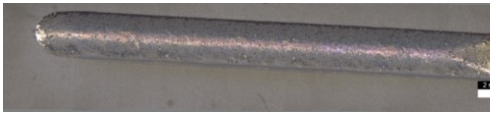
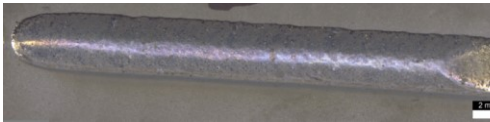
Condition	Power [W]	Speed [mm/s]	Visual aspect
1	2000	8	
2	1500	8	
3	2000	16	
4	1500	16	
5	1750	12	

Table 3.14: Visual aspect of the traces of deposition

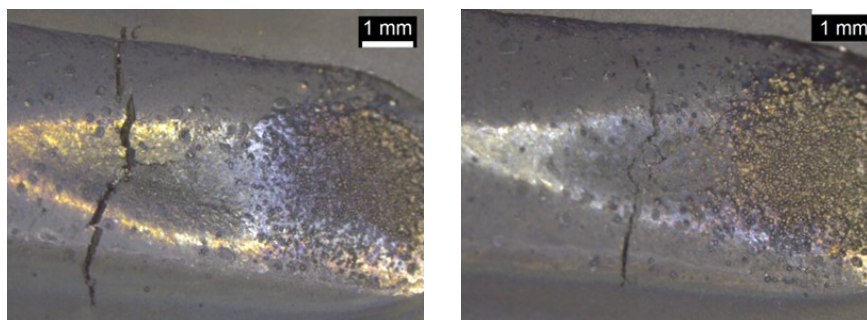


Figure 3.37: Detail of the cracks on the depositions under conditions 1 and 2

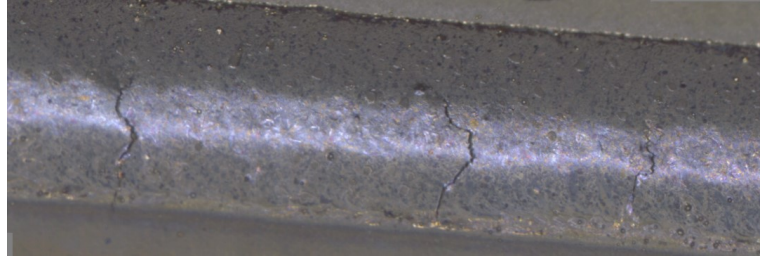




Figure 3.38: Detail of the cracks on the conditions 3

Indications have not been found in conditions 4 and 5 which have been replicated (4B and 5B conditions) to the purpose of deeper inspections. The visual aspects are shown in Table 3.15.

Table 3.15: Visual aspects of replicas in according to conditions 4 and 5

Condition	Power [W]	Speed [mm/s]	Visual aspect
4B	1500	16	
5B	1750	12	

With respect to deposition of C1023, processing of CM247LC has been found to be challenging. Therefore, proper additional studies are required before shifting the application to a real component.

3.7 Conclusions

In this chapter, the effectiveness of DMD of Ni-based powder over homologous surfaces has been proven. The trends of the main responses as a function of the main governing factors power and speed have been discussed; it has been shown that dilution can be restrained below 25%, hence resulting in low affection of the base metal. In this frame, upon preliminary investigation of single-trace depositions, a proper processing condition has been found; it is worth noting that although wider and higher traces may result otherwise, higher thermal input would be required, with consequent possible cracks and increased amount of detrimental Laves phases.

In agreement with similar findings in the literature about Ni-based superalloy, a condition with low thermal input has been preferred indeed, then shifted to multi-trace repairing within a defined bound. A square-shaped groove slot has been repaired. Although a number of micropores have been found, the process is deemed to comply with usual referred standards.

References chapter III

- 1) E. Toyserkani, A. Khajepour e S. Corbin, Laser Cladding, CRC Press LLC, 2005.
- 2) L. Li e J. Mazumder, «Study of the mechanism of laser cladding processes. Laser processing of materials.» in AIME Annual Meeting, Los Angeles, CA, USA, 1985.
- 3) E. Foroozmehr, Laser Powder Deposition, VDM Verlag Dr. Muller, 2010.
- 4) W. Steen, «Laser Material Processing» Springer, 2003.
- 5) P. Vuoristo, J. Tuominen e J. Nurminen, «Laser coating and thermal spraying-process basics and coating properties».
- 6) Weerasinghe e W. Steen, «Laser cladding by powder injection» in ASME, New York, 1983.
- 7) H. Mei, G. Tao e R. Kovacevic, «Closed loop control of 3D laser cladding based on infrared sensing» Advanced Manufacturing, pp. 129-137
- 8) B. Graf, S. Ammer, A. Gumenyuk e M. Rethmeier, «Design of experiments for laser metal deposition in maintenance, repair and overhaul applications» Elsevier, vol. 11, pp. 245-248, 2013.
- 9) P. Balu, P. Leggett e R. Kovacevic, «Parametric study on a coaxial multi-material powder flow in laser-based powder» Journal of Materials Processing Technology, vol. 212, p. 1598– 1610, 2012.
- 10) Y. Kathria, «Some aspects of laser surface cladding in the turbine industry» Surface and coating technology, vol. 132, pp. 262-269, 2000.
- 11) Z. Xiong, G. Chena e X. Zeng, «Effects of process variables on interfacial quality of laser cladding on aeroengine blade material GH4133» Journal of materials processing technology, vol. 209, pp. 930-936, 2009.J.
- 12) Caiazza F, Alfieri V, Sergi V, Tartaglia A, Di Foggia M, Niola A (2016) Technical feasibility of laser dissimilar welding of superalloys on casted nozzle guide vanes. Procedia CIRP 41:963-968.
- 13) Hernandez I, Subinas A, Madariaga I, Ostolaza K (2007) Improving C1023 manufacturability using two-step heat treatment. Heat Treating Progress 3:25-31.
- 14) Graf B, Ammer S, Gumenyuk A, Rethmeier M (2013) Design of experiments for laser metal deposition in maintenance, repair and overhaul applications. Procedia CIRP 11:243-248.
- 15) Caiazza F, Alfieri V, Argenio P, Sergi V (2017) Additive manufacturing by means of laser-aided directed metal deposition of 2024 aluminium powder: investigation and optimization. Advances in Mechanical Engineering 9(6):1-12.

- 16) Paul CP, Ganesh P, Mishra SK, Bhargava P, Negi J, Nath AK (2007). Investigating laser rapid manufacturing for Inconel-625 components. *Optics & Laser Technology* 39:800–805.
- 17) A. D17.1, «Specification for Fusion Welding for Aerospace Applications» American Welding Society, Miami, FL, 2010.
- 18) Ya W, Pathiraj B, Liu S (2016) 2D modelling of clad geometry and resulting thermal cycles during laser cladding. *Journal of Materials Processing Technology* 230:217-232.
- 19) American Welding Society (2001) D17.1—Specification for Fusion Welding for Aerospace Applications. AWS, Miami.
- 20) Kakinuma Y, Mori M, Oda Y, Mori T, Kashihara M, Hansel A, Fujishima M (2016) Influence of metal powder characteristics on product quality with directed energy deposition of Inconel 625. *CIRP Annals - Manufacturing Technology* 65(1):209-212.
- 21) Riveiro A, Mejías A, Lusquiños F, del Val J, Comesaña R, Pardo J, Poub J (2013) Optimization of laser cladding for Al coating production. *Physics Procedia* 41:327-334.
- 22) Kraemer KM, Ammer S, Gumenyuk A, Rethmeier M (2017) Application-oriented description of time-temperature dependent crack growth in a conventionally cast nickel-based superalloy. *International Journal of Fatigue* 96:78–88.

Chapter_IV

Reduction of surface roughness by means of laser processing over additive manufacturing metal parts

Additive manufacturing is receiving increasing interest in a wide range of industrial applications. In particular, new possibilities in lightweight design and direct fabrication of functional end-use parts are offered by selective laser sintering and melting of metal powders by means of laser irradiation [1, 2]. Extensive research, experimental trials and computational prediction are aimed to optimization of the processing parameters and the exposure strategies to set up the process [3, 4]; nevertheless, surface quality may limit the application of the part if compared with conventional metal manufacturing processes such as machining.

4.1 Surface roughness of additive manufacturing metal parts

Namely, as for any additive layer manufacturing, since the CAD model of the object is preliminary sliced into layers, the resulting contour of the real part is a stepped approximation of the nominal surface; it has been proved [5] that a staircase effect is induced (Figure 4.1: Staircase effect on the nominal surface in selective laser melting upon layering) depending on both the local theoretical curvature and the sloping angle with the building direction.

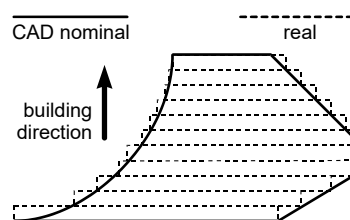


Figure 4.1: Staircase effect on the nominal surface in selective laser melting upon layering

Although the thickness of the building layers can be reduced theoretically to improve surface finish, a threshold of minimum slicing is given by the

average powder grain size. A distinct lay pattern (i.e., a distinct directional feature) is hence produced on the surface depending on the building direction. Further unevenness results on overhanging surfaces, due to either dross formation and removal of the supporting structures. As a consequence of these, depending on the technology and the average powder grain size, standards for surface finish may not be evenly matched on a single complex part. Depending on the manufacturer and the powder size, arithmetic as-built roughness usually ranges from 8 to 20 μm [6], whereas tighter standards could be required [7].

4.2 Post processing treating for surface modification

Therefore, post processing treating to the purpose of surface modification in terms of morphology and roughness is required. A number of methods can be considered: CNC machining, shot peening, sandblasting and infiltrating are suggested [8]; some are deemed to be unsuitable for local improvement on complex shapes; some are not fit to the purpose of generating different surface features on the same component; some are not capable of reliable monitoring and automation.

4.2.1 Laser surface modification

When finishing is driven by a laser beam instead, laser surface modification (LSM) is in place: namely, surface peaks are melted to fill the valleys, resulting in a smoother surface, provided that overmelting is prevented [9]. Depending on the laser operation mode, two processes are reported [10]: macropolishing with continuous wave emission and micropolishing with pulsed radiation. As a consequence of tight focusing, laser energy is effectively delivered where required, thus suitably affecting the surface and preventing uncontrolled thermal penetration, distortion of the base metal and thermal stresses leading to possible cracking and fatigue failure; furthermore, non contact processing and automation are allowed. Nevertheless, reflectivity to the laser beam in heat treating, thus absorbed energy in turn and eventual response, depend on the surface type [11], hence on the starting surface texture: the higher the starting roughness, the lower the reflectivity; the intensity distribution and pulse duration are also involved [12] on metals.

It has been shown [29, 30, 31] that the main parameter in macropolishing is energy density E_s depending on delivered power P , focus diameter D_0 and processing speed s :

$$E_s = \frac{P}{D_0 \cdot s}$$

An energy density in the order of 30 J/mm² has been proven to be effective [9] in reducing the roughness in a measure of 80% at least over metal sintered parts of bronze-infiltrated stainless steel; similar values have been considered in optimizing post processing on 316L stainless steel [6].

4.2.2 Laser surface modification by means of scanning optics

LSM by means of scanning optics can be effectively performed. Galvanometers moving laser-grade mirrors with low mass and inertia are arranged to deflect the laser beam in two dimensions [14] so to conveniently position the focus on the work-piece (Figure 4.2).

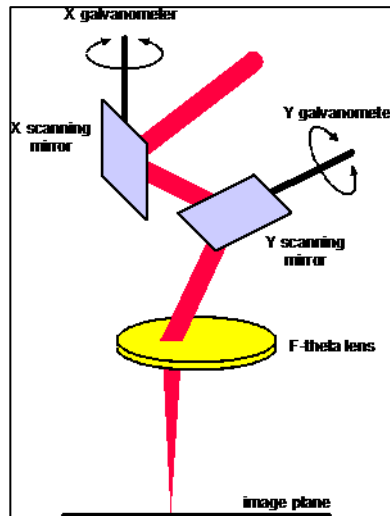


Figure 4.2. Base components and principle of laser scanning head

To provide uniform irradiance and scanning rate across the focal plane, a F-theta lens must be considered; with respect to standard flat-field scanning lenses, the need for complex electronic correction of the scanning speed is prevented. Higher speed, optimized exposure strategies and larger working distances are allowed in addition to general advantages of laser material processing with robot-moved laser heads; accuracy and capability to address complex 3D geometries are benefited. Given these reasons, processing via scanning optics is a subject of considerable interest both in research and industry to perform laser cutting, engraving, marking and surface finishing [15].

Wobbling of the laser beam along the scanning path is allowed as well (Figure 4.3). A prolate trochoid is set, being it helpful in welding in particular, to the purpose of better covering the gap or eventual fixing of possible imperfection [16]. In the frame of LSM, beam wobbling is deemed to be a valid tool to widen the scanning traces, thus reducing the overall processing time on the surface to be polished. Defocusing would result in increased width of the scanning traces as well [11]; nevertheless this would require increased beam power or reduced processing speed for a given optimum energy density.

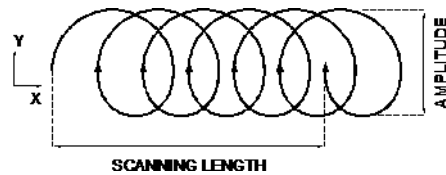


Figure 4.3: A prolate trochoid as a result of laser beam wobbling along the scanning path

For a given processing speed s , the trace width is given by the wobble amplitude A , whilst the longitudinal step between two consecutive loops is only driven by wobble frequency f according to equations:

$$X = s \cdot t + \frac{A}{2} \cos(2\pi f t)$$
$$Y = \frac{A}{2} \sin(2\pi f t)$$

Based on these, it is worth noting that s results as mean processing speed along the scanning length.

4.3 Experimental setup

LSM to improve surface topography by means of laser beam wobbling and linear scanning is discussed in this chapter; a comparison is given in terms of roughness, geometry of the fusion zone, microstructural modification and Vickers microhardness in the cross-section in order to assess the effectiveness of the process. Namely, as the starting roughness resulting from additive manufacturing depend on the sloping angle with the building direction, flat-, 45°- and upright-built samples have been considered in order to test post processing against different surface conditions. The operating window for the experimental plan has been found based on preliminary trials, a mixed experimental plan has been arranged, the main governing factors of beam laser wobbling being the wobble amplitude A to be set to 1 and 2 mm, the wobble frequency f to be set to 200 and 400 Hz, the building orientation of the sample as categorical factor. Linear scanning has also been performed to compare the results. Irrespective of the scanning strategy, LSM has been conducted at 1 kW operating laser power in continuous wave emission mode at $2 \text{ m}\cdot\text{min}^{-1}$ scanning speed, which is intended to be processing linear speed in case of linear macropolishing, mean speed in case of circular wobble path instead. A focused beam, 1 mm diameter, has been delivered to the surface.

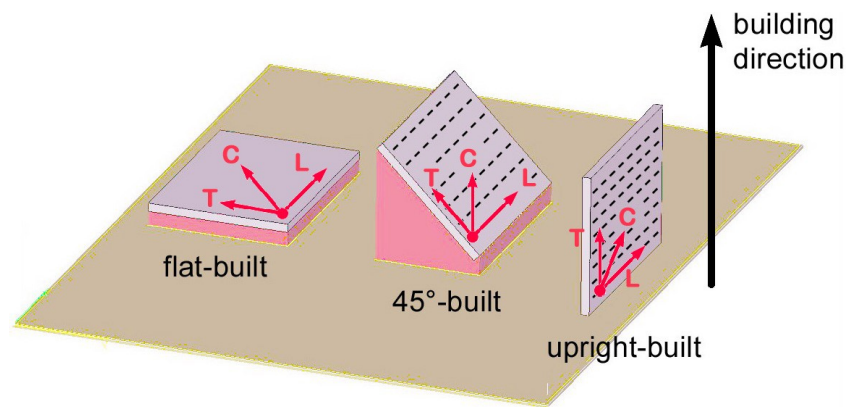


Figure 4.4: Manufacturing of the samples via selective laser melting; flat, 45° and upright building

4.3.1 Materials and methods

An EOSINT M270 commercial laser sintering system has been used to manufacture a suitable number of testing samples, 3 mm thick. Pre-alloyed, argon gas atomized, commercial EOS GP1 stainless steel powder, $20 \mu\text{m}$ mean grain size, corresponding to standard UNS S17400 chromium-copper

Reduction of surface roughness by means of laser processing
over additive manufacturing metal parts

precipitation hardening steel in terms of nominal chemical composition (Table 4.1) has been considered.

Table 4.1: Nominal composition (wt.%) of the powder; single values to be intended as maximum

Cr	Ni	Cu	Mn	Si	Mo	Nb	C	Fe
15.0÷17.5	3÷5	3÷5	1	1	0.5	0.15÷0.45	0.07	balanced

Processing power, speed, layer thickness and hatching strategies are based on preliminary trials aimed to optimization of selective laser sintering and full dense structure (Table 4.2); a nitrogen inert atmosphere has been arranged.

Table 4.2: Main features and processing parameters in selective laser melting of stainless steel powder

Gain medium	Fibre, Yb:YAG
Operating laser power [W]	195
Linear processing speed [mm·s⁻¹]	1
Hatch spacing [mm]	0.10
Layer thickness [μm]	20
Focused spot diameter [μm]	90

Flat, 45° and upright building orientations have been addressed with respect to the building plate in order to test the effectiveness of the post processing scanning strategy against different surface conditions. Supporting structures have been required on downward facing surfaces of overhanging samples as a threshold angle is exceeded, as well as below flat-built samples; nevertheless, roughness on the unsupported side has been investigated. No post processing neither heat treating for stress relieving have been conducted upon fabrication, before performing LSM.

To perform LSM, a prototype scanning optic has been used with a fibre laser (Table 4.3) and fibre delivered.

Table 4.3: Laser source and scanning optics for LSM, main technical data

Gain medium	Fibre, Yb:YAG
Operating nominal wavelength [nm]	1030
Beam parameter product [mm × mrad]	6.0
Core diameter of the delivering fibre [mm]	0.300
Scan head aperture [mm]	35
Effective focal length [mm]	1000
Image field [mm × mm]	400 × 400

A resulting scanning focus diameter D_0 of 1 mm approximately is given by:

$$D_0 = \frac{\lambda \cdot F \cdot k_G \cdot M^2}{D_{in}}$$

being λ the operating nominal wavelength of the laser beam, F the effective focal length of the F-theta lens, k_G the factor accounting for laser beam diffraction of the theoretical corresponding Gaussian beam, M^2 the beam propagation parameter and D_{in} the diameter of the laser beam when entering the optics. For a given focus diameter of 1 mm, power and speed have been conveniently set in the experimental plan aiming to provide an energy density in the order of 30 J/mm² which has been proven to be effective to the purpose of surface polishing, as discussed in the literature [6, 13]. LSM in form of single 50 mm long scanning trace, the laser beam being normal with respect to the surface of the sample, has been performed; replications of each testing conditions of LSM have been considered to average the responses.

As a carryover of a prior patented device [22], a diffuser has been developed for inert shielding to the mere purpose of this research; argon has been supplied at a constant flow rate, 40 l/min, atmospheric pressure.

As a consequence of slicing along the building direction, it is worth noting that a lay pattern would be expected over 45°- and upright-built samples; therefore, measuring traces to assess the starting roughness before LSM should be taken at right angle to the main lay, hence the same angle should be considered for LSM processing and the same should be taken for measurements upon LSM as well. All of the measurements have been conducted in compliance with the ISO standard for surface roughness testing [21]; the results are averaged among three traces at least to assess statistical significance.

Measurements on the responses in terms of heat affection have been conducted by means of conventional optical microscopy and Vickers microhardness testing; an indenting load of 0.200 kg has been used for a dwell

_____ Reduction of surface roughness by means of laser processing
over additive manufacturing metal parts

period of 10 s; a step of 100 μm has been allowed between consecutive indentations, in compliance with ISO standard [23] for hardness testing on metallic materials.

4.4 Results and discussion

The following figure shows the specimens made by selective laser melting. Flat, 45° and upright building orientations have been addressed with respect to the building plate in order to test the effectiveness of the post processing scanning strategy against different surface conditions.

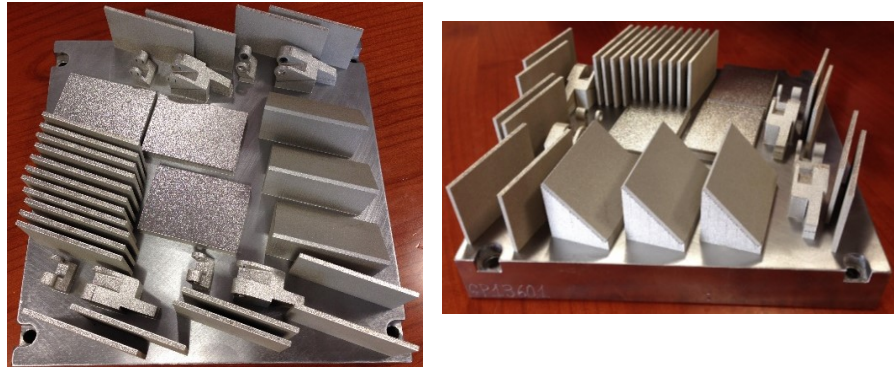


Figure 4.5: Manufacturing of the samples via selective laser melting: flat, 45° and upright building

4.4.1 Starting roughness for as-built samples

Arithmetic roughness R_a and peak-to-valley height R_z have been measured on as-built samples either in longitudinal (L), transverse (T) and crossed (C) direction with respect to layering, so to investigate any possible directional feature on as-built samples before LSM processing. It is worth noting that since no lay patterns are expected on flat build samples instead, the surface being formed by a single building layer, longitudinal and transverse direction of scanning are intended to be mere directions of the sample sides in this case.

Surface texture and resulting roughness clearly depend on the sloping angle with the building direction (Figure 4.6); namely, average roughness is higher for 45°- and upright-built samples (Table 4.4). Nevertheless thin layering led to uniform surfaces preventing any clear main pattern in terms of mean spacing of profile irregularities; hence, no deviation is found among longitudinal, transverse and crossed roughness. As a consequence, a single average reference value for starting roughness is considered in the following for each given building direction to assess the effectiveness of LSM.

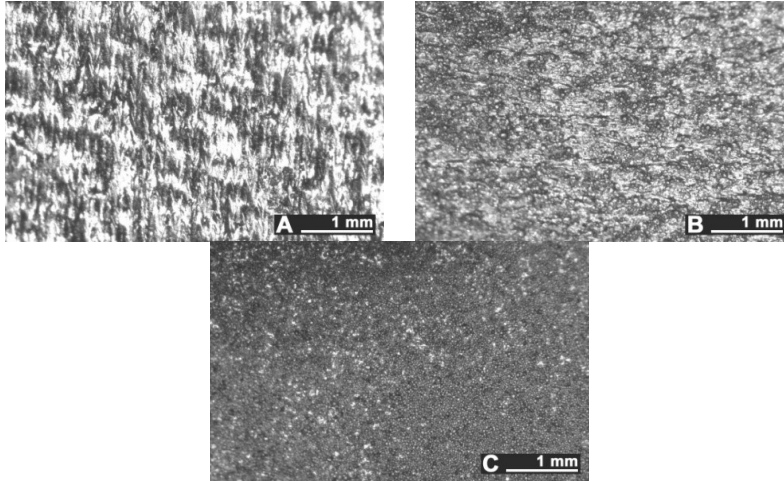


Figure 4.6: Surface texture, as-built samples: (A) flat-built, (B) 45°-built and (C) upright-built

Table 4.4: Longitudinal, transverse and crossed average as-built roughness

	Measuring direction	Arithmetic roughness R_a		Peak-to-valley height R_z	
		Average [μm]	Std. deviation [μm]	Average [μm]	Std. deviation [μm]
Flat-built	Longitudinal	6.06	0.60	34.33	3.59
	Transverse	6.87	0.74	35.50	3.10
	Crossed	7.44	0.10	43.50	3.15
45°-built	Longitudinal	14.40	0.70	106.80	6.77
	Transverse	15.07	0.55	111.30	3.54
	Crossed	14.83	1.17	109.27	12.65
Upright-built	Longitudinal	16.20	1.75	107.47	12.82
	Transverse	15.83	0.32	104.83	4.39
	Crossed	16.50	1.04	109.77	3.97

4.4.2 Roughness and geometry of the fusion zone upon LSM

Based on visual inspections upon LSM (Figure 4.7), shielding is deemed to be effective. Furthermore, no cracks neither macropores resulted from any of the processing conditions (Table 4.5). Surface modification of each texture are then discussed in terms of percentage reduction of roughness $\Delta R\%$; the depth of the fusion zone (i.e., the remelted layer, Figure 4.8) with respect to the nominal surface in the cross-section has also been considered as response (Table 4.5); due to shading boundaries, the depth of the heat-affected zone (HAZ) should be discussed via microhardness testing instead.

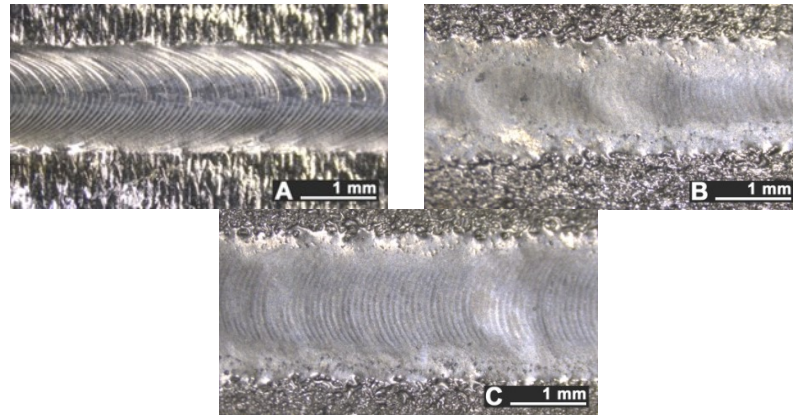


Figure 4.7: Examples of visual inspections upon LSM with laser beam wobbling, 2 mm amplitude at 400 Hz frequency: (A) flat-built, (B) 45°-built and (C) upright-built samples

Table 4.5: Transverse cross-sections; 1 kW power, 2 m·min⁻¹ scanning speed, 1 mm diameter focus

	Flat-built sample	45°-built sample	Upright-built sample
Beam wobbling: 1 mm amplitude, 200Hz frequency			
Beam wobbling: 1 mm amplitude, 400Hz frequency			
Beam wobbling: 2 mm amplitude, 200Hz frequency			
Beam wobbling: 2 mm amplitude, 400Hz frequency			
Linear scanning			

Reduction of surface roughness by means of laser processing
over additive manufacturing metal parts

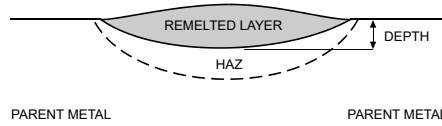


Figure 4.8: Scheme for width and depth of the remelted layer in the cross-section

Table 4.6: Responses for each processing condition

Conditions		Arithmetic roughness R_a			Peak-to-valley height R_z			Depth [mm]	
		Average [μm]	Std. dev. [μm]	$\Delta R\%$	Average [μm]	Std. dev. [μm]	$\Delta R\%$		
A [mm]	f [Hz]								
Flat built	1	200	3.09	0.19	54	17.11	2.06	55	0.17
	1	400	2.26	0.19	67	13.66	0.78	64	0.19
	2	200	2.27	0.21	67	12.81	0.21	66	0.12
	2	400	2.54	0.16	63	13.15	0.61	65	0.14
	Linear scanning		1.73	1.21	74	9.35	4.62	75	0.18
45° built	1	200	2.66	0.31	84	13.85	1.49	87	0.19
	1	400	1.92	0.32	88	10.59	1.01	90	0.19
	2	200	1.91	0.24	88	11.12	0.94	90	0.12
	2	400	1.85	0.37	89	10.38	1.68	90	0.10
	Linear scanning		1.34	0.26	92	7.41	1.30	93	0.19
Upright built	1	200	3.11	0.12	79	16.67	0.61	85	0.17
	1	400	1.69	0.33	89	10.38	2.30	90	0.16
	2	200	2.59	0.15	82	14.55	1.15	87	0.11
	2	400	1.71	0.32	88	9.47	1.26	91	0.15
	Linear scanning		1.54	0.27	90	9.16	0.79	92	0.19

Decreased roughness resulted in all of the conditions of the experimental plan; therefore, overmelting of the surface, which would increase roughness due to improper energy density, is prevented. Namely, major improvements are achieved when considering 45°- and upright-built samples, the process being capable of reducing R_a below 2 μm under certain processing conditions. Two reasons are inferred. First, irrespective of the scanning strategy in LSM, a dependence of absorption on the surface type is assumed: the higher the starting roughness, the lower the reflectivity, the more effective the overall process; moreover, as LSM is driven by melting of surface peaks, the higher them, the better the response.

Further findings result from the discussion of the main effects plots (Figure 4.9) when referring to scanning in case of laser beam wobbling. For a given building direction, both wobble amplitude and frequency have mild affection on either R_a and R_z roughness reduction. Interestingly, as a general rule, increasing wobble frequency for a given wobble amplitude results in decreasing roughness but concurrent increasing depth of the remelted layer,

as more loops per length are engraved along a given scanning length; increasing wobble amplitude for a given wobble frequency results in decreasing roughness as well, with concurrent decreasing depth of the fusion zone instead, since wider scanning traces are processed and overlapping among consecutive loops is affected.

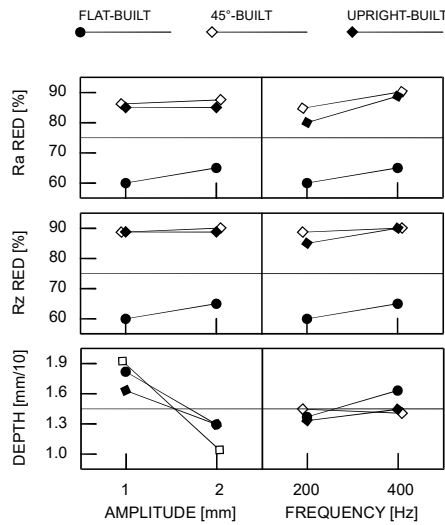


Figure 4.9: Main effects plots for roughness reduction percentage and depth of the remelted layer

Since heat affection and deterioration of bulk properties in the parent metal must be proven to be reasonable upon LSM, the suggestion of an optimum condition for processing would be pointless when based on mere discussion of reduction of roughness. Therefore, higher weight must be awarded to the technical constrain involving depth; as a consequence of this, although better polishing results from linear scanning in terms of roughness, wobbling with 2 mm amplitude at 200 Hz frequency is suggested within the current investigating domain.

4.4.3 Microstructure and microhardness

The depth of thermal penetration is worth investigating. In the unaffected parent metal, the appearance of lenticular-shaped melting pools is clear as a result of building and layer development (Figure 4.10); moreover, as heat flows toward the building plate during manufacturing, columnar growth along the building direction is shown in magnified view (Figure 4.11).

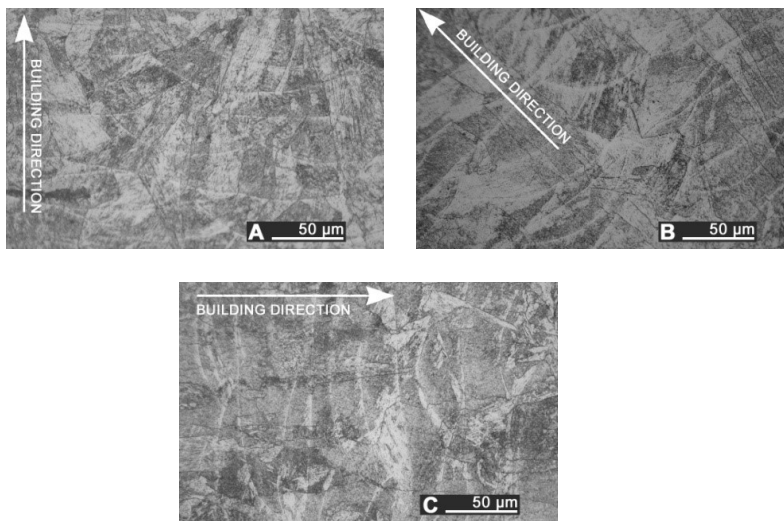


Figure 4.10: Melting pools in the cross-section: (A) flat-built, (B) 45°-built and (C) upright-built samples

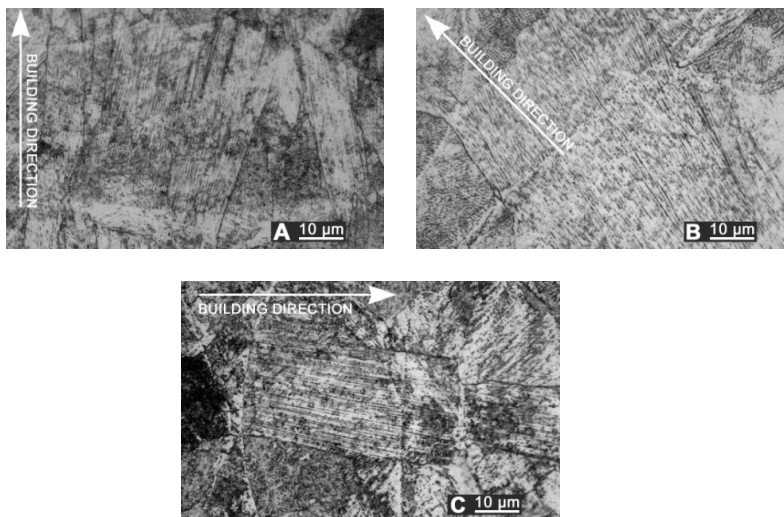


Figure 4.11: Micrographs, grain growth: (A) flat-built, (B) 45°-built and (C) upright-built samples

In agreement with the literature [17], specific grain size and microstructure strongly depend on both the building strategy and the supporting structures; nevertheless, irrespective of these, a fully martensitic transformation is prevented due to nickel and chromium addition in the base powder, leading to large solidification undercooling and residual metastable austenite; moreover, tempering is promoted in the lowest layers during additive fabrication. Indeed, as-built samples are approximately composed of 70% mass fraction austenite and 30% martensite on average [18]; a reference microhardness of 265 HV is found, in agreement with similar results on the same alloy [19] and the material data sheet of the supplier.

As a consequence of LSM, softening to 235 HV on average is experienced in the fusion zone, austenite being retained as the main phase. Solution annealing is thought to be in place in the HAZ instead (Figure 4.12), based on referred metallographic analyses [20].

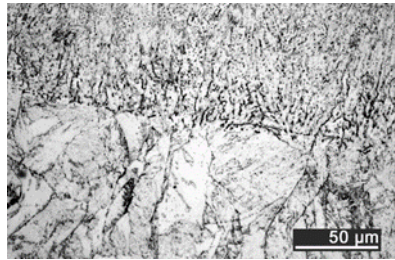


Figure 4.12: Heat-affected zone at the interface with the remelted layer; LSM with laser beam wobbling, 2 mm amplitude at 200 Hz frequency on flat-built sample

Namely, referring to the suggested condition for LSM with beam wobbling on flat-built samples, one may assume the parent metal is unaffected at an average depth of 250 μm, based on the trend of Vickers microhardness as a function of the distance from the nominal top surface; a depth of 400 μm at least is found instead when considering linear scanning with no wobble (Figure 4.13), although a dependence from the position on the building plate is inferred as reason for different hardness of the parent metal. Similar trends of microhardness have been found for 45°- and upright-built samples.

Reduction of surface roughness by means of laser processing
over additive manufacturing metal parts

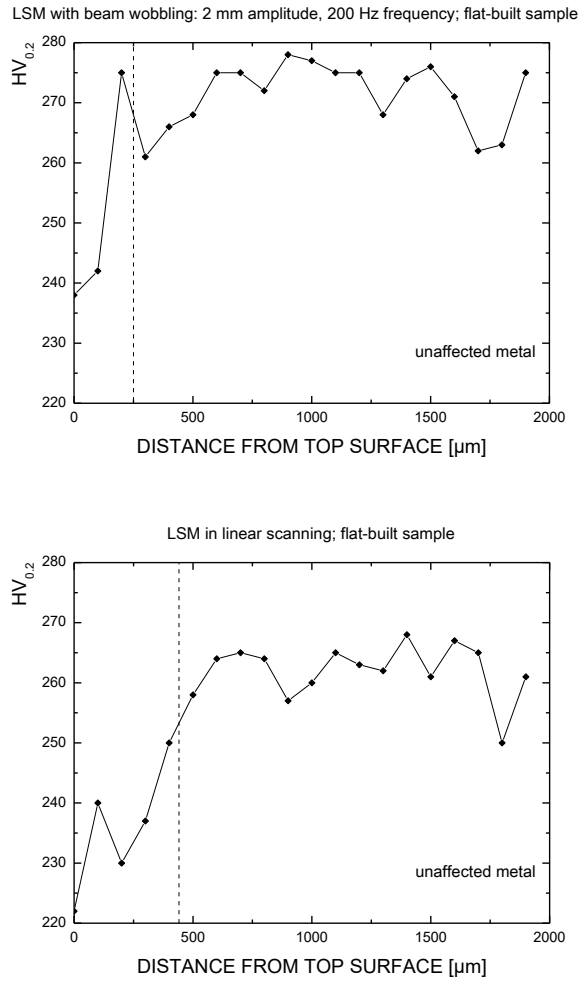


Figure 4.13: Vickers microhardness trend as a function of distance from top surface, as a result of LSM with beam wobbling and LSM in linear scanning on flat-built samples

4.5 Conclusions

Surface modification by means of laser beam is effective as possible post processing treatment over stainless steel components resulting from additive manufacturing, in order to improve the surface topography. The response has been proven to depend on the starting features of the samples; namely, major improvements are achieved over 45°- and upright-built samples, the process being capable of reducing arithmetic roughness below 2 μm on average, thus matching the requirement for real parts in valid operating conditions.

Nevertheless, a change in the microstructure is induced as a consequence of lasing, therefore the affection of the parent metal must be addressed. Some benefits are offered when performing laser beam wobbling compared with linear scanning: heat affection is proven to be lower indeed, based on the depth of the fusion zone as well as on the extent of the HAZ resulting from Vickers microhardness testing. For given operating power of 1 kW and processing speed of 2 $\text{m}\cdot\text{min}^{-1}$, wobbling with 2 mm amplitude at 200 Hz frequency is suggested.

Interestingly, additional opportunities are offered as the resulting features of the surfaces can be conveniently graded by means of proper setting of frequency and amplitude, with reliable monitoring from the laser source. For these reasons, grounds for application on real parts are given, although additional studies on overlapping traces must be conducted to perform the process over larger surfaces.

References chapter IV

1. Emmelmann, C., Sander, P., Kranz, J., Wycisk, E. Laser additive manufacturing and bionics: redefining lightweight design. *Physics Procedia* 2011, 12 (A), 364–8.
2. Santos, E.C., Shiomi, M., Osakada, K., Laoui, T. Rapid manufacturing of metal components by laser forming. *Int. J. Mach. Tools Manuf.* 2006 46 (12-13), 1459–68.
3. Strano, G., Hao, L.,m Everson, R.M., Evans, K.E. Surface roughness analysis, modeling and prediction in selective laser melting. *J. Mater. Process. Technol.* 2013, 213 (4), 589-597.
4. Luis Pérez, C.J., Calvet, J.V., Pérez, M.A.S. Geometric roughness analysis in solid free-form manufacturing processes. *J. Mater. Process. Technol.* 2001, 119 (1), 52-57.
5. Calignano, F. Design and optimization of supports for overhanging structures in aluminum and titanium alloys by selective laser melting. *Mater. Des.* 2014 64, 203-13.
6. Alrbaey, K., Wimpenny, D., Tosi, R., Manning, W., Moroz, A. On optimization of surface roughness of selective laser melted stainless steel parts: a statistical study. *J. Mater. Eng. Perform.* 2014 23 (6), 2014-139.
7. Lü, L., Fuh, Wong, Y.S. *Laser Induced Materials and Processes for Rapid Prototyping*; Springer Science + Business Media: New York, United States of America, 2001.
8. Kumbhar, Mulay, A. Post processing methods used to improve surface finish of products which are manufactured by Additive Manufacturing (AM) technologies – A review. *J. Inst. Eng. India Ser. C* 2016.
9. Lamikiz, Sanchez, J.A., Lopez de Lacalle, L.N., Arana, J.L. Laser polishing of parts built up by selective laser sintering. *Int. J. Mach. Tools Manuf.* 2007 47, 2040-50.
10. Kumstel, Kirsch, B. Polishing titanium- and nickel-based alloys using cw-laser radiation. *Physics Procedia* 2013 41, 362-71.
11. Steen, Mazumder, J. *Laser Material Processing*; Springer-Verlag: London, United Kingdom, 2010.
12. Nüsser, C., Wehrmann, I., Willenborg, E. Influence of intensity distribution and pulse duration on laser micro polishing. *Physics Procedia* 2011 12, 462-71.

13. Ukar, E., Lamikiz, A., Martinez, S., Tabernero, I., Lopez de Lacalle, N.L. Roughness prediction on laser polished surfaces. *J. Mater. Process. Technol.* 2012 *212*, 1305-13.
14. Marshall, G.F., Stutz, G.E. *Handbook of Optical and Laser Scanning*; CRC Press: Boca Raton, United States of America, 2011.
15. Engelmayer, A. Galvanometer scanning speeds laser processing. *Industrial Laser Solutions for Manufacturing* 2005 *2*.
16. Kuryntsev, S.V., Gilmudinov, A.K. The effect of laser beam wobbling mode in welding process for structural steels. *Int. J. Adv. Manuf. Technol.* 2015 *81*, 1683–91.
17. Luecke, W.E., Slotwinski, J.A. Mechanical properties of austenitic stainless steel made by additive manufacturing. *J. Res. Nat. Inst. Stand. Technol.* 2014 *119*, 398-418.
18. Facchini, L., Vicente, N. Jr., Lonardelli, I., Magalini, E., Robotti, P., Molinari, A. Metastable austenite in 17-4 precipitation-hardening stainless steel produced by Selective Laser Melting. *Adv. Eng. Mater.* 2010 *12* (3), 184-7.
19. Gratton, A. Comparison of mechanical, metallurgical properties of 17-4PH stainless steel. Proceedings of National Conference on undergraduate research (NCUR), Ogden, Utah, United States of America, March 28-31, 2012.
20. Vander Voort, G.F., Lucas, G.M., Manilova, E.P. Metallography and microstructures of stainless steels and maraging steels. In *ASM Handbook 9 – Metallography and Microstructures*. Publisher: ASM International, Materials Park, United States of America, 2014.
21. EN ISO 4288:1997. Geometrical product specifications (GPS) – Surface texture: Profile method – Rules and procedures for the assessment of surface texture, 1997.
22. Caiazzo, F., Sergi, V., Corrado, G., Alfieri, V., Cardaropoli, F. Apparato automatizzato di saldatura laser. Patent no. SA2012A000016, 2012.
23. EN ISO 6507-1:2005. Metallic materials – Vickers hardness test – Part 1: test method, 2005.

Conclusions

The aim of this work was to investigate the application of additive manufacturing techniques in the field of aerospace industry.

The following application topics have been investigated:

- Redesign and production of moulds for investment casting of turbine blade with powder-bed based additive manufacturing instead of conventional technique of machining by CAD/CAM technologies;
- Job-design and optimization with powder-bed based additive manufacturing. Application of this process has been investigated as an advanced industrial prototyping tool to manufacture Inconel 718 turbine blade at a pre-design stage before flow production. The mechanical properties of the base metal have been discussed via tensile testing;
- Repair and overhaul of condemned parts of high complexity and expensive manufacturing cost with Directed Metal Deposition (DMD) of powder. This process is receiving increasingly interest in aerospace industry since it allows minimal distortion of the work-piece, reduced heat-affected zones and better surface quality in comparison with conventional coating and repairing techniques such as arc welding or plasma spraying. Namely, manufacturing of C1023 and CM247LC components have been repaired through a suitable deposition scheme, that is side-by-side and overlapping deposition;
 - Surface optimization: since surface quality may limit the application of the AM part if compared with conventional metal manufacturing processes such as machining, proper means to address the surface roughness have been investigated. Flat, 45° and upright building orientations have been addressed with respect to the building plate in order to test the effectiveness of the post processing scanning strategy against different surface conditions. Experimental trials and computational prediction have hence been aimed to optimization of the processing parameters and the exposure strategies. This approach has been proven to be effective as possible post processing treatment over stainless steel components resulting from AM, in order to improve the surface topography.

All these topics have been considered and possible real applications have been demonstrated for each of them in complex and challenging fields such as the aerospace industry. Specific conclusions have been provided in the relevant chapters in comparison with conventional technologies.

Despite higher costs in comparison with conventional technologies, a number of advantages are benefited thanks to Additive Manufacturing.

Nevertheless, the Technology Readiness Level (TRL) of these applications is different, depending on the efforts made so far in terms of research. Laser Cladding to the purpose of repairing is currently employed in the industry, although specific research is required depending on the materials; on the other hand, deeper and wider studies are still needed in the frame of direct fabrication of turbine blades via AM, hence a lower TRL is in place. Therefore, further developments are expected in the industrial world in the frame of Industry 4.0.